PROTON RADIATIVE CAPTURE TO ^{13}N IN THE REGION OF THE SECOND HARMONIC GIANT DIPOLE RESONANCE COLLECTIVE EXCITATION

by

Alessandro ZUCCHIATTI

A thesis submitted to the
Faculty of Science
University of the Witwatersrand, Johannesburg
for the degree of
Doctor of Philosophy

1988

ABSTRACT

This work embraces the measurement of angular distributions and excitation functions for proton radiative capture to the ground and excited states of ^{13}N, in energy steps from $E_p = 40$ to $E_p = 52$ MeV.

Legendre polynomial fits to the angular distributions are made and the energy variation of Legendre coefficients is established for several (p,γ) transitions involving states up to an excitation energy of 15 MeV. The polynomial coefficients are explained by large dipole-quadrupole interference effects, particularly interesting at excitation energies corresponding to twice ($E_x \approx 46$ MeV) the centroid value of the ground state based Giant Dipole Excitation. Broad resonances are found in the (p,γ_0) and the (p,γ_{2+3}) channels, which involve final states that are members of the same rotational band and therefore should present very similar internal structures as the almost equivalent Legendre coefficients substantiate. For other excited states similar trends have been found although within limits imposed by larger experimental errors.

The $2\hbar\omega \rightarrow 1\hbar\omega$ transition is found largely superimposed on inelastic proton scattering channels, contrary to what was established in previous experiments. Upper limits for the excitation functions are extracted and only for the highest measured energy point are the two contributions clearly separated.

This reasearch program is based on a newly-developed anti-coincidence large-volume scintillation spectrometer designed by means of a Monte Carlo simulation code. Specific tests performed with Tandem accelerator beams, and routine application at higher energies, demonstrate the excellent correspondence of the design expectations with the performance as measured, for this spectrometer.

DECLARATION

I declare that the results presented in this theses are my own work performed under the supervision of Professor J.P.F. Sellschop.

The realisation of the Monte-Carlo simulation code for the study of electromagnetic showers development in detection media and of the data analysis codes has been largely conducted at the Istituto Nazionale di Fisica Nucleare of Genova (Italy).

This material has not been submitted for a degree in any other university.

25 MARCH 1988

To Rosanna, Andrea and Elena

ACKNOWLEDGEMENTS

This work would not have been possible without the support and collaboration of many persons, to whom I would like to express my deep gratitude.

- Professor J.P.F. Sellschop, my supervisor, has supported me at all stages of this difficult task with essential discussions, vital decisions and warm and endless encouragement. But he has also made my stay at the Schonland Research Centre for Nuclear Sciences, which he directs, a most profitable scientific experience for which I really am grateful.
- Prof. H.J. Annegarn, Prof. R.J. Keddy, Dr. R.W. Fearick, Dr. M.C. Stemmet, Dr. J. Carter, Prof. D.G. Aschman and Mr. D. Steyn have shared with me the difficulties of the experiment contributing a great deal to the success of this initiative and to the achievements upon which this thesis is based.
- The technical staff of the Schonland Research Center have provided essential back-up in the construction of the complex detector developed as part of this thesis. To the mechanical workshop foreman Mr. L.Verga, to the head of the electronics laboratory Mr. A.H. Andeweg and to our target maker Mr. M. Rebak goes, in particular, my deep gratitude.
- My colleagues at the Istituto Nazionale di Fisica Nucleare of Genova, Prof. P. Corvisiero and Dr. M.Taiuti have assisted me with great dedication in the delicate task of preparing the computer codes for data analysis.
- I would also like to acknowledge the warm hospitality of the National Accelerator Center in Faure. The Director, Dr. D. Reitmann, the chief engineer, Dr. A. Botha and the technical staff have contributed to the success of our experiment.
- The financial support of Foundation for Research Development of the Council for Scientific and Industrial Research of South Africa and of the Istituto Nazionale di Fisica Nucleare of Italy is gratefully acknowledged.
- I would also like to thank the University of the Witwatersrand for hospitality and support and the use of their laboratory facilities at the Schonland Research Centre for Nuclear Sciences, during my two year secondment and several subsequent visits.

CONTENTS

CHAPTER 1

RADIATIVE CAPTURE TO LIGHT AND MEDIUM NUCLEI

1-1 General comments

Polarized and unpolarized deuteron and proton radiative capture studies from about 1 MeV to a few hundred MeV have covered final nuclei from ^{3}He to ^{40}Ca. A review of the literature so far produced on this subject, even if the analysis has to be limited to the ensemble of papers which have led so far to the major break-throughs in the field, can give a comprehensive picture of the actual situation and the opportunity of identifying the problems and goals of an experimental program in the range of energies available at the National Accelerator Centre (NAC).

The extent of radiative capture physics studies emerges immediately from the plots of the "relative production" (figure 1) of (p,γ), $(\vec{p},\gamma)$, (d,γ), $(\vec{d},\gamma)$ and of the "energy distribution" (figure 2) based on a set of about eighty relevant papers and classified with respect to the final nucleus mass. Most of the attention has been dedicated to double closed shell nuclei or to nuclei having one nucleon off a doubly closed shell. This is understandable, experiment-wise, in terms of the high Q-values involved in capture reactions to even-even nuclei which allow reaching the Giant Dipole Resonance even with low energy beams and therefore reduced neutron background but also in terms of the relatively large spacing of low-lying states in the final nucleus which readily allows correct identification of at least the first couple of γ transitions, even with elementary medium resolution γ spectrometers. Theory-wise it is clear that calculations in closed shell or nearly closed shell nuclei can be performed under simplifying assumptions, as for example in the schematic GDR model [64]. It is also of relevance that in light nuclei (and they represent most of our ensemble) one channel carries often a significant fraction of the dipole sum rule and the capture reaction measures just the GDR decay through one channel only. These are the basic reasons for the trend of the data in figure 2 where, with the exception of ^{12}C and ^{28}Si, the majority of the experimental points appears clustered in the excitation energy region corresponding to the GDR, with only few but extremely important inroads into higher energies, and few but important polarized projectile experiments.

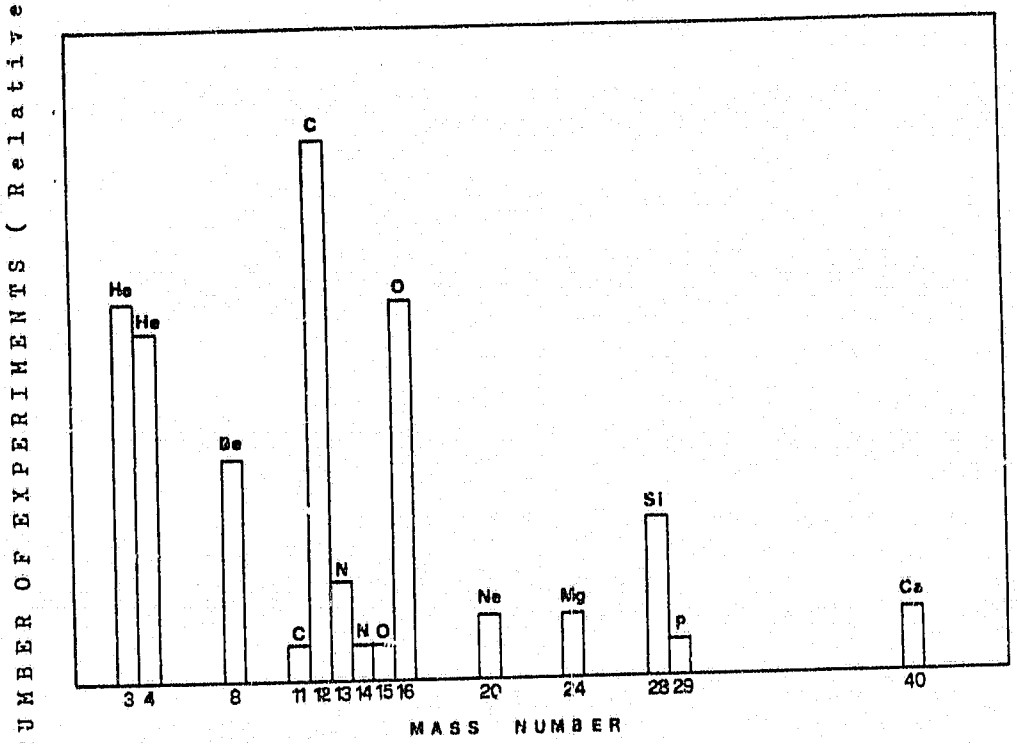

FIGURE 1 Distribution of proton and deuteron radiative capture experiments as a function of the compound nucleus mass.

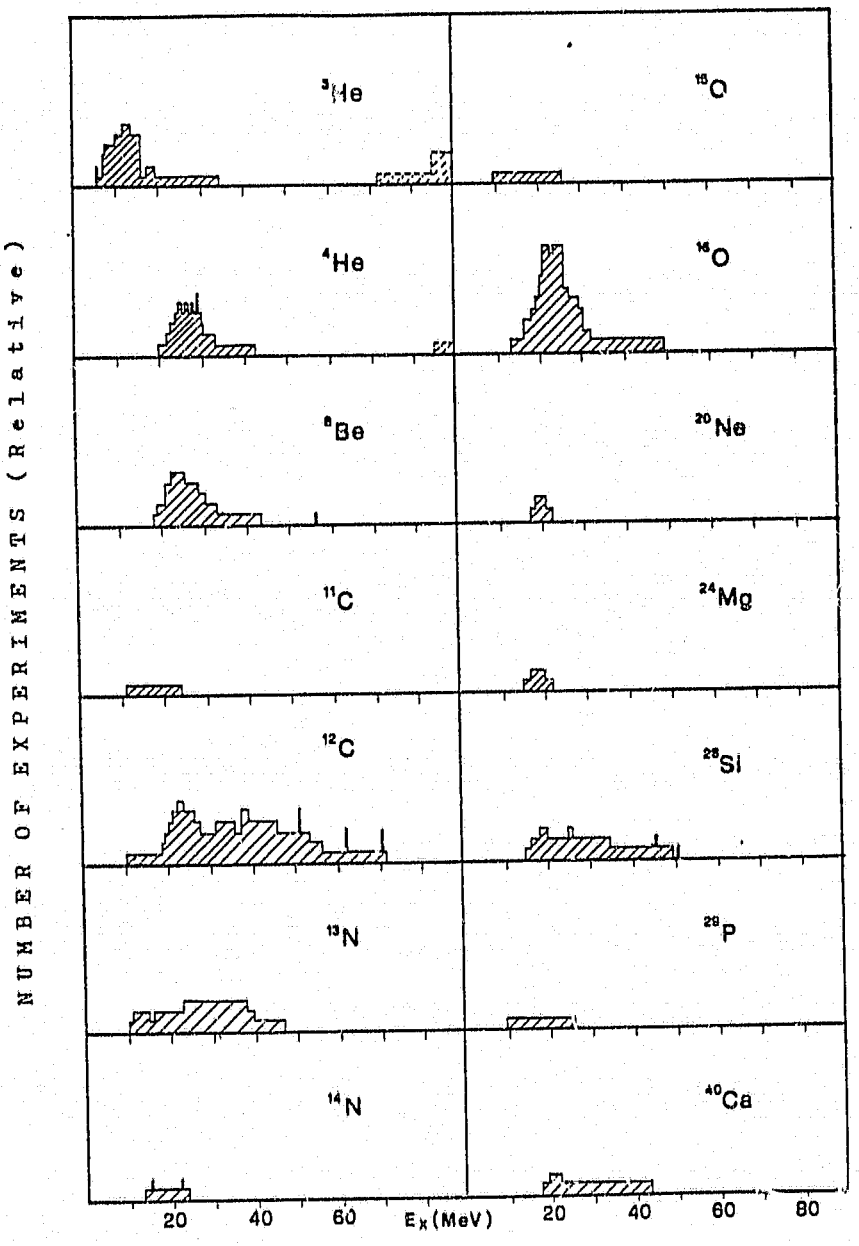

FIGURE 2 Energy distribution of proton and deuteron radiative capture experiments in different compound nuclei.

The data on capture reactions to the ground state of the final nucleus are obviously complementary to those obtained by direct photonuclear reactions and experimental points can be easily compared for equivalent energies through the detailed balance. This characterized the use of capture reactions in their inception, as a fruitful tool for the complementary study of photonuclear reactions. But a large amount of original information, given by radiative captures to excited nuclear states, has subsequently started to be collected and has opened up a most interesting field of research in recent years. This draws to attention the possibilities offered at NAC, where the beam features available can make significant additions to the data set in figure 2, in those parts which our analysis shall attemp to specify.

1-2 Polarized and unpolarized p and d capture to ^{3}He

For few body systems like ^{3}He, radiative capture reactions are essentially an important complement to direct photonuclear reactions since the ground state (p,γ_0) cross section is related through the detailed balance formula to the (γ,p_0), but with the advantage, common to all capture reactions, of having definite kinematics corresponding to monochromatic photons in the (γ,p) channel and with charged particle beam monitoring that is much more precise than any γ dose measurement. The $D(p,\gamma)^3$He as well as the $^1H(d,\gamma)^3$He, the $D(\vec{p},\gamma)^3$He and the $^1H(\vec{d},\gamma)^3$He reactions have been studied extensively and details of the cross section obtained by capture reactions from threshold to about 500 MeV, contribute, with the corresponding two body photodisintegration data, a great deal of information on nuclear forces between bound nucleons [1]. Furthermore the analysis of precision angular distributions allows us to establish the composition of the ground state wave function in ^{3}He and the excitation mechanism responsible for the capture reaction, bringing evidence over the influence of the D state and the S' (mixed symmetry) components in the ^{3}He wave function. Finally, very recent polarized projectile capture studies allowed the singling out, rather unambiguously, of the contribution of various multipolarities to the photonuclear cross section and precise measurements of the interference between contributing waves in the entrance channel. Below 50 MeV the two body photodisintegration total cross section of ^{3}He(γ,p)D (as obtained from both photonuclear reactions and

radiative captures), peaks at $E_x \approx 13$ MeV with measured values scattered between 0.7 and 1 mb. The low values are more likely candidates for the true value, since the measurements have smaller statistical errors and they are supported by the accurate $^2H(p, ^3He)$ calibration experiment [2] at $E_p = 16.1$ MeV. Realistic ^{3}He g.s. wave functions have been obtained by numerical solutions of the Fadeev equations [3] or by variational methods [4], with similar results. This exact g.s. wave functions has been used to calculate the two body photodisintegration of ^{3}He by adopting a one-body current operator and final proton undistorted, or by using one-body current operator and distorted proton waves, and Siegert theorem and distorted waves to acccunt for meson exchange currents [5]. The importance of distortion in the final scattering state is proved by the rather good fitting to the experimental data peaking at 0.7 mb, while meson exchange currents (MEC) could account for the large measured peak values (1.2 mb) as observed in some experiments.

Angular distributions should be more dependent on the details of the three body wave function. This can be written as [6]:

$$\psi_a = \phi_a U_s + \phi_s U_a + (\phi' U'' + \phi'' U') \qquad [1-1]$$

where $a\,(s)$ denotes complete asymmetry (symmetry) with respect to the spatial coordinates of any pair of nucleons in states ϕ_a, ϕ_s or to spin and isospin coordinates in U_a, U_s. The ϕ', ϕ'', U', U'' are symmetric or antisymmetric not for the exchange of any pair of nucleons but of only two of them and arise physically from the different average separation of the n-p pair compared to that of the p-p pair. The second term is the spatially symmetric S component while the third is the so-called S' component of mixedsymmetry. Furthermore there is a non-negligible probability of finding the final nucleus in a D state and it is expected that the angular distribution is sensitive to both the S' and D states of the final nucleus.

The Legendre expansion of the angular distribution for unpolarized particles and photons is given by:

$$\frac{d\sigma}{d\Omega} = A_0 \left[1 + \sum_{k=1}^{2L} a_k P_k(\cos\vartheta)\right] \qquad [1-2]$$

TABLE 1

Multipole dependence of angular distribution Legendre coefficients

$a_n\ b_n$	1^{st} ord kR	2^{nd} ord kR	3^{rd} ord kR	4^{th} ord kR	5^{th} ord kR
a_0	$\|E1\|^2$		$\|E2\|^2 + \|M1\|^2$		$\|E3\|^2 + \|M2\|^2$
$a_1\ b_1$		$(E1, E2)$		$(E2, E3)$	
		$(E1, M1)$		$(E2, M2)$	
				$(M1, M2)$	
$a_2\ b_2$	$\|E1\|^2$		$\|E2\|^2$		$\|E3\|^2$
	$(E1, E1')$		$\|M1\|^2$		$(E^\circ, E3')$
			$(E1, E3)$		$\|M2\|^2$
			$(E1, M2)$		$(M2, M2')$
			$(M1, E2)$		$(E3, M2)$
			$(E2, E2')$		
			$(M1, M1')$		
$a_3\ b_3$		$(E1, E2)$		$(E2, E3)$	
				$(E2, M2)$	
				$(M1, M2)$	
				$(M1, E3)$	
$a_4\ b_4$			$\|E2\|^2$		$\|E3\|^2$
			$(E1, E3)$		$(E3, E3')$
			$(E2, E2')$		$\|M2\|^2$
					$(M2, M2')$
					$(E3, M2)$
$a_5\ b_5$				$(E2, E3)$	
$a_6\ b_6$					$\|E3\|^2$
					$(E3, E3')$

each coefficient is sensitive to multipoles contained in the interaction expansion and to interference terms between the various amplitudes [1], as shown in Table 1.

For ^{3}He and few body systems, a different parametrisation [7] is used and allows straightforward connection between angular distribution expansion coefficients and the involved multipolarities.

$$\frac{d\sigma}{d\Omega} = A(\sin^2\vartheta + \beta\sin^2\vartheta\cos\vartheta + \gamma\sin^2\vartheta\cos^2\vartheta + \delta + \epsilon\cos\vartheta) \qquad [1-3]$$

where the $\beta, \gamma, \delta, \epsilon$ coefficients are related to the different multipolarities according to table I, since the connection between these coefficients and the a_k is straightforward:

$$\begin{aligned} A &= -\frac{3}{2}a_0(a_2 + \frac{5}{12}a_4) \\ \beta &= \frac{1}{A}(-\frac{5}{2}A_0a_3) \\ \gamma &= \frac{1}{A}(-\frac{35}{8}A_0a_4) \qquad [1-4] \\ \delta &= -\frac{A_0}{A}(1 + a_2 + a_4) \\ \epsilon &= \frac{A_0}{A}(a_1 + a_3) \\ \sigma_{tot} &= 4\pi A_0 = \frac{8\pi}{3}(1 + \frac{\gamma}{5} + \frac{3}{2}\delta) \end{aligned}$$

Now it is statistically justified in all data to limit the Legendre polynomial expansion to $k = 2$, at least below 50 MeV excitation energy. Furthermore for spatially symmetric ^2S waves, the M1 matrix element is expected to make a negligible contribution due to the orthogonality of initial and final state wave function. So we can expect the coefficients of the angular distributions to depend on only a few transition modes to the ^{3}He g.s.; more precisely

A	pure dipole	E1 ($^2P \rightarrow {}^2S$)
β	E1 E2 interference	E1($^2P \rightarrow {}^2S$), E2($^2D \rightarrow {}^2S$)
γ	pure quadrupole	E2($^2D \rightarrow {}^2S$)
δ	isotropic M1 contribution	M1($^4S \rightarrow {}^2S$)
ϵ	basically =0 at low energy	M1 , M2 interference at high energy

In the work of Griffith et al. [8] the angular distribution is perfectly compatible with a limited form of [1-3] namely $d\sigma/d\Omega = A(\sin^2\vartheta + \delta)$. The predominant $\sin^2\vartheta$ term indicates

that the reaction proceeds essentially through direct p wave proton capture in a continuum $^{2s+1}L = {}^2P$ state with a dipole emission to the final ^2S ground state of ^{3}He. The isotropic component δ, is essentially fixed by the 90 deg cross section and should correspond to the capture of an s wave proton and subsequent M1 transition. The contribution of the two parts can be separated; this gives after integration of [1-3], $\int A\delta d\Omega = \sigma_s$ and $\int A \sin^2\vartheta d\Omega = \sigma_p$:

$$\sigma_p = \frac{\sigma_T}{1+3/2b} \qquad \sigma_s = \frac{3/2b}{1+3/2b} \qquad \frac{\sigma_s}{\sigma_p} = \frac{3}{2}b \qquad [1-5]$$

The ratio σ_s/σ_p decreases from 0.12 at $E_p = 250\,\text{keV}$ to about 0.025 at $E_p = 2\,\text{MeV}$ indicating that p wave capture has relevance even at very low energies.

Wolfli et al. [9] investigated the region between $E_p = 2$ and $E_p = 12\,\text{MeV}$. Their angular distributions are sensitive to β and δ coefficients. The δ coefficient is accounted for using a Gunn-Irving wave function including an S' admixture of 0.5% . But discrepancies arise with the experimental data at proton energies higher than $\approx 3\,\text{MeV}$, requiring the inclusion of D state components in the ground state of the three body nucleus. The β values are in agreement with the calculation performed using the same Gunn-Irving wave function.

Belt et al. [10] measured the $^1\text{H}(d,\gamma)^3\text{He}$ reaction by detecting the recoiling ^{3}He nuclei in a broad range magnetic spectrometer and inferring the γ emission angle from the ^{3}He angle and the reaction kinematics. Their angular distributions are sensitive to the β, γ and δ coefficient but do not require the inclusion of higher order terms, as found at 100 MeV [11]. Their results are noticeably in disagreement with most other experiments, in particular the δ coefficient is found to increase with energy and the β coefficient to decrease. Furthermore the ratio $\gamma = \beta^2/4$ [12], that is obtained assuming a pure spatially symmetric ^{3}He state and a phase difference between E1 and E2 amplitudes close to zero, is not confirmed by this experiment which gives $\gamma = \beta^2/1.5$, a value more similar to that ($\gamma = \beta^2/2.6$) computed when including higher multipoles [12]. A resonance at $E_x = 19.5\,\text{MeV}$ to which $T = \frac{1}{2}$ is attributed, shows up from their data[10] but is not confirmed by other experiments in the same range.

King et al. [13] measured angular distributions at excitation energies from 10 to 16 MeV and focused attention on the behaviour of the a_2 coefficient [14] of the Legendre polynomial expansion [1-2]. Statistical uncertainties of less than ± 0.02 on values from -0.87 to -0.93 are obtained. They performed an effective two body direct capture calculation including E1, E2 and E3 radiation. Gibson and Lehman ^{3}He g.s. wave functions including variable D state probability are used [15], while the initial continuum wave function is obtained from the optical model potential that describes elastic scattering of protons (neutrons) off deuterium. The optical model parameters are those of Guss [16]. Values of 0%, 4% and 7% for the D state probability are tested with the last value giving the best fit to the data, substantiating that high quality angular distribution data, taken over a reasonable energy range, are indeed sensitive to a D state presence in ^{3}He.

A group (including the author) [17], has extended proton capture on deuterium up to $E_x = 32.1$ MeV. The γ-ray spectrometer used to detect photons from about 35 deg to 140 deg, had good resolution (fig 3) and detection efficiency. A Legendre polynomial expansion [1-2], including terms up to $L = 2$ was fitted to the data (Figure 4) and the coefficients converted by means of equations [1-4]. A review of data, covering the range of excitation energies from 3 to 52 MeV, was carried out and is presented in fig. 5. This shows a rather smooth trend for all coefficients. The isotropy coefficient δ can arise at $E_x \leq 15$ MeV from spin-flip M1 ($^4S \rightarrow {}^2S'$) transitions and is compatible with a $1-2\%$ admixture of the mixed symmetry component in ^{3}He g.s. wave function. The full curves values compared to the measured σ_{tot}, β and γ, are those of Barbour and Hendry [18] who assume a pure spatially symmetric $^2S_{1/2}$ state in order to compute

$$A = \frac{3}{8\pi}\sigma(\mathrm{E1}) \quad \beta = 2\sqrt{\frac{5\sigma(\mathrm{E2})}{\sigma(\mathrm{E1})}}\cos\varphi_{E1\,E2}$$

$$\gamma = \frac{5\sigma(E2)}{\sigma(E1)} \quad \delta = \frac{2\sigma(M1)}{3\sigma(E1)} \quad \epsilon = 0 \qquad [1-6]$$

The experimental cross section is quite well reproduced, confirming the poor sensitivity of the total cross section, in this energy range, to the details of the g.s. wave function. On the contrary the departure of this simple model from the actual experimental points above

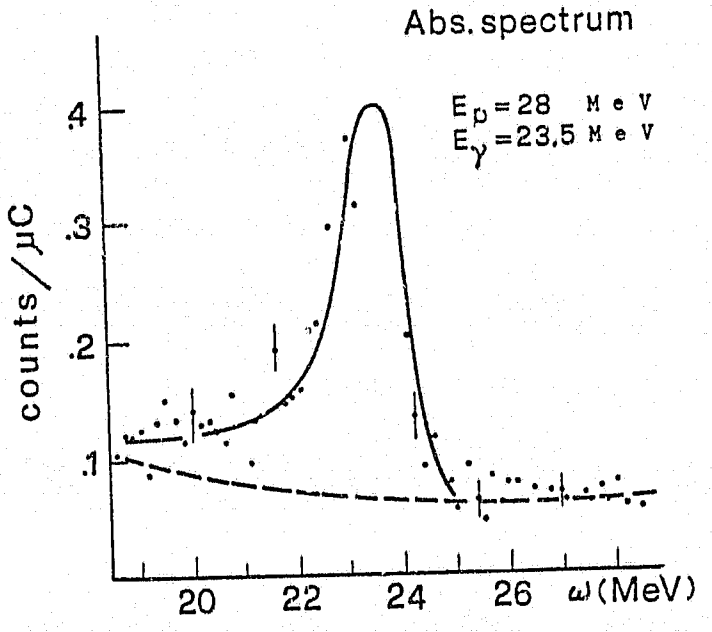

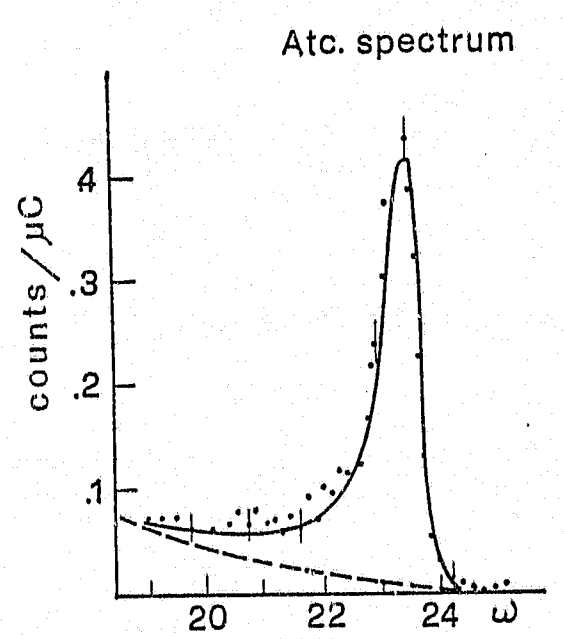

FIGURE 3 Photon spectra for the reaction $^2H(p,\gamma_0)^3He$ as detected by an anticoincidence scintillation spectrometer in the ungated (Abs.) and gated (Atc.) anticoincidence condition to show the resolution improvement due to tail events rejection. ω is the photon energy

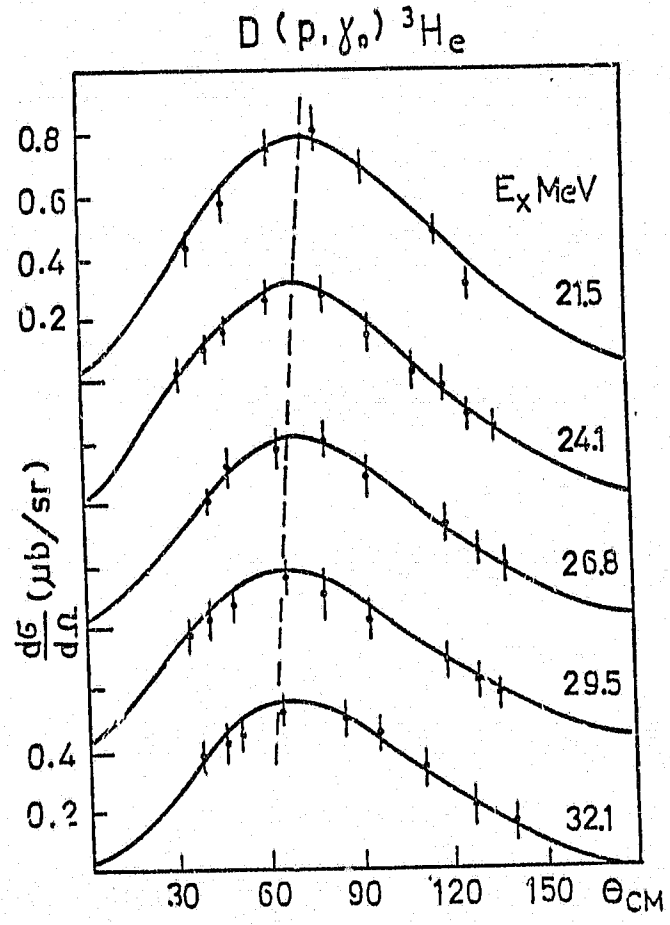

FIGURE 4 Angular distributions for the $^2H(p,\gamma_0)^3He$ reaction from $E_x = 21.5$ MeV to $E_x = 32.1$ MeV

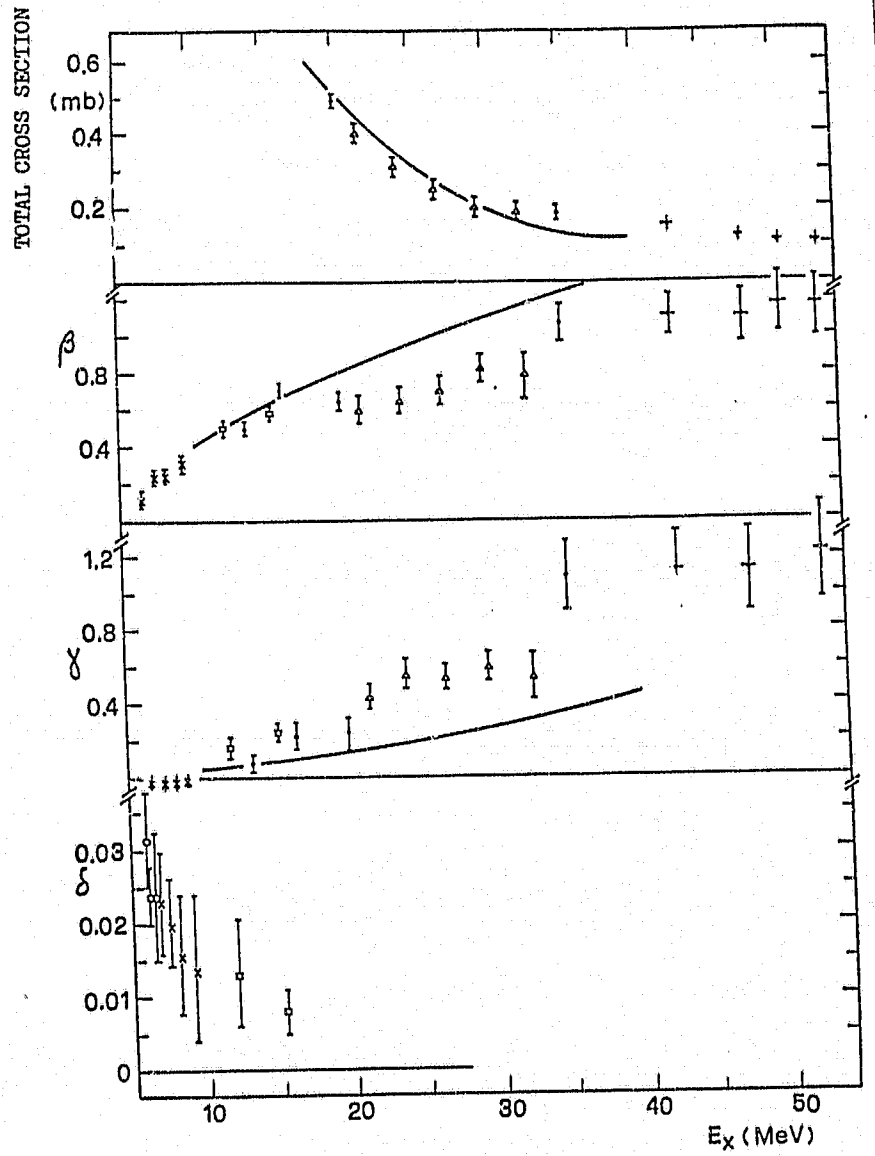

FIGURE 5 Absolute total cross section and angular distribution coefficients from the analysis of $^2H(p,\gamma_0)^3He$ angular distributions. Solid lines are from calculations in [18].

about 12 MeV is a significant indication of transitions involving the $^4D_{1/2}$ component of the ground state wave function. It is not probable, at least at these energies, that a contribution comes from multipolarities higher than $L = 2$.

With polarized projectiles the amount of information collected is doubled and it is possible to resolve rather unambiguously the contributions from individual multipolarities. The measured quantities are the cross section and the analyzing power, the latter being defined as

$$A = \frac{1}{P}\left(\frac{N_+ - N_-}{N_+ + N_-}\right) \qquad [1-7]$$

P is the beam polarization and $N_+(_-)$ the counts recorded alternatively for spin up (+) spin down (-) beams. This has been carried out in the energy range from $E_x = 9.83$ MeV to $E_x = 16.3$ MeV by King et al.[14]. Their expressions for the two quantities are

$$\frac{d\sigma}{d\Omega} = A_0\left[1 + \sum_{k=1}^{4} a_k P_k(\cos\vartheta)\right] \qquad [1-8]$$

$$\frac{A(\vartheta)\sigma(\vartheta)}{A_0} = \sum_{k=1}^{4} b_k P_k^1(\cos\vartheta) \qquad [1-9]$$

where the P^1 are the associated Legendre functions and terms of order higher than 4 are not statistically justified by the data. A model independent analysis of these data in terms of amplitudes and phases of the matrix elements in not possible. Simplifying assumptions to connect these quantities to the 9 observables provided by the experiment are however possible. Even if only E1 and E2 radiation is assumed, the number of amplitudes is 11 and 10 relative phases are needed.In the assumption of only no spin-flip E1 and E2 transitions, the amplitudes reduce to 4 and the relative phases to 3. The relative phase between waves having the same j is found very close to 0 and the phase between E1 and E2 radiation around 70-80 deg [19]. But the E2 strength extracted in this simplified analysis [19] was anomalously large, of the order of 12% of the total cross section . Nevertheless, from this analysis, the indication of zero phase difference between waves of equal j and also the indication of the influence of the D state upon the a_2 coefficient, allows us to perform a

more complete analysis of the revised data set assuming one $s = \frac{1}{2}$ E1 term, one $s = \frac{1}{2}$ E2 term and one $s = \frac{3}{2}$ E1 term giving three amplitudes and two phases (indicated by $^{2s+1}\ell$ and Φ_{2s+1}) to be determined. Here ℓ and s refer to the orbital angular momentum and the spin of the entrance channel. The quantities are related through the equations:

$$
\begin{aligned}
1.0 &= 6(^2p)^2 + 6(^4p)^2 + 10(^2d)^2 \qquad \text{for normalisation} \\
a_1 &= 20.78^2p^2d\cos(\phi_{^2d} - \phi_{^2p}) \\
a_2 &= -6.0(^2p)^2 + 7.14(^2d)^2 + 2.87(^4p)^2 \\
a_3 &= -20.78^2p^2d\cos(\phi_{^2d} - \phi_{^2p}) \qquad [1-10] \\
a_4 &= -17.14(^2d)^2 \\
b_1 &= 6.79^4p^2d\sin(\phi_{^4p} - \phi_{^2d}) \\
b_2 &= 3.924^2p^4p\sin(\phi_{^4p} - \phi_{^2p}) \\
b_3 &= 4.524^4p^2d\sin(\phi_{^4p} - \phi_{^2d}) \\
b_4 &= 0.0
\end{aligned}
$$

It should be noted that both $s = \frac{1}{2}$(E1) and $s = \frac{3}{2}$(E2) strengths affect the a_2 coefficient, which would became $a_2 = -1$ for pure $s = \frac{1}{2}$(E1). The results obtained between 10.83 and 16.12 MeV show the dominance of $s = \frac{1}{2}$(E1) (amounting to 93-95% of the total cross section) with a 3-5% contribution from spin-flip E1 and a 2-3% contribution from E2 radiation. This latter value is in agreement with a similar one found by Skopik et al.[20] and confirmed by the theoretical calculations of Aufloger and Drechsel [5].

The importance of capture in channel spin $\frac{3}{2}$ is reinforced by King et al. [14] by a comparison of polarized deuteron and proton capture to ^{3}He at the same $E_x = 6$ MeV excitation energy. For $^2\mathrm{H}(\vec{p},\gamma)^4\mathrm{He}$ the measured quantities and their decomposition in Legendre polynomials are

$$
\begin{aligned}
\sigma_p(\vartheta) &= \sigma_{pu}[1 + PA_p(\vartheta)] \\
\sigma_{pu} &= A_0\left[1 + \sum_k a_k P_k(\cos\vartheta)\right] \qquad [1-11]
\end{aligned}
$$

where N_+ (N_0) is the number of counts recorded with polarized (unpolarized) beam, Q_+ (Q_0) is the integrated beam charge and P is the beam polarization.

$$A_p(\vartheta) = \frac{1}{P}\left[\frac{N_+ Q_0}{N_0 Q_+} - 1\right]$$

$$A_p(\vartheta)\sigma_{pu}(\vartheta) = A_0 \sum_{k=1} b_k P_k^1(\vartheta)$$

For the $^1\mathrm{H}(\vec{d},\gamma)^3\mathrm{He}$ the same quantities are expressed by

$$\sigma_d(\vartheta) = \sigma_{du}(\vartheta)\left[1 + \frac{3}{2} P A_d(\vartheta)\right]$$

$$\sigma_{du} = A_0\left[1 + \sum_k a_k P_k(\cos\vartheta)\right] \qquad [1-12]$$

$$A_d(\vartheta) = \frac{2}{3}\frac{1}{P}\frac{r-1}{r+1} \quad \text{where} \quad r^2 = L_+ R_- / L_- R_+$$

$$\frac{3}{2} A_d(\vartheta)\sigma_{du}(\vartheta) = A_0 \sum_k \iota_k P_k^1(\vartheta)$$

The quantity that is very sensitive to the presence of the $s = \frac{3}{2}$ case of the reaction channel spin is

$$\frac{b_k(d,\gamma)}{b_k(p,\gamma)} = -\frac{3}{2}\frac{W[1s\,1s';(1/2),1]}{W[(1/2)\,s\,(1/2)\,s';1\,1]} \qquad [1-13]$$

W being the Wigner's symbols. The b_1 coefficient is non-zero for the p on d data thus beeing attributable to (E1,E2) + (E1,M1) interferences to first order. Transition matrix elements are computed using g.s. wave functions generated from Fadeev type equations with separable interactions and continuum wave functions from an optical potential that describes the elastic scattering from protons [19]. A D state component in the g.s. wave function is included and inclusion of 1 to 8% of M1 strength, predominantly of $s = \frac{3}{2}$ type gives 90% confidence limits on the fits performed.

At higher energies ($E_p = 1.56$ MeV, Didelez et al. [11] measured the angular distribution of emitted photons with a lead glass detector in coincidence with recoiling ^{3}He nuclei and found a non negligible $\epsilon = 0.045$ value for the usual Fetisov expansion [1-3], indicating the presence of (M1,M2) interference at these energies. Transition matrix elements

are computed assuming direct capture, Born plane wave approximation, and treating the electromagnetic field and incident proton non-relativistically. The use of other different types of radial wave functions for the ^{3}He final state (Gaussian, double Gaussian, Irving, Irving-Gunn, Gibson) gives poor matching of the computed angular distributions to the experimental points, with particularly insensitivity to the choice of helium wave functions. The use of a distorted wave born approximation does not change the shape of the computed angular distributions as satisfactorily, while inclusion of the spin part can change height and position of the maximum ($\approx$ 45 deg) in the right direction . Semidirect mechanism and inclusion of mesonic effects is claimed to be the correct ingredient for the explanation of the observed $d\sigma/d\Omega$ behaviour.

Polarized protons from 200 to 500 MeV have been used by Cameron et al. [21] and angular distributions and analyzing powers have been determined. The tendency for radiative capture to give higher cross sections than photodisintegration experiments with the consequent implication of time reversal invariance violation [22], is rejected by the results of this extensive experiment at all energies involved. Nevertheless the spread in the different sets of direct photodisintegration data cross section is the major source of complication in the global interpretation of the data. The angular distribution at 200 MeV seems well reproduced by the model calculation of Prats [23] who includes in the reaction amplitude contributions of quasi-deuteron in addition to ordinary deuteron and proton Born terms. A distorted wave Born approximation calculation of Fearing [24] compares favourably to the experimental points, when distortion is included for the incoming proton and the ^{3}He wave function is adjusted to reproduce the electromagnetic form factor. A microscopic calculation from Laget [25] is fitted to the the same data showing again the need of an operator that includes meson exchange currents. The analyzing power is not as well reproduced but a better fit is obtained by the inclusion of a nucleon rescattering diagram corresponding to the quasi deuteron contribution.

1-3 Polarized and unpolarized p and d capture to ^{4}He

Direct photonuclear reactions [1] through the various possible channels (γ,p), (γ,n), (γ,pn), (γ,dd), $(\gamma,2n2p)$ and polarized or unpolarized proton radiative capture to ^{4}He

cover the range of excitation energies up to about 60 MeV, with proton capture itself covering the range from 20 to 43 MeV.

Perry and Bame [26] covered from $E_x = 19.9$ to $E_x = 24.5$ MeV providing a cross section at 90 deg that shows a steady increase from threshold to a maximum of $\approx 10\,\mu$b/sr at $E_p = 4$ MeV and then a slow decrease. This is in general agreement with that calculated using the principle of detailed balance from photodisintegration of ^{4}He and the excitation function behaviour is in fair agreement with the calculation of Gunn and Irving [27]. Angular distributions were produced and expanded in terms of the usual Fetisov expansion [1-3] where they retain the $\sin^2\vartheta$ and the $\sin^2\vartheta\cos\vartheta$ terms only and analyzed in terms of the possible interaction states of ^{4}He which might be formed in the reaction. These are summarized in table 2.

TABLE 2

^{4}He *possible interaction states*

$s_p\, s_T$	S	ℓ_p	Transition	Type	Ang. Distr.
u-d	0	0	$^1S_0 \rightarrow {}^1S_0$	Forbid.	
u-d	0	1	$^1P_1 \rightarrow {}^1S_0$	E1	$\sin^2\vartheta$
u-d	0	2	$^1D_2 \rightarrow {}^1S_0$	E2	$\sin^2\vartheta\cos^2\vartheta$
u-u	1	0	$^3S_1 \rightarrow {}^1S_0$	M1	Isotropic
u-u	1	1	$^2P_0 \rightarrow {}^1S_0$	Forbid.	
u-u	1	1	$^2P_1 \rightarrow {}^1S_0$	E1	$1+\cos^2\vartheta$
u-u	1	2	$^2D_1 \rightarrow {}^1S_0$	M1	$5-3\cos^2\vartheta$
u-u	1	2	$^2D_2 \rightarrow {}^1S_0$	E2	$1-3\cos^2\vartheta+4\cos^4\vartheta$

Their angular distribution results in predominantly a $\sin^2\vartheta$ indicating that the reaction proceeds mainly by capture of p wave protons. The β coefficient that increases with energy from $\beta = 0.01$ at $E_p = 0.5$ MeV to $\beta = 0.06$ at $E_p = 5.8$ MeV may be attributed to capture of d wave protons. The states formed by the capture of a p wave proton ($^1P_1$) and of a d wave proton ($^1D_2$), interfere in their decay in agreement with the observed angular distribution shape. The increase of the asymmetry coefficient is accounted for by the barrier penetration.

Gardner and Anderson [28] extended the (p,γ) measurements from $E_x = 24.7\,\text{MeV}$ to $E_x = 26.7\,\text{MeV}$. Their absolute cross section matches the Perry and Bame data [26] and does not show evidence of sharp resonances as found in the inverse photonuclear reaction. Angular distribution analysis requires only the first two terms of equation [1-3] and confirms a trailing trend for the asymmetry coefficient that raises up to $\beta \approx 0.1$ at $E_p = 9.2\,\text{MeV}$. Poorer angular distribution fits at the higher proton energies were interpreted as an indication of a possible presence of an isotropic triplet component neglected in the Fetisov expansion.

Almost the same range ($E_x = 22.8$ to $E_x = 28.1\,\text{MeV}$) was covered by Gemmel and Jones [29]. The 45 deg, 90 deg and 135 deg yield curves slowly decrease with energy. Analysis of the angular distributions gave a δ coefficient consistent with zero. The asymmetry term β is in agreement with that of Perry and Bame and confirms that the radiation is essentially E1 resulting from the capture of p wave protons into a singlet state with interference between this decay mode and an E2 component following the capture of d wave protons into a singlet state. Since no isotropic component is found, in contrast to the result for direct photonuclear reactions, there is no support for an interaction in a triplet state the result of which would be the emission of M1 radiation following s wave capture.

Meyerhoff et al. [30] measured relative 90 deg cross section and angular distributions from $E_x = 22.1$ to $E_x = 33.3\,\text{MeV}$. After normalisation to the data of Perry and Bame, the cross section at 90 deg results in agreement with previous measurements and seems to reject the hypotesis [31] of energy dependent fine structures in this energy region. From the 0 to 90 deg cross section ratio is deduced the δ coefficient, connected to the other coefficients of [1-3] by the equation

$$\delta = \frac{\sigma(0)}{\sigma(90)}(1+\delta) - (1+\beta+\gamma)\frac{\Omega}{2\pi} \qquad [1-14]$$

where $\Omega(<< 4\pi)$ is the finite solid angle subtended by the detector at $\vartheta = 90\,\text{deg}$. The δ value is not taken equal to zero but is constrained within the range 0.015 -- 0.020. The subsequent development of the angular distribution in terms of the β, γ coefficients

is especially sensitive to the δ value and this is reflected particularly in the γ coefficient which is about 30% lower if δ is assumed equal to zero. If the hypotesis of pure S wave is made for the ^{4}He g.s.,the E1 photodisintegration cross section can be deduced from the 90 deg yield curve via detailed balance and from the equation

$$\sigma_{E1}(\gamma,p) = \frac{8\pi}{3}(1+\delta)^{-1}\sigma_{tot}(90) \qquad [1-15]$$

The E2 cross section can be deduced from the relation:

$$\sigma(E2) = \frac{\gamma}{5}\sigma(E1) \qquad [1-16]$$

but a lower limit can be set when considering the β coefficient alone, viz.

$$\sigma(E2) \geq \frac{1}{20}\beta^2\sigma(E1) \qquad [1-17]$$

These experimental points compare smoothly and favourably with other experimental results and give a rather complete data set for the interpretation of the reaction mechanism up to about 30 MeV excitation energy (the upper limit being imposed by the presence of large neutron background in the angular distributions as collected). The general trend of the angular distributions is compatible with a dominant E1($\Delta S = 0$) radiation, interfering with E2($\Delta S = 0$) radiation, while the term δ is attributed to radiation with $\Delta S = 1$, namely M1. The integrated (γ,p) cross section reaches a maximum value of $\approx 2\mu$b at $E_\gamma = 25$ MeV and then slowly decreases without evidence of any sharp structure. The integrated E2 cross section alone amounts to $\approx 4\%$ of the total cross section and is not resonant. Shell model calculations predict several $2^+(T=0,T=1)$ states in ^{4}He in the neighbourhood of 25 MeV [32] but it is speculated that these states are so broad that no resonant shape is evident in the cross section. The Crone and Werntz interpretation [33] of E1 transitions proceeding via two $T = 1, 1^-$ levels, each being a mixture of $^1P_1$and$^3P_1$ configurations, is compared with the data, but the experimental evidence is not in favour of the lower 1^- state being predominantly $^1P_1$, contrary to the theoretical calculations. The E1-E2 phase difference appears to be constant along the energy range of this experiment and not too different from results at much higher ($E_\gamma = 136$ MeV) energy [34].

An effort to produce accurate absolute cross sections has been made by Calarco et al. [35] who measured simultaneously the 90 deg (p,γ) and the 30 deg (p,p') elastic scattering cross sections at $E_x = 26.1\,\mathrm{MeV}$ and $E_x = 30.0\,\mathrm{MeV}$. Corrections to the total cross section, were performed using the King [36] angular distribution results and the principle of detailed balance. This procedure should have allowed an order of two decrease in absolute uncertainties. It is observed that while the (p,γ) cross sections are all compatible within their statistical uncertainties, the (γ,p) cross sections show somewhat lower average values and larger uncertainties due, it is claimed, to the uncertainties in the absolute flux measurements,and to difficulties in the subtraction of the many-body break-up processes. After careful revision of the entire ensemble of (p,γ) data, a "consensus" cross section for the $^4\mathrm{He}(\gamma,p)^3\mathrm{H}$ reaction, derived from the two precise absolute measurements and all the observations surveyed, is produced and the average (γ,p) cross section between $E_\gamma = 26-30\,\mathrm{MeV}$ is measured to be $1.80\pm0.12\,\mathrm{mb}$. Above 30 MeV the $(\gamma,p)/(\gamma,n)$ ratio is compatible with 1 in all the experiments performed, while below 30 MeV the measured cross sections show discrepancies as large as 100% but tend to cluster around the value of 1.0 mb. Together with the previous result this would give $\sigma(\gamma,p)/\sigma(\gamma,n) = 1.8$, implying a $T = 0/T = 1$ isospin mixing in the excited ^{4}He wave function, of the order of 0.14 ± 0.02, definitely exceeding the predictions from a pure Coulomb effect.

Data from McBroom et al. [37] were not included in the survey of Calarco [35]; certainly these would have changed to some extent the overview. These points, measured from $E_x = 15$ to $E_x = 43\,\mathrm{MeV}$, were calibrated according to the $^3\mathrm{H}(p,p')^3\mathrm{H}$ reaction cross section but the reported values sit some 20-25% above the "consensus curve", though still compatible with it if one considers the experimental errors. Angular distributions were measured from $E_p = 13$ to $E_p = 30\,\mathrm{MeV}$ and their deconvolution is performed in terms of Legendre polynomial expansion [1-8]. The indications are that the $^3\mathrm{H}(p,\gamma)^4\mathrm{He}$ cross section should proceed through an E1 mechanism with some E2 mechanism present, as indicated by the fact that there is no need to include terms of order higher than 4 in the angular distribution expansion. As already seen, in the channel spin representation, there will be two E1 terms with spin $S = 0\,\mathrm{or}\,1$ $({}^1P_1, {}^3P_1 \leftarrow {}^1S_0)$ as well as two E2 terms with spin $S = 0\,\mathrm{or}\,1$ $({}^1D_2, {}^3D_2 \leftarrow {}^1S_0)$. If $S = 1$ the E1 amplitude $({}^3P_1 \leftarrow {}^1S_0)$ is small, so

that then $a_1 = -a_3$ and, if $S = 2$ the E2 amplitude ($^3D_2 \leftarrow {}^1S_0$) is small so that then $a_1 = -a_3$ and $1 + a_2 + a_4 = 0$. This is in fact the experimental indication although the measured angular distributions are not sensitive to small percentages of $^3P_1$ or $^3D_2$ states in the entrance channel.

Polarized proton capture has been reviewed by Weller and Roberson [38] at excitation energies from 24 to 32 MeV, and offers remarkable insight into the different strengths of the triplet and singlet E1 or E2 amplitudes. The four contributing complex T-matrix elements are expressed as

$$T_{10} = {}^1P_1 e^{i\phi_{1P}}(\mathrm{E1}) \qquad T_{11} = {}^3P_1 e^{i\phi_{3P}}(\mathrm{E1}) \qquad [1-18]$$

$$T_{20} = {}^1D_2^{i\phi_{1D}}(\mathrm{E2}) \qquad T_{21} = {}^3D_1 e^{i\phi_{3D}}(\mathrm{E2})$$

The experiment provides coefficients $A_0, a_1, \ldots, a_n$ [1-8] and $b_1, \ldots, b_n$ [1-9]; the number of unknowns is only the four amplitudes and the three relative phases. The possible presence of an M1 component will affect only a_1 and b_1 so one can proceed to a fitting strategy that excludes a_1 and b_1 from the computation of the seven unknowns. With the normalisation condition $0.75({}^1P_1^2 + {}^3P_1^2) + 1.25({}^1D_2^2 + {}^3D_2^2) = 1.0$ the results are that $^1P_1$ remains almost constant in the energy range explored, while $^3P_1$ smoothly increases with energy and accounts for about 1.5% of the total E1 cross section. The D amplitude follows a similar trend with the E2 triplet being the same size as the E2 singlet at $E_x = 28$ MeV, which is rather surprising. Total E1 and E2 cross sections, measured in this experiment and normalized to the values of Meyerhoff et al. [30] (by $\sigma_{tot}(p,\gamma) = \frac{8}{3}\pi\sigma(90)$), agree rather well with previous measurements [29]. Particular attention was dedicated to the b_2 coefficient. The E2 contribution to b_2 should configure through the product of the $S = 0$ and $S = 1$ E2 T-matrix elements and these can be reasonably neglected. Then b_2 can be written in terms of the E1 amplitudes only as

$$b_2 = -0.07\,{}^1P_1\,{}^3P_1 \sin(\Phi_{1P} - \Phi_{3P}) \qquad \text{with } ({}^3P)^2 + ({}^1P)^2 = 1.0 \qquad [1-19]$$

resulting in a value of 0.059 ± 0.09 that is well reproduced if one considers a continuum

shell model calculation [39] which leads to the conclusion that b_2 depends on the spin-orbit odd component of the effective nuclear force.

1-4 Symmetric ^{4}He break-up

Also relevant in its importance is the ^{4}He break-up into two deuterons observed by the $^4\mathrm{He}(\gamma,d)D$ and its inverse reaction $^2\mathrm{H}(d,\gamma)^4\mathrm{He}$. Deuteron-deuteron radiative capture is largely determined by strong selection rules. First the identity of the two particles permits only states having L and S with the same parity to be formed in the entrance channel. The electromagnetic multipole transitions expected after application of this selection rule and the predicted angular distributions are summarized in Table 3.

TABLE 3

Expected $^2\mathrm{H}(d,\gamma)^4\mathrm{He}$ *angular distributions*

Ent. ch. S	Ent. Ch. L	Ent. Ch. J^π	Transition	Ang. Distrib.
0	0	0^+	$^1S_0 \rightarrow {}^1S_0$	forbidden
0	2	2^+	$^1D_2 \rightarrow {}^1S_0$ E2	$\sin^2\vartheta\cos^2\vartheta$
1	1	0^-	$^1P_0 \rightarrow {}^1S_0$	forbidden
1	1	1^-	$^3P_1 \rightarrow {}^1S_0$ E1	$1+\cos^2\vartheta$
1	1	2^-	$^5P_2 \rightarrow {}^1S_0$ M2	$1+\cos^2\vartheta$
1	3	2^-	$^5F_2 \rightarrow {}^1S_0$ M2	$1+\cos^2\vartheta-5\cos^4\vartheta$
2	0	2^+	$^5S_2 \rightarrow {}^1S_0$ E2	isotropic
2	2	0^+	$^1D_0 \rightarrow {}^1S_0$	forbidden
2	2	1^+	$^3D_1 \rightarrow {}^1S_0$ M1	$1+\cos^2\vartheta$
2	2	2^+	$^5D_2 \rightarrow {}^1S_0$ E2	$2+3\sin^2\vartheta+12\sin^4\vartheta$

Some of the dacay modes would involve $J=0 \rightarrow J=0$ transitions and are therefore forbidden. Isospin selection rules, related to the basic T_3 dependence of the interaction Hamiltonian, determine that a γ transition must have $\Delta T = 0,1$ but no $T=0 \rightarrow T=0$ decay can take place. Looking only at the isospin dependence of the E1 operator, the selection rule is such that $\Delta T = 0,1$ if T_3 is different from 0 but $\Delta T = 1$ only, if $T_3 = 0$. Consequently in $N=Z$ nuclei ($T_3=0$) and for the most probable T values (0 or 1) for excited states in such nuclei, E1 transitions between two $T=0$ levels or two $T=1$ levels

are forbidden. In $D(d,\gamma)^4$He both entrance and exit channels have $T = 0$ so that E1 transitions are ruled out. There are no selection rules deduced by magnetic operators. However in the case of $T = 0 \rightarrow T = 0$ transitions, M1 is reduced by a factor of 100 due to the form of its isospin dependence. Therefore the $^3D_1 \rightarrow {}^1S_0$ is basically ruled out from table 3. The d capture should therefore be largely dominated by transition $^1D_2 \rightarrow {}^1S_0$ (E2), with other E2 or M2 transitions expected to be still negligible in comparison to the former. This picture is independently confirmed when we assume a central nuclear force. In this case the deuteron will be in a pure ^3S state and ^{4}He in a pure ^1S state. In this hypothesis L and S are good quantum numbers and it can be shown that, for $L = 0$ states like the ^{4}He $^1S_0$, electric type transition operators act only on the ordinary space, while magnetic type operators act only on spin space, and have a form which does not change the spin value. For the S states the magnetic operators rule out spin-flip transitions, and that excludes M2 transitions from Table 1.

Zurmhule et al. [40] first observed the $D(d,\gamma)^4$He reaction at deuteron energies $E_d =$ 0.8, 1.35 and 1.25 MeV at three different angles 0 , 45 and 90 deg. Only a qualitative deduction could be made from this work and this was to infer an upper limit to the 90 deg cross section of the order for example of $0.5\,10^{-33}\,\mathrm{cm}^2/\mathrm{sr}$ at 1.35 MeV as opposed to a value of $2.0\,10^{-33}\,\mathrm{cm}^2/\mathrm{sr}$ at 45 deg. This was interpreted as due to the effect of the dominant $^1D_2 \rightarrow {}^1S_0$ E2 transition.

Meyerhoff et al. [41] extended the measurements from $E_d = 6$ to $E_d = 9$ MeV measuring the yield curve at 135 deg and a complete center of mass angular distribution at 10 MeV. Their angular distribution is found to be compatible with the expected E2 behaviour i.e.

$$\sigma(\vartheta) \propto \sin^2\vartheta\cos^2\vartheta \qquad [1-20]$$

and the total cross section is therefore computed converting the 135 deg point through detailed balance

$$2[2I(^4\mathrm{He})+1]k_\gamma^2\frac{d\sigma(\gamma,d)}{d\Omega} = [2I(^3\mathrm{H})+1]k_d^2\frac{d\sigma(d,\gamma)}{d\Omega} \qquad [1-21]$$

where $I(^4\mathrm{He}) = 0$ and $I(^3\mathrm{H}) = 1$ and k_d and k_γ are the wave numbers of the photon and deuteron in their respective reactions. Assuming a $\sin^2\vartheta\cos^2\vartheta$ behaviour over the range explored, the total cross section takes the value

$$\sigma(\gamma,d) = \frac{4\pi}{15}\left[\frac{d\sigma(\gamma,d)}{d\Omega}\right]_{\vartheta=\vartheta_0}(\sin\vartheta_0\cos\vartheta_0)^{-2} \qquad [1-22]$$

and the results are compared with photodisintegration values in an attempt to establish the presence of a broad $2^+\,T=0$ state in ^{4}He at ≈ 30 MeV excitation energy. A compilation of resonance parameters computed from $(\gamma,d)\,(d,\gamma)$ and (p,n) reactions does not compare to a Breit Wigner resonance factor [33] but closely resembles the trend expected of a direct capture process.

More detailed (d,γ) data on the deuteron were collected by Poutissou and Del Bianco [42] from $E_d = 4$ to $E_d = 12.5$ MeV. Complete angular distributions were measured at $E_d = 6.05, 8.96$ and 11.67 MeV. If a Legendre polynomial expansion [1-2] is used, then a pure E2 transition corresponding to $\sigma(\vartheta) \propto \sin^2\vartheta\cos^2\vartheta$, would give $A_2 = 0.712$ and $A_4 = -1.694$, not too different from the experimental findings of this (Table 4) and other experiments.

TABLE 4

Legendre polynomial expansion coefficients

E_d(MeV)	A_2	A_4
6.05	0.814 ± 0.101	-1.661 ± 0.148
8.96	0.683 ± 0.114	-1.590 ± 0.165
11.67	0.831 ± 0.260	-1.287 ± 0.372

The poorer agreement at $E_d = 11.6$ MeV is ascribed to the poorer statistics obtained in the measured γ-ray spectra. This would substantiate the dominance of the E2 $(^1D_2 \rightarrow {}^1S_0)$ transition at these energies, as expected from the stringent selection rules. If anywhere small percentages of E1 $(^3P_1 \rightarrow {}^1S_0)$ or E2 $(^5S_2 \rightarrow {}^1S_0)$ transitions were present, the angular distribution should assume the form

$$\frac{d\sigma}{d\Omega} = A[\sin^2\vartheta\cos^2\vartheta + B(1+\cos^2\vartheta) + C] \qquad [1-23]$$

But B and C values are here found of the same order as their statistical errors, and unpolarized deuteron capture does not enaable us to disentangle multipolarities different from the main E2 component.

Low energy cross sections and angular distributions were measured by Weller et al. [43] starting from $E_d = 0.7\,\mathrm{MeV}$ up to $E_d = 4.5\,\mathrm{MeV}$ and analyzed together with data from a similar experiment [42]. The aim was to investigate the D-state effects upon the total cross section and angular distributions. The E2 transition from the $^5S_2$ scattering state to the final $^5D_0$ component of the ^{4}He g.s., should be more and more evident as the energy decreases, since it has to compete with the dominant E2 transition from the $^1D_2$ scattering state. At low energies we have the advantage of the centrifugal barrier that tends to suppress states with $L \neq 0$ and enhance consequently the $L = 0$ scattering state $^5S_2$. If one neglects, as it is legitimate at these energies, $J = 2$ mixing amongst the $^1D_2$, $^5S_2$, $^5D_2$ and $^5G_2$ scattering states,one expects a $\sigma(\vartheta) \propto \frac{E_a^5}{p} T(\vartheta)$, where p is the incident deuteron c.o.m. momentum and the angular dependence is

$$T(\vartheta) = (|A|^2 + \frac{2}{7}|C|^2)\sin^2\vartheta + 2|B - \frac{C}{2\sqrt{14}}(3\cos^2\vartheta - 1)|^2 + \frac{9}{28}|C|^2(1 - \cos^4\vartheta)$$
$$+ \frac{|D|^2}{126}(17 + 60\cos^2\vartheta - 45\cos^4\vartheta) + \frac{2}{3\sqrt{14}}\mathrm{Re}(BD^*)(-35\cos^4\vartheta + 30\cos^2\vartheta - 3)$$
$$+ \frac{2}{21}\mathrm{Re}(CD^*)(25\cos^4\vartheta - 24\cos^2\vartheta + 3) \qquad [1-24]$$

that in the absence of D state in the ^{4}He wave function, reduces ($B = C = 0$) to the well known $\sin^2 2\vartheta$ expression. Measured angular distributions show a significant departure from the latter behaviour and are sensitive to the asymptotic D state to S state ratio ρ which is found in the range $-0.25 < \rho < -0.15$. The ratio of the 90 deg to the 135 deg cross section $R = \sigma(\pi/2)/\sigma(3\pi/4)$ is rapidly increasing when $E_d < 4\,\mathrm{MeV}$ and this is found compatible with a ρ value of -0.2. The total cross section computed in this experiment is also compared to other experimental results and shows great sensitivity to the assumed ρ value at least below 1 MeV, as does the R ratio. D state percentages between 5 and 13% are deduced from the ρ results.

Polarized projectile captures are intrinsically much richer in information. Two experiments, very similar in their techniques, have been performed at $E_{\vec{d}} = 9.7\,\text{MeV}$. Weller et al. [44] consider the expansion of the c.m. cross section in terms of the beam polarization tensor moments $T_{kq}(\vartheta)$ as:

$$\sigma(\vartheta,\varphi) = \sigma_u(\vartheta)[1 + 2it_{11}iT_{11}(\nu) + t_{20}T_{20}(\vartheta) + 2\text{Re}t_{21}T_{21}(\vartheta) + 2\text{Re}t_{22}T_{22}(\vartheta)] \quad [1-25]$$

Taking the spin symmetry axis along the beam momentum direction, reduces to negligible amounts the contributions of it_{11}, t_{21} and t_{22}. Choosing two different polarizations, namely $t_{20}^{(1)} = P/\sqrt{2}$ and $t_{20}^{(0)} = -2/\sqrt{2}P$, where P is the percentage beam polarization, makes

measurable the tensor T_{20} given by:

$$T_{20}(\vartheta) = \frac{\sqrt{2}}{P}\frac{Y_1(\vartheta) - Y_0(\vartheta)}{2Y_1(\vartheta) + Y_0(\vartheta)} \quad [1-26]$$

The cross section $\sigma(\vartheta)$ is obviously always measurable but, while this gives results compatible with a $\sin^2 2\vartheta$ behaviour consequent on the dominant ${}^1D_2 \rightarrow {}^1S_0$ E2 capture mechanism, the observed T_{20} tensor result is isotropic at a value of -0.22 ± 0.014. Taking into consideration only E2 processes and assuming the presence of a finite D state probability in the g.s. wave function of ${}^4\text{He}$, requires including the following E2 modes in the capture process: ${}^5S_2 \rightarrow {}^5D_0$, ${}^5D_2 \rightarrow {}^5D_0$, ${}^5G_2 \rightarrow {}^5D_0$, still fulfilling the requirement of the selection rules previously mentioned. Neglecting products of two $S = 2$ terms that should give absolutely negligible contributions to the cross section, one can define the quantities

$$\begin{aligned} A &= {}^2D_2\cos(\phi_{{}^2D_2 - {}^5S_2}) \\ B &= {}^2D_2{}^5D_2\cos(\phi_{{}^2D_2 - {}^5D_2}) \\ C &= {}^2D_2{}^5G_2\cos(\phi_{{}^2D_2 - {}^5G_2}) \end{aligned} \quad [1-27]$$

and formally compute the analyzing powers as

$$iT_{11} = 0$$

$$T_{20} = +0.497A - 0.594B + 0.797C$$
$$T_{22} = -0.203A - 0.242B - 0.055C \qquad [1-28]$$
$$T_{21}(\vartheta) = (-0.145A + 0.087B + 0.155c)(2.8 - 5.6\cos^2\vartheta)/\sin(2\vartheta)$$

The T_{20} has been found to be isotropic as expected, and its value has been successfully fit even with a simple model calculation. This assumes direct capture followed by E2 radiation to a ground state formed from two Wood-Saxon potentials binding the two point-like deuterons to 23.84 MeV, one having $L = 0$ and one having $L = 2$. The correct percentage to fit the experimental value had 4.8% admixture of $L = 2$ strength, thus showing the sensitivity of T_{20} to D state presence in the g.s. of ^{4}He.

Mellema et al. [45] used the expansion of the differential cross section in terms of the Cartesian analyzing powers:

$$\sigma(\vartheta,\varphi) = \sigma_u(\vartheta,\varphi)[1 + \frac{3}{2}p_y A_y(\vartheta) + \frac{1}{2}p_{yy}A_{yy}(\vartheta)] \qquad [1-29]$$

and performed four different measurements with $p_y = \pm 0.3$ and $p_{yy} = \pm 0.9$, thus determining the unpolarized cross section σ_u, the analyzing power $A_y(\vartheta)$ and the vector analyzing power $A_{yy}(\vartheta)$ for which expansion coefficients have been determined according to

$$\sigma_u(\vartheta) = A_0[1 + \sum a_l P_l(\cos\vartheta)]$$
$$\sigma_u(\vartheta)A_y(\vartheta) = \frac{2}{3}A_0 \sum b_l P_l^1(\cos\vartheta) \qquad [1-30]$$
$$\sigma_u(\vartheta)A_{yy}(\vartheta) = 2A_0 \sum c_l P_l^2(\cos\vartheta)$$

where P_l^1 and P_l^2 are associated Legendre functions. The angular distribution of the differential cross section deviates only slightly from the expected $\sin^2(2\vartheta)$ form. The product $\sigma_u A_y$ should have all the odd coefficients equal to zero in the case of a pure E2 transition; therefore the presence of significant b_1 and b_3 coefficients suggests possible interferences of the main E2 mode with either E1 or M2 amplitudes. Furthermore the relatively large value

of $A_{yy}(\vartheta)$ can only arise from interference between E1 or M2 amplitudes. No calculation on D state percentages is reported.

Data from various experiments have been reviewed by Weller [46], in connection to the measured quantities $\sigma(\vartheta)/A_0$, $T_{20}(\vartheta)$, $iT_{11}(\vartheta)$, $T_{22}(\vartheta)$ and $\sigma(\vartheta)A_y(\vartheta)/A_0$. It is observed that there is a large superposition $(6-7\%)$ between the "physical" ground state of ^{4}He and a two deuteron like configuration that should be largely responsible for the expected D state admixture. As said already four amplitudes are involved in pure E2 transitions: $^5S_2 \rightarrow {}^5D_0$ $^5D_2 \rightarrow {}^5D_0$ $^5G_2 \rightarrow {}^5D_0$ $^2D_2 \rightarrow {}^2S_0$. The angular distributions, in which states of different channel spin are not interfering, are expected to be little sensitive to $S = 2$ terms. On the co ntrary a large amount of information is available from the tensor and vector analyzing powers expressed by equation [1-28]. Assumption of pure E2

radiation leads to the result that, if second order terms (products of two $S = 2$ terms) are neglected, then T_{20} and T_{22} are isotropic, with departure from isotropy expected at 0, 90 and 180 deg, where the dominant E2 transition is going to zero and small second order contributions can play a significant role. When transition matrix elements are computed constructing the ^{4}He g.s. wave function in a two deuteron like form, by means of a pair of Wood Saxon potentials, which bind the two deuterons to 23.84 MeV with $L = 0$ and $L = 2$ respectively, making use of the Siegert form of the E2 spin independent operator, and including second order contributions, the fits to the data are remarkably good if 5% D state admixture is included in the ^{4}He g.s. wave function. The inclusion of M2 transition matrix elements due to capture in the $^3P_2$ and $^3F_2$ continuum states, followed by decay to the $^1S_0$ component of the g.s. wave function, produces

also tremendous effects on the $A_{yy} = 2/\sqrt{3}T_{11}$ observable, while slightly improving the fit to other quantities, specially around the critical angles 0, 90 and 180 deg. The M2 contribution used represents $\approx 3\%$ of the total integrated capture cross section . Cartesian tensor analyzing power A_{yy} and spherical tensor analyzing power T_{kq} are related through

$$A_{yy}(\vartheta) = -\frac{1}{\sqrt{2}}T_{20}(\vartheta) - \sqrt{3}T_{22}(\vartheta) \qquad [1-31]$$

which, using the previous hypotheses, is equal to $0.839B - 0.468C$ i.e. independent from

the A that represents the $^2D_2 \rightarrow {}^5S_2$ interference term. Phase shift analysis shows that S waves are largely distorted in the entrance channel and A_{yy} should be insensitive, within this simplified model, to such effects. A significant advance in the correct interpretation of data is the use [47] of variational wave functions having a pair correlation operator containing central tensor and spin correlations, and the use of an Hamiltonian incorporating three nucleon interactions. Two realistic two body interactions have been used, having a D state parameter D_2 respectively at -0.16 and $-0.24\,\mathrm{fm}^2$. When continuum wave functions were extracted including distorsion and E1, M1, E2, M2 multipoles in the long wavelength approximation were employed, a reasonable description of A_y was obtained when either M1, E2 or both were included. The results on A_{yy} are already good if one uses only E2 and either values of D state parameter, but improve to fit the slight asymmetry in the experimental data if inclusion of multipoles other than E2 are included. Finally Weller draws attention to the behaviour of A_{yy} and A_y with energy, that are both constant at a value of 0.07 for E from 3 to 12 MeV and linearly increasing from -0.2 to ≈ 0, also from 3 to 12 MeV. This behaviour seems to be reproduced by the preliminary results of the same model used to reproduce so nicely A_y and A_{yy} at 10 MeV.

1-5 Radiative capture at and above the GDR region in ^{8}Be

Since the beginning of experimental investigations of proton radiative capture reactions, the $^7\mathrm{Li}(p,\gamma_0)^8\mathrm{Be}$ process enjoyed great attention because the high Q value of this reaction (+17.2 MeV) allowed cross section measurements in the GDR region even at low projectile energies, and because of the interest in establishing, through the detailed balance rule [1-21], the trend of the direct photonuclear $^8\mathrm{Be}(\gamma,p)^7\mathrm{Li}$ cross section that is impossible to measure in nature due to the spontaneous break-up of ^{8}Be into two α particles.

Gemmel et al. [48] measured the reaction yield in the range from $E_p = 4$ MeV to $E_p = 7.7$ MeV on two different ^{7}Li targets for the purpose of identifying eventual structures in the yield curves and of calibrating their gamma spectrometer. A 145 keV thick target (to 4.8 MeV) gives a yield curve which rises from lower proton energies, where it matches points from Bair et al. [49], and then flattens off above $E_p = 6.0$ MeV as could be expected as a consequence of large pile-up induced distortions. A thicker target (280 keV), run

at a reduced current of 0.05 μA gives a resonant yield curve having a maximum value of 0.14 μb centered at $E_p = 5.8$ MeV or at an excitation energy of 23.3 MeV in ^{8}Be. There is no evidence of structures in the cross section within the limits of statistics and their spectrometer resolution.

Extension to higher energies was performed by Perry et al. [50] using the 12 MeV van de Graaff of Rice University. Decay of the highly excited ^{8}Be nucleus to the 0^+ g.s. and to the 2^+ $E_x = 2.9$ MeV first excited state, were in evidence in this experiment, although gamma rays from the two transitions could not be resolved. A 90 deg yield curve was produced therefore for the sum of the two peaks. The giant resonance is centered at $E_p = 7.3$ MeV and is about 5 MeV wide. Its asymmetric shape suggests some structure with a possible second peak at about $E_p = 6$ MeV. The main peak corresponds to a state at 23.6 MeV in ^{8}Be, while the other minor peak should correspond to a state near 22.5 MeV. No change in the ratio of the γ_0 and γ_1 gamma peaks over the whole energy range was observed. All angular distributions measured up to 7 MeV, where neutron background started to noticeably distort the collected spectra, were isotropic within 25% and when expanded in terms of $\sigma(\vartheta) = 1 + a_1 P_1 + a_2 P_2$ gave a_1 coefficients from 0.0 to 0.09 and a_2 coefficients from 0.04 to 0.17. This is explainable assuming s wave proton capture by the ^{7}Li core in its $\frac{3}{2}^-$ g.s. This leads to 1^- or 2^- compound states that can decay to both the ground and first excited state in ^{8}Be. An E1 transition should largely dominate the process as shown by the smallness of the a_1 coefficient that is in principle due to (E1,E2) or (E1,M1) interference. The differential cross section at 90 deg and $E_p = 3$ MeV was measured to be 0.043 mb/sr for the sum of the two peaks.

A slightly better separation of the γ_0 and γ_1 peaks was achieved by Mitchell and Taylor [51], who explored the region between $E_p = 2.5$ and $E_p = 9$ MeV providing the 90 deg yield curve and few angular distributions both for separated and combined γ_0, γ_1 cases. The γ_0 yield shows a broad maximum at $E_p = 5$ MeV with a width of about 5 MeV. The γ_1 yield curve increases up to 7 MeV where it starts flattening. At higher energies, the separation of the two components, is doubtful, due to the large intrinsic width (≈ 1 MeV) of the 2.9 MeV 2^+ state in ^{8}Be, but the combined yield curve confirms the structure at 6

and 7.3 MeV already observed by Perry et al. [50]. The shape of the γ_1 yield, although not completely collected across the resonance, seems compatible with a width of about 8 MeV. The great width observed for these peaks prevents measurement with sufficient accuracy of their separation in energy. Nevertheless a value of 2.0 ± 0.5 MeV, not too different from the excitation energy of the first state in ^{8}Be,

is observed similar to what is deduced in other (p,γ) reactions on ^{27}Al and ^{11}B. This gives evidence of possible giant resonances, built upon excited states, an hypothesis that has been further clarified and to which we will come back considering the large amount of data collected so far for the ^{12}C system. Angular distributions have been fitted by the expansion [...] and show isotropy within 30%, requiring the inclusion of only small percentages of P_1. Assuming dominance of E1 excitation, only 1^-, 2^- and 3^- states can be excited through electric dipole absorption by the 0^+ g.s. and the 2^+ $E_x = 2.9$ MeV states in ^{8}Be. So both s or d capture can contribute to the population of these levels in (p,γ) capture when coupled to the $J^\pi = \frac{3}{2}^-$ g.s. of ^{7}Li, but the s wave capture hypothesis is the simplest one although d wave admixture is not completely ruled out by these unpolarized beam results.

More information was obtained on the nature of γ_0 and γ_1 transitions in ^{8}Be by Reay et al. [52] at proton energies from about 4.3 MeV to 8 MeV. But since the first excited state transition was found to be larger in intensity, it was almost impossible to separate the two transitions, lying approximately 2.5 MeV apart. However a rough qualitative separation of ground and first excited state transitions was done and shows an excited state giant resonance 3.0 ± 0.5 MeV above the g.s. GDR, giving once more evidence for a gamma deexcitation linearly superimposed on the 2.9 MeV level in ^{8}Be, similar to what has been observed for example in ^{12}C. The combined $\gamma_0 + \gamma_1$ results are in agreement with those in the literature, showing two structures at about $E_x = 22$ MeV and $E_x = 25$ MeV. A combined c.o.m. angular distribution was measured at a c.o.m. energy of 8.0 MeV including points from 45 deg to 145 deg. A least squares fit gave:

$$\sigma(\vartheta) = [(0.454 \pm 0.068) + (0.462 \pm 0.087)\sin^2\vartheta + (0.298 \pm 0.054)\sin^2\vartheta\cos\vartheta] \times 10\,\mu\text{b/sr} \qquad [1-32]$$

The appreciable odd terms are attributed, within the assumption of a dominant E1 mechanism, to interference with E2 or M1 strengths, but most probably E2 that should be favoured with respect to M1 at these large excitation energies.

The most comprehensive analysis of the $^7\mathrm{Li}(p,\gamma_0)^8\mathrm{Be}$ and $^7\mathrm{Li}(p,\gamma_1)^8\mathrm{Be}^*$ reactions has been performed by Fisher et al. [53] at Stanford, using the Tandem van de Graaff accelerator from $E_p = 0.8$ to $E_p = 17.6$ MeV and a compound NaI-plastic anticoincidence spectrometer that allowed complete resolution of the two reaction channels over the whole energy range explored. Standard line shapes for this instrument were obtained from the $^{11}\mathrm{B}(p,\gamma_0)^{12}\mathrm{C}$ gamma peaks. This result was perfectly suitable to deconvolute the $^8\mathrm{Be}$ γ_0 peak, which displays only detector resolution, while the γ_1 peak is broadened by the 1.5 MeV natural width of the first excited state. Escape tails for the two transitions could be taken into account carefully and subtracted down to the low energy extremes of the spectra. Both γ_0 and γ_1 yields at 90 deg and for an excitation energy region extending from $E_x = 18$ to $E_x = 32.5$ MeV were produced and exhibit a pronounced giant resonance in each channel with little additional structure. Detailed angular distributions were measured in steps of 100 keV to 500 keV and were subsequently fit by the usual expansion [1-2] limited to $k = 2$, or alternatively with the same expansion extended up to $k = 4$. The γ_0 resonance peaks at $E_x = 21.6$ MeV at a value of $\approx 2.7\,\mu$b/sr. Integrated between 18 and 33 MeV the $^8\mathrm{Be}(\gamma,p_0)^7\mathrm{Li}$ obtained through detailed balance exhausts only 11% of the classical Thomas-Reiche-Khune sum rule

$$\int_{18}^{33} \sigma(E)dE \approx 13 \pm 4\,\mathrm{MeV\,mb} \approx 60\frac{NZ}{A}\,\mathrm{MeV\,mb} \qquad [1-33]$$

Over a similar integration region in the GDR of 4N nuclei this is the smallest value, since it compares with 35% in ^{4}He, 31% in ^{12}C and 18% in ^{16}O. The ^{8}Be to ^{12}C cross section ratio results give 0.23. This can be understood in the framework of a schematic 1p-1h model. Assuming a $(s_{\frac{1}{2}})^4_{J=0}(p_{\frac{3}{2}})^4_{J=0}$ configuration for the ^{8}Be g.s. and $(s_{\frac{1}{2}})^4_{J=0}2(p_{\frac{3}{2}})^4_{J=0}$ for ^{12}C, it is straightforward to calculate p $\rightarrow$ h transitions in a harmonic oscillator well at $\hbar\omega = 41/A^{1/3}$ MeV, based upon the statistical factor of the initial (hole) and final (particle) state. As seen from Table 5 the $(1p_{\frac{3}{2}})^{-1}(1d_{\frac{5}{2}})$ configuration dominates the absorption

although the other configurations give substantial contributions.

After correction for the $A^{1/3}$ factor, one has

$$B(E1, {}^{8}\mathrm{Be})/B(E1, {}^{12}\mathrm{C}) = 0.60 \qquad [1-34]$$

When the B-factors are introduced to calculate the cross section ratio via the integral

$$\int \sigma(\gamma, p_0) dE = E_\gamma^3 B(E1, \uparrow)(\Gamma_{p_0}/\Gamma) \qquad [1-35]$$

where E_γ is the peak energy of the resonance, Γ its total width and Γ_{p_0} is related to the proton reduced width by $\Gamma_{p_0} = 2P\gamma_{p_0}^2$. The computed ratio is 0.28 which is in good agreement with the experimental value of 0.23. Thus the smaller strength observed in ^{8}Be relative to ^{12}C can simply be ascribed to the smaller amount of $p_{\frac{3}{2}}$ particles in the g.s. of ^{8}Be. The missing strength goes naturally to excited states.

TABLE 5

Relative contributions of 1p-1h transitions to E1 absorption in ^{8}Be

Configuration	$\lvert < \lvert E1 \rvert > \rvert^2$	Rel. Cont. ($A^{\frac{1}{3}}$ unit)
$(1s_{\frac{1}{2}})^{-1}1p_{\frac{3}{2}}$	0.477	0.239
$(1s_{\frac{1}{2}})^{-1}1p_{\frac{1}{2}}$	0.239	0.239
$(1p_{\frac{3}{2}})^{-1}1d_{\frac{5}{2}}$	1.433	0.17
$(1p_{\frac{3}{2}})^{-1}1d_{\frac{3}{2}}$	0.159	0.080
$(1p_{\frac{3}{2}})^{-1}2s_{\frac{1}{2}}$	0.318	0.359

As concerns γ_0 angular distributions, they are expanded in two or four Legendre polynomials. The a_1 coefficient is found to be positive with an average value between 0.1 and 0.4, increasing with an energy above $E_x = 24$ MeV. This means that interference between configurations of opposite parity, occurs most probably (E1,E2) with the E2 strength concentrated at higher excitation energies. The a_2 coefficient is virtually constant at a value of -0.05 for $E_x \geq 20$ MeV and this means that the GDR is dominated by a single collective state. The a_3 coefficient depends intrinsically on the (E1,E2) interference and since it it found to be positive and constant up to $E_x = 28$ MeV, it indicates that a small amount of E2 radiation mixes with the dominant E1 mode. The fact that above 28 MeV a_3 starts

decreasing as the energy increases, indicates a relatively large and perhaps resonant E2 contribution located at higher energies, but confined in any case to a very small intensity as compared to the E1 contributions as the a_4 coefficient (never distinguishable from zero) confirms. No significant attempt to deduce E2 strengths is possible from this set of unpolarized data. The small value of a_2 can be fitted by an almost pure $s_{\frac{1}{2}}$ wave, but solutions with large $d_{\frac{5}{2}}$ or $d_{\frac{3}{2}}$ components are not formally excluded, and only polarized particle data should allow separation of these components. The γ_1 resonance is shifted upwards from the γ_0 one at about 2.3 MeV, which is not too different from the excitation energy of the first excited state at 2.9 MeV. This is what one would expect if an E1 excitation is built upon the first excited state and the coupling of the two excitations is weak. This is a rather general experimental evidence and will be discussed in more detail when considering the ^{12}C case. The characteristics of the γ_1 angular distributions are that the a_1 coefficient is generally positive and increases with energy, the a_2 coefficient decreases with increasing energy, being positive at low energies, crossing the zero line in the vicinity of the resonance peak, and becoming large and negative at higher energies. The a_3 coefficient is small, but becomes definitely negative and increases in magnitude with energy, while a_4 is consistent with zero throughout the energy range covered. As for the γ_0 case, a broad giant quadrupole resonance built upon the first excited state can be assumed to explain the behaviour of the a_1 and a_3 coefficients, but again the intensity of this resonance must be very small as compared to that of the E1 so to justify the negligible values assumed by the a_4 coefficient. It is further observed that the different shape of the γ_0 resonances in ^8Be and ^4He does not support strong α clustering in ^8Be.

Weller et al. [54] report on radiative capture to highly excited states of ^8Be, confirming this peculiar aspect of radiative capture, observed primarily in ^{12}C and ^{28}Si. The most evident transition is to unresolved states around 16.6 MeV, where two 2^+ ^8Be states are expected at 16.62 and 16.92 MeV respectively. The 16.92 MeV level is a single neutron state, while the 16.6 MeV level is a single proton state and has a large matching with the entrance channel configuration. Therefore it should be the most valid candidate for the final ^8Be state involved in the proton radiative capture. The 90° γ yield curve has been extended from $E_p = 12$ MeV to $E_p = 30$ MeV, which corresponds to excitation

energies above the 16.62 MeV level from 11 to 26 MeV. This curve is compatible with a direct $E1 + E2$ calculation but the lack of data in the region around $E_x = 16$ MeV and $E_x < 11$ MeV prevents any conclusion on a possible resonance. If this exists it should be compact and strong enough to be observed in the p_0 channel, and should be built upon this state and shifted upwards by ≈ 22 MeV as are those built upon the g.s. and first excited state in ^{8}Be. On the other hand, if the direct capture mechanism gives a reliable description of the reaction, then this type of experiment should provide a useful means for studying single particle strengths at high excitation energies [55].

1-6 Radiative proton capture in the GDR region of ^{12}C

Measurements over the ^{12}C GDR via radiative proton capture by ^{11}B were started with the work of Bair et al. [56] who measured from approximately 2 to 5 MeV proton energy, the 0 and 90 deg yields for the ^{11}B$(p,\gamma_0)^{12}$C and ^{11}B$(p,\gamma_x)^{12}$C* leading to the first excited state at 4.43 MeV in ^{12}C, detecting gamma rays with a 3″ × 3″ NaI crystal that gave 8% FWHM resolution at the ^{137}Cs peak (0.661 MeV). Below the neutron production threshold ($E_p = 3.015$ MeV), the 4.43 MeV peak and the peaks corresponding to capture transitions to the ground and first excited states in ^{12}C, clearly identified by their energy dependence going as $E_\gamma = 15.95 + \frac{11}{12}E_p$, are the main structures observed in the gamma spectra. Above the neutron production threshold, a large background, due to neutron capture in the NaI(Tl) crystal, extends up to 9 MeV and swamps the 4.43 MeV peak. The γ_0 capture can be however measured in all the explored range. Resonant radiative capture shows at proton energies of 2.6, 3.14,3.6, 4.94 and 5.12 MeV and the trailing edge of the GDR is already evident.

Extension of these measurements to just above the GDR peak, was performed by Gemmel et al. [48] who produced a 90 deg yield curve from $E_p = 4$ to $E_p = 7$ MeV, and first remarked on the great advantage of capture reactions, that provide an energy assignement determined only by the incoming proton energy and an energy resolution limited only by the gamma spectrometer performance. In their experiment, the g.s. and the first excited state are identified except at low energies, where the transition to the 4.43

MeV state is merged into the background edge. Only the (p,γ_0) yield was produced and this leads to a peak cross section at $E_p = 7.2$ MeV of $(2.7 \pm 0.5) \times 10^{-28}$ cm^2, assuming isotropy. In the region of overlap there is good agreement with the data of B air et al. [56]. The curve reveals small peaks at 21.4 and 22.1 MeV excitation energy but is otherwise smooth, within the resolution of the experiment. Application of detailed balance gives a peak value

for the photoproton cross section of ^{12}C of (29 ± 5) mb at 90 deg, the peak being located at 22.5 MeV. This is in agreement with direct photonuclear reaction measurements. Support for the existence of compound $p+^{11}$B states can be found in the ^{11}B$(p,n)^{11}$C yield curve [58] that shows peaks at 21.3 and 21.8 MeV and from the ^{12}C$(e,e'p)^{11}$B excitation function [59] that shows a peak at $E_p \approx 6$ MeV and discontinuities at approximately the excitation energy of 21.2 and 22.1 MeV. Nevertheless, if one has to substantiate the fact that only few 1^- states of ^{12}C are responsible for absorption in the GDR region, one has to improve the overall experimental resolution by an order of magnitude to separate sharp and low spaced (≤ 0.25 MeV) states in ^{12}C.

The 90 deg yield of capture gamma rays leading to the ground and first excited states in ^{12}C has been measured in the proton energy range from 3 to 11 MeV by Gove et al. [60] [61] together with a few angular distributions at critical energies. Capture gamma rays were observed by a a 12 cm Ø×15 cm NaI detector. Pulse height spectra are characterized by two high energy peaks, corresponding to capture gamma rays leading to the ground and first excited states of ^{12}C, a fairly steep rise at lower energies due to neutron background, a series of sharp gamma lines resulting from particle emission by the compound nucleus and a smooth cosmic background. The γ_0 and γ_1 peaks follow a linear variation with E_p expected from reaction kinematics and a rather careful deconvolution of the spectra has been made assuming reasonable energy tails for the γ_0 peak, despite the absence of information on detector response to real monochromatic photons. The 90 deg yield curve is produced for excitation energies from ≈ 18 to ≈ 26.5 MeV. The γ_0 yield displays a broad resonance centered at (22.5 ± 0.02) MeV and a half maximum width of ≈ 3.1 MeV in the c.o.m. system; there is also indication for a small peak at $E_x = 25.5$ MeV. No sharp structure is observed, though from $E_x = 21$ to $E_x = 22.6$ MeV two or three secondary

maxima with widths of ≈ 200 keV and intensities of the order of 10% of the total yield are observed around 21.8, 22.15 and 23.3 MeV. Whether these structures can be responsible for, or associated with, the breaks in the integrated yield curve of neutrons from bremsstrahlung irradiation of ^{12}C, reported by Katz [57], is really questionable since the results of the two experiments are not easily compared. The γ_1 yield shows more structure, although the statistical errors are much higher due to the subtraction of the γ_0 low energy tail from the γ_1 peak contribution. The γ_1/γ_0 ratio is low at the GDR peak and thereafter it increases continuously up to a value of about 2 at the highest measured proton energy of 11.4 MeV. At this energy one has unfortunately not yet reached an excitation in ^{12}C of 4.43 MeV above the peak of the g.s. GDR and although the γ_1 yield curve seems to flatten at 11.4 MeV, there is too little evidence to substantiate the existence of a dipole resonance built upon the first excited state in ^{12}C. A series of angular distributions for the γ_0 and the γ_1 radiations was made and fitted, in the laboratory system, by the Legendre polynomial expansion [1-2] limited to $k = 2$. When compared, the γ_0 results from this experiment and from a (γ, p) photoproton experiment [62] agree with each other in the region of superposition and result (Table 6) in an a_1 coefficient always distinct from zero and an a_2 coefficient that clusters around a value of -0.6.

TABLE 6

Angular distribution coefficients

E_x(MeV)	a_1	a_2	Reference
19.2	0.08 ± 0.03	-0.12 ± 0.04	Gove
21.5	–	-0.47 ± 0.02	Gove
22.1	0.09 ± 0.04	-0.56 ± 0.04	Penfold
22.5	0.12 ± 0.03	-0.69 ± 0.05	Gove
24.4	0.11 ± 0.03	-0.57 ± 0.05	Gove
25.3	0.27 ± 0.04	-0.59 ± 0.06	Penfold
25.5	0.29 ± 0.06	-0.57 ± 0.09	Gove

If one assumes, together with Courant [63], that the (p, γ) reaction proceeds in the giant resonance region by a direct process, in which a single proton of angular momentum

ℓ makes a transition $\ell \rightarrow \ell + 1$ emitting an E1 photon and being captured without the creation of a compound state, the angular distribution should be (see also ch.4):

$$W(\vartheta) = 2(\ell+2) + \ell \sin^2\vartheta = 1 - \frac{1}{2}\left(\frac{\ell}{2\ell+3}\right) P_2(\cos\vartheta) \qquad \ell \rightarrow \ell+1 \qquad [1-36]$$

and

$$W(\vartheta) = 2(\ell-1) + (\ell+1)\sin^2\vartheta = 1 - \frac{1}{2}\left(\frac{\ell+1}{2\ell-1}\right) P_2(\cos\vartheta) \qquad \ell \rightarrow \ell-1 \qquad [1-37]$$

In the case of $^{11}B(p,\gamma)$, possible proton transitions are $s \rightarrow p$ with $W(\vartheta) =$ constant and $d \rightarrow p$ with $W(\vartheta) = 1 - 0.5P_2$. Extension of the Legendre polynomial expansion to $k = 4$ performed in the region of the GDR gives no statistical evidence for P_3 and P_4 terms different from zero. The dipole resonance should give, at the peak, an a_2 value of -0.5, close to what is experimentally observed, but interference with even a small quadrupole strength should produce a_1 and a_3 coefficients changing sign upon passing through the dipole resonance, a fact that is contradicted by the experimental evidence. The γ_1 angular distribution has been measured at $E_p = 7.12$ MeV, where it was deconvoluted to give $W(\vartheta) = 1 + (0.22 \pm 0.01)P_1 + (0.40 \pm 0.014)P_2$ and at 8.4 MeV where it presented as spherically isotropic. The positive $a_2 = 0.4$ value at the peak of the γ_0 resonance, cannot be given by capture to a $J^\pi = 1^-$ state. Therefore the 1^- states involved in the γ_0 resonance do not emit gammas to the first excited state in ^{12}C, confirming the suggestion of Brown and Bolsterli [64] that the giant resonance is intimately related to the final state in the dipole emission.

The entire GDR region has been covered by Becker and Fox [65] who measured the 90 deg yield of the γ_0 and γ_1 radiations using protons from $E_p = 6$ to $E_p = 13.2$ MeV in steps of 100 keV, with the aim of confirming the γ_0 trend to higher energies and to explore structures in the γ_1 yield better than it was done previously. A single NaI crystal detector was used which allowed a rather easy deconvolution of the spectra into a γ_0, plus γ_1, plus background contribution, with the limitation of a larger statistical error on the γ_1 peaks, due to the subtraction of tails from highly populated γ_0 transitions and

of the neglect of energy dependent factors in the subtracted γ_0 response function. No evidence of fine structure appears in the giant resonance region for the ground state. The γ_0 excitation function is characterized by a broad maximum around 22.5 MeV and a secondary peak at 25.5 MeV. The γ_1 excitation function exhibits four prominent peaks at 22.1, 23.6, 25.5 and 26.9 MeV, in agreement with the less complete data of Gove et al. [61]. The γ_1 contribution exceeds the γ_0 one above $E_p = 9$ MeV and remains higher at higher energies. The integrated yield ratio $Y_{\gamma_0}/Y_{\gamma_1}$ is equal to 0.79. The data are compared to $T = 1$ states calculated by Vinh-Mau and Brown [66] in the framework of a particle-hole formalism, using harmonic oscillator wave functions and a δ–force. The qualitatively predicted behaviour finds support from the two yield curves as seen from Table 7.

TABLE 7

Particle hole state energies in ^{12}C

Configuration	Spin	Theory	Experiment
$(1p_{\frac{3}{2}})^{-1}(1d_{\frac{5}{2}})$	1^-	22.2	22.25
$(1p_{\frac{3}{2}})^{-1}(1d_{\frac{3}{2}})$	1^-	23.9	25.5
$(1s_{\frac{1}{2}})^{-1}(1p_{\frac{1}{2}})$	1^-	34.3	34.0
$(1p_{\frac{3}{2}})^{-1}(1d_{\frac{5}{2}})$	2^-	19.2	22.1
$(1p_{\frac{3}{2}})^{-1}(2s_{\frac{1}{2}})$	2^-	22.9	23.6
$(1p_{\frac{3}{2}})^{-1}(1d_{\frac{3}{2}})$	3^-	26.4	26.9

The predicted 22.2 MeV level is in good agreement with the peak of the G.D.R. This level should be, together with almost all others in the table, easily formed in proton capture by boron, which has a ground state configuration $(1p_{\frac{3}{2}})^{-1}$. Its decay to the 4.43 MeV 2^+ state should be largely inhibited since it involves spin-flip. But it carries, as predicted, the major part of the dipole strength for the ground state transition. The next structure in the γ_0 yield curve at 25.5 MeV is not distant from the predicted 23.9 MeV 1^- level, though it is much more intense than the calculation predicts. The following 1^- level at ≈ 34 MeV should not easily be excited by proton capture, since its configuration has a hole in the $1s_{\frac{1}{2}}$ shell. But data at higher energy [67] seem to support some influence of this level upon the γ_0 excitation function although the strength is two orders of magnitude lower than that

of the main 22.25 MeV transition. The 2^- levels at 19.2 and 22.9 MeV are predicted to strongly deexcite to the first excited state in ^{12}C as is

confirmed by the presence of peaks in the γ_1 excitation function at 22.1 and 23.6 MeV. Of the four peaks (22.1, 23.6, 25.5 and 26.9 MeV) in the γ_1 excitation function, one is common to the γ_0 curve at 25.5 MeV. The last can be identified with a $(1p_{\frac{3}{2}})^{-1}(1d_{\frac{5}{2}})$ level that should lead to non spin flip dipole radiation to the 4.43 MeV 2^+ state. An estimate of 1.0 MeV for the energy difference between the 1^- and the 3^- states, gives for this state, not calculated by Vinh-Mau, a value of 25.5 + 1.0 = 26.5 MeV, not far from the 26.9 MeV experimentally found.

Excitation functions for the ground and first excited state transitions in ^{12}C have been studied by Re_ay et al. [67] in the range from $E_p = 15.0$ to $E_p = 25.0$ MeV making use, for the first time, of a plastic scintillator ring surrounding the main 10 cm Ø×12.7 cm NaI crystal, to reduce cosmic radiation induced spurious contributions by a factor of ten, but no the low energy escapes from the crystal boundaries. The 90 deg yield function shows the presence of a weak resonance at 34.4 MeV, that decays both to the ground and the first excited state, being the γ_1 contribution two to three times larger than the corresponding γ_0. The total width of the 34.4 MeV state is ≈ 4 MeV compared to ≈ 2.8 MeV for the 22.5 MeV resonance. The integrated (γ, p_0) cross sections across the 22.5 MeV and the 34.4 MeV resonances, give a total of 55 ± 13 MeVmb and of 4.1 MeVmb respectively. Angular distributions are not given, but the $\sigma(41)/\sigma(90)$ ratio is measured to be 1.04 ± 0.30 for the g.s. and 1.33 ± 0.25 for the first excited state transition. The data are discussed in terms of the Gillet and Vinh-Mau [68] calculations for ^{12}C dipole states reported in Table 8.

TABLE 8

Configuration and strength of ^{12}C computed dipole states

E(MeV)	Strength rel.	$(1p_{\frac{3}{2}})^{-1}2s_{\frac{1}{2}}$	$(1p_{\frac{3}{2}})^{-1}1d_{\frac{5}{2}}$	$(1p_{\frac{3}{2}})^{-1}1$.'	$(1s_{\frac{1}{2}})^{-1}1p_{\frac{1}{2}}$
17.7	0.09	0.992	0.078	-0.097	-0.007
21.5	0.73	0.106	-0.116	0.989	-0.062
24.2	0.01	-0.060	0.967	0.133	0.210
33.6	0.17	0.028	-0.217	0.036	0.977

It is seen that the main component of the 34 MeV state is $(1s_{\frac{1}{2}})^{-}(1p_{\frac{1}{2}})$ and this cannot be reached by direct capture since ^{11}B has the $1s_{\frac{1}{2}}$ shell completely filled in its ground state. Applying the Breit-Wigner one level formula to the dipole states at 22 and 34 MeV, one has for the integrated cross section ratios

$$\frac{S_{34}}{S_{22}} = \frac{E_{22}}{E_{34}} \frac{\Gamma_p^{34}}{\Gamma_p^{22}} \frac{\Gamma_\gamma^{34}}{\Gamma_\gamma^{22}} \frac{\Gamma^{22}}{\Gamma^{34}} \qquad [1-38]$$

where Γ_p, Γ_γ and Γ are the partial widths for proton decay, for gamma decay to the ground state and the total width. In the single particle shell model the widths are proportional to $E^3 A^{2/3}$ which gives, considering the Gillet Vinh-Mau values for the relative dipole strengths,

$$\frac{\Gamma_\gamma^{34}}{\Gamma_\gamma^{22}} = \frac{0.17}{0.73} \left(\frac{34.4}{22.5}\right)^3 = 0.83 \qquad [1-39]$$

With this ratio for the gamma decay partial widths, the measured total widths (2.8 MeV and 4.0 MeV respectively) and the integrated cross sections (55 MeV mb and 4.1 MeV mb respectively) one gets an experimental ratio for proton decay of the two resonances $\Gamma_p^{34} = 0.20\Gamma_p^{22}$, which is in strong contradiction to the value of 4 that is obtained assuming that both dipole states were due to proton decay entirely through their $(1p_{\frac{3}{2}})^{-1}1d_{\frac{5}{2}}$ component. The disagreement could only be accounted for by a decay of the dipole state via small admixtures of continuum configurations. Support for this view is given by the measured $\sigma(41)/\sigma(90)$ ratio at 1.04, i.e. almost isotropic. This ratio should be 2.33 in the case of direct $p \rightarrow s$ capture, which is obviously ruled out, and 1.52 in the case of $d \rightarrow p$ direct capture. But the observed value can be as well explained if one assumes interference between s and d wave capture to a final p state. The possibility of the 34 MeV state being identified with one of the $T = 1, 2^+$ states predicted by Vinh-Mau and Brown at 35 and 36.6 MeV has been considered. These states should carry 19% and 13% of the quadrupole strength and contribute 23% and 18% of the total gamma absorption from the ^{12}C g.s.. Since they are based upon a $(p_{\frac{3}{2}})^{-1}$ configuration, they should be accessible by proton capture on ^{11}B. But to reproduce the integrated value of 4.1 MeV mb, consistently

with pure quadrupole absorption, would require $\Gamma_{p_0}/\Gamma = 0.36 - 0.6$ i.e. 30% to 60% of the 2^+ 35 and 36.6 MeV states decay should be proton decay to the g.s. and this seems exceedingly large in view of the numerous n, α, p open channels. The conclusion is that the state observed at 34 MeV is the $T = 1, 1^-$ state of Table 8.

A very detailed set of data, namely excitation functions at 90 deg for the γ_0 and γ_1 transitions and angular distributions at 5 or 6 angles in steps of 50 keV or less, covering the range $E_p = 4$ to $E_p = 14$ MeV, has been produced by Allas et al. [69] at the Argonne tandem laboratory. The emphasis was in fact given to achieving maximum resolution and as well, for the first time, the trend of the angular distributions for the γ_0 and the γ_1 transitions over the entire GDR energy region and above it. This was certainly obtained due to the clear separation of the γ_0 and γ_1 peaks and the validity of the unpeeling procedure to resolve the total gamma spectrum into γ_0 plus γ_1, plus cosmic ray, plus background contributions. The 90 deg yield curve for γ_0 is dominated by a broad (FWHM ≈ 3 MeV) structure centered at $E_p = 7.2$ MeV ($E_x = 22.6$ MeV), accompained by smaller reproducible structures at $E_p = 6.0$, 6.7 and 8.3 MeV. Above the main resonance the 90 deg yield decreases with secondary peaks showing up at $E_p = 10.4$ and 13.2 MeV. The γ_1 90 deg yield curve shows a more complex structure that involves few "equally" strong resonances, although above 6 MeV one can observe a slow growth and subsequent decay in the average yield, that can be ascribed to a broad ($\Gamma \approx 7$ MeV) resonance centered at about $E_p = 11$ MeV. Resonances are distinguishable from this average behaviour at 6.7, 8.3, 10.5, 11.8 and 13.1 MeV. A doublet of states is confirmed around $E_p = 5$ MeV and a new sharp ($\Gamma = 100$ keV) resonance is observed at 10.15 MeV. These data confirm and extend previous results except for the newly observed 10.15 MeV resonance, with the advantage of extreme detail on the whole energy range and of lower statistical errors resulting from a good single crystal resolution and a computer-assisted unpeeling procedure. Angular distributions for the γ_0 transitions show little variation across the resonance and are characterized by a peak at about 90 deg and a quite large anisotropy, the yield being concentrated more towards the forward angles. Angular distributions for the γ_1 transition are less anisotropic and show considerable variation across the huge structure observed in the yield curve. Cross sections

are fitted by the usual Legendre polynomial expansion [1-2], restricted to four terms only. The $a_1 - a_4$ coefficients are plotted in steps of 50 keV or less as a function of energy. The behaviour is extremely different for the two cases. For the γ_0 component the a_1 coefficient is always positive and, after some fluctuations between 4.0 and 5.5 MeV, it stabilizes at +0.03 around 5.5 MeV, then increasing with energy to reach a value of +0.3 at 13.8 MeV. The a_2 coefficient is always negative at an average value of -0.6 from 4.3 MeV upwards. The a_3 value is positive with large fluctuations below 5.0 MeV; thereafter it remains very close to zero showing perhaps a tendency to go towards negative values above 11.5 MeV. The a_4 coefficient is never distinguishable from zero over the entire energy range. On qualitative grounds, one can say that the 90 deg peaking

is reflected in the negative a_2 value, while the forward angle predominance has the consequence of a positive increasing a_1 coefficient. The γ_1 coefficients show in general large fluctuations. The a_1 value is generally positive, but assumes a steadily increasing trend only above 5.0 MeV. The trend of a_2 is completely different as it has large but negative fluctuations below 6.0 MeV and then averages to about zero up to 9.0 MeV. From there on, the trend is consistently downwards. Both a_3 and a_4 are not distinguishable from zero around which they largely fluctuate, even though more positive values are found for a_3 below 5.5 MeV. After integration is performed, the total (p,γ_0) cross section clearly resembles the 90 deg yield. The peak value is 1.2×10^{-28} cm^2, as compared with the value of 1.3×10^{-28} cm^2 given by Gove et al. [61] and 2.1×10^{-28} cm^2 of Gemmel et al. [48] The (p,γ_1) total cross section peaks at 0.83×10^{-28} cm^2 at about 10.3 MeV. Extrapolating this curve with the data at higher energy of Re_ay et al. [67], one has a FWHM of about 7.0 MeV. Energy integration over the two peaks gives 630 eV b for the γ_0 case and 850 eV b for the γ_1 case. These values require that, in both cases, the bulk of the capture must proceed through E1 transitions. This could be reflected in the relative simplicity of the γ_0 yield, to which E1 contributions come only from 1^- capturing states, and the evident complexity of the γ_1 yield to which E1 contributions may come from either 1^-, 2^- or 3^- capturing states due to the high spin value of the final 4.43 MeV 2^+ state. However, the appearence of secondary maxima in the γ_0 yield, suggests that the strength of the transition is not exhausted by a single level. In $j-j$ coupling, one can predict the behaviour of the

angular distribution. Assuming the dominance of E1 transitions, although the forward asymmetry indicates interference with multipolarities of opposite parity like M1 or most probably E2, one can reach a capture 1^- state coupling to the $^{11}\mathrm{B}\ \frac{3}{2}^-$ ground state, with a proton in either a $s_{\frac{1}{2}}$, $d_{\frac{3}{2}}$ or $d_{\frac{5}{2}}$ state. In this case the angular distribution is completely determined by the set of equations

$$\begin{aligned} W(\vartheta) &= 1 + a_2 P_2(\cos\vartheta) \\ a_2 &= 0.40(d_{\frac{3}{2}})^2 + 0.40(d_{\frac{5}{2}})^2 + 0.60(d_{\frac{3}{2}})(d_{\frac{5}{2}}) \\ &\quad + \cos(sd)[0.45(s_{\frac{1}{2}}, d_{\frac{3}{2}}) - 1.34(s_{\frac{1}{2}}, d_{\frac{5}{2}})] \\ 1 &= (s_{\frac{1}{2}})^2 + (d_{\frac{3}{2}})^2 + (d_{\frac{5}{2}})^2 \end{aligned} \qquad [1-40]$$

where ℓ_j is the amplitude of the partial wave of orbital angular momentum ℓ and total spin j. The $\cos(sd)$ can be computed from the nuclear radius and,if $r = 1.2A^{1/3}$ fm, one finds a decreasing trend from 1.0 at $E_p = 4\,\mathrm{MeV}$ to 0.5 at $E_p = 14.0\,\mathrm{MeV}$. Obviously the exact determination of the three amplitudes is impossible with only two equations relating them, but the path that represents the possible combinations can be computed and gives some important information, viz. i) The $s_{\frac{1}{2}}$ intensity cannot be zero and must vary from 1% to 80%; ii) the $d_{\frac{5}{2}}$ intensity is always greater than 10% and can be as high as 98% keeping the same sign of $s_{\frac{1}{2}}$; iii) the $d_{\frac{3}{2}}$ intensity can be zero and not greater than 50%. If one reproduces the energy behaviour of a_2 from 14 MeV, taking into account possible uncertainties in the nuclear radius the situation is

$(s_{1/2})^2$ from 1% to 3%; $d_{3/2}|d_{3/2}|$ from 0% to -32%; $d_{5/2}|d_{5/2}|$ from 66% to 97%

which strongly supports d-wave proton capture. Energies, transition probabilities and angular distributions for $T = 1, 1^-$ states have been computed by Vinh-Mau and Brown [66] within the particle-hole formalism and are reported in Table 9.

Then the strongest transition is at 22.2 MeV in excellent agreement with the γ_0 centroid energy at 22.5 MeV. The E1 transition is dominated by a $(1p_{\frac{3}{2}})^{-1}1d_{\frac{5}{2}}$ as the analysis of angular distributions confirmed, assigning to $d_{\frac{5}{2}}$ capture a probability of between 66 and

98%. The experimental a_2 value of −0.6 is not distant from the predicted −0.4 with the difference expected to be easily removed by the addition of small ($\leq 5\%$) percentages of $d_{\frac{3}{2}}$ or $s_{\frac{1}{2}}$ amplitudes in the theoretical calculations. Further support of this picture comes from the calculations of Gillet [70] which predict, for the dominant giant resonance state, the $[(1p_{\frac{3}{2}})^{-1}1d_{\frac{3}{2}}]/[(1p_{\frac{3}{2}})^{-1}1d_{\frac{5}{2}}]$ amplitude ratio to be −0.12 with an angular distribution $W(\vartheta) = 1 - 0.46P_2$, not far from what is experimentally found. The Becker and Fox [65] assignment of a $(p_{\frac{3}{2}})^{-1}d_{\frac{3}{2}}$ configuration to the structure at 25.5 MeV in the γ_0 yield is not supported here by the detailed angular distribution measurements. Still in the spirit of pure $j-j$ coupling, one can consider radiative transitions to the first excited state from the $T = 1\, J^\pi = 1^-\, 2^-\, 3^-$ states of ^{12}C as predicted by Vinh-Mau and Brown [66], as in Table 9. The small characteristic a_2 coefficient found experimentally, is supported by the calculated values, that are ≤ 0.04 for five of the eight possible configurations. The $j-j$ coupling scheme also accounts for the weak role in the γ_1 yield of the $(p_{\frac{3}{2}})^{-1}d_{\frac{3}{2}}$ configuration, that dominates the γ_0. In fact the 2^+ 4.43 MeV state configuration, $(1p_{\frac{3}{2}})^{-1}1p_{\frac{1}{2}}$ does not connect through single particle E1 transitions to the 22.5 MeV 1^- states ($\Delta J = 2$). The angular distributions do not contradict the Becker and Fox arguments of peaks in the γ_1 yield, i.e. $22.2[(1p_{\frac{3}{2}})^{-1}1d_{\frac{3}{2}}; 2^-]$, $23.7[(1p_{\frac{3}{2}})^{-1}1s_{\frac{1}{2}}; 2^-]$, $25.6[(1p_{\frac{3}{2}})^{-1}1d_{\frac{5}{2}}; 1^-]$, and $26.8[(1p_{\frac{3}{2}})^{-1}1d_{\frac{3}{2}}; 3^-]$. The latter agreement is supported by the fact that theory assigns

TABLE 9

Particle hole states in ^{12}C

Configuration	J^π	E_x(MeV)	E1(%)	$W(\vartheta)$
$(1p_{\frac{3}{2}})^{-1}2s_{\frac{1}{2}}$	1^-	18.7	6.5	1
$(1p_{\frac{3}{2}})^{-1}1d_{\frac{5}{2}}$	1^-	22.2	75	$1 - 0.04P_2$
$(1p_{\frac{3}{2}})^{-1}1d_{\frac{3}{2}}$	1^-	23.9	0.5	$1 + 0.04P_2$
$(1p_{\frac{3}{2}})^{-1}1d_{\frac{5}{2}}$	2^-	18.11		$1 + 0.143P_2$
$(1p_{\frac{3}{2}})^{-1}1d_{\frac{3}{2}}$	2^-	19.2		1
$(1p_{\frac{3}{2}})^{-1}1s_{\frac{1}{2}}$	2^-	22.9		1
$(1p_{\frac{3}{2}})^{-1}1d_{\frac{3}{2}}$	3^-			$1 - 0.24P_2$
$(1p_{\frac{3}{2}})^{-1}1d_{\frac{5}{2}}$	3^-			$1 - 0.19P_2$
$(1s_{\frac{1}{2}})^{-1}1F_{\frac{7}{2}}$	3^-	34.3		1

to 1^- and 2^- states energies all below 24 MeV.

1-7 Resonant radiative capture to the first excited states in ^{12}C

Absolute cross sections at 90 deg and at other 7 angles (30, 45, 60, 90, 120, 135, 145 deg) measured by Brassard et al. [71] provided angular distributions from $E_p = 14$ to $E_p = 22$ MeV for the $\gamma_0(g.s.)$, $\gamma_1(4.43\,2^+)$ and $\gamma_3(9.64\,3^-)$ transitions in ^{12}C. The weakness of the $\gamma_2(7.65\,0^+)$ transition, prevented any reasonable assignment except for an upper limit set at 20% of the γ_1 value at any energy in this range. Gamma rays were detected by a single 9 in Ø×12 in NaI crystal, where counting pile-up was reduced by means of an electronic counting system 40 times faster than any traditional double delay line amplifier system. Good resolution was achieved by an automatic gain adjustment associated with a light pulser peak. Peak shapes of various γ lines in the spectra detected were inferred by extrapolating a measured [71] 12.5 MeV shape, scaling the resolution according to $(E_\gamma)^{-\frac{1}{2}}$. Compton contributions, due to rescattering in the surrounding media were added, maintaining the peak tail slightly above zero at zero energy. This was the shape used in fitting spectra, while the original, going to zero, shapes were used to calculate absolute cross sections. The γ_0 and γ_1 angular distributions were fitted by a four-terms Legendre polynomial expansion [1-2], while the γ_3 angular distributions are simply fitted in the form $\sigma(\vartheta) = A_0[1 + a_2P_2]$. Apart from relative normalisation, all available (p, γ_0) points, define quite clearly the trend of the cross section, except for the case of the resonance at $E_x = 3.3$ MeV observed by Reay [67] but not confirmed elsewhere. In particular the data points of Allas et al. [69] are normalized to the present values, since Allas used a somewhat overestimated tail contribution. Rather smooth experimental curves, are obtained by the combination of different data sets, ranging from about 19 to over 35 MeV excitation energy in ^{12}C. Theoretical indications are based on the one particle one hole model wave functions of Gillet and Vinh-Mau [72] and the use of a complete R-matrix formalism. All 64 states calculated by Gillet were included and 60 reaction channels considered, some of these, corresponding to excited configurations of ^{11}B and ^{12}C, though more likely to be seen in the direct (γ, p) or (γ, n) reactions, do however contribute additional width to the capture

resonances. The ^{11}C and ^{11}B ground states have been simply described as pure $1p_{\frac{1}{2}}$ hole states. A channel radius of $R_c = 4.5$ fm, based on ^{12}C experimentally determined charge distribution, has been used, with a boundary condition for the radial wave functions to which a logarithm derivative equal to -1 was imposed at R_c. The reduced width amplitudes of the 1p-1h configuration are defined by

$$\gamma = (\hbar c)(2mc^2 R_c)^{-1/2} R_c u(R_c) = (2.247\,\mathrm{MeV}^{1/2}) R_c u(R_c) \qquad [1-41]$$

with the radial wave function normalized to $\int_0^{R_c} |ru(r)|^2 dr = 1$ Values are reported in Table 10.

TABLE 10

Reduced width amplitudes of 1p-1h configurations in ^{12}C

Single particle state	$\gamma(\mathrm{MeV}^{\frac{1}{2}})$
$1p$	0.427ω
$1d$	1.450
$1f$	1.850
$2S$	1.638
$2p$	1.883

The reduced widths for configurations like the $(1s_{\frac{1}{2}})^{-1}1p_{\frac{1}{2}}$ require some attention as indicated in Table 10 by the presence of the factor ω, the only free parameter in all these calculations. As a matter of fact Gillet predicts a bound state at 34 MeV excitation energy with an almost pure $(1s_{\frac{1}{2}})^{-1}1p_{\frac{1}{2}}$. Since it is bound, the reduced width should approach zero and, in this circumstance, a narrow resonance should appear in the excitation function. The fact that there is no evidence of it, apart from a weak increase in the excitation function observed by Re..ay et al. [67], reflects the fact that numerous other configurations including many particle-many holes or 1p-1h across two major shells (there are six with $(1s_{\frac{1}{2}})^{-1}1p_{\frac{1}{2}}$), have not been included. This can be done approximately by introducing the parameter ω, which has limited influence on the overall excitation function and affects only the predicted 34 MeV resonance. In particular the comparison of calculated and measured cross sections is meaningful since no normalization has been introduced in the calculations.

For the calculated contributions of the various elements to the γ_0, γ_1 and γ_3 transitions, one can say that the γ_0 is dominated by the $(1p_{\frac{3}{2}})^{-1}(1d_{\frac{5}{2}})$ configuration, while the main contribution to γ_1 arises from the $(1p_{\frac{3}{2}})^{-1}(1d_{\frac{3}{2}})$ coupled to 3^- 2^- and 1^- in order of importance. But there is no simple evidence that the many structures experimentally observed in the γ_1 excitation function, are due to the greater number of levels which can contribute an E1 transition to the first excited state, since the calculated widths of such levels are quite large and their combination does not give rise to appreciable structure. Rather the interpretation is that these structures are clear evidence for the presence of more complex configurations. The γ_3 total cross section results appear to be dominated by the $[(1p_{\frac{3}{2}})^{-1}(1d_{\frac{5}{2}})]_{3^-}$ configuration at low energy implying a strong M1 transition, and by the $[(1p_{\frac{3}{2}})^{-1}(1f_{\frac{7}{2}})]_{4^+}$ configuration at higher energies. Referring to the γ_0 transition comparison with calculations allows us to extract a few fundamental statements. First the huge structure at 34 MeV disappears completely if ω is chosen at a perfectly reasonable value of 2.8. The fact is consistent with the configuration $[(1s_{\frac{1}{2}})^{-1}(1p_{\frac{1}{2}})]_{1^-}$ being excited with several complex states, which are not efficiently reached in proton capture. Secondly the apparent resonance phenomena observed at 25 MeV and 28 MeV have such magnitudes that they certainly involve dipole transitions as could result from interference between these states and the main component of the GDR. However the state predicted at 25 – 28 MeV by Gillet, consisting primarily of $(1p_{\frac{3}{2}})^{-1}(1d_{\frac{3}{2}})$ included in these calculations is not able to reproduce the experimental structures. The hypothesis of this author is that the resonances are predominantly many particles-many holes, with a substantial admixture of 1p-1h states through which they are populated and observed. It is emphasized that these conclusions are only possible after a complete calculation, being direct comparison to computed strengths of the many 1p-1h states present in this

energy region completely misleading,if it is not known how the strength is distributed. A much larger predicted value gives further support to the presence of substantial admixtures of different configurations although the 1p-1h computed angular coefficients seem not to have enough sensitivity to reflect this fact. Much larger experimental values and overall discrepancies are observed in the decay to the 4.43 MeV 2^+ first excited state in ^{12}C which is mainly a $(1p_{\frac{3}{2}})^{-1}(1p_{\frac{1}{2}})$ configuration. On a general basis, considering the

reverse experiment of photon absorption from such a $(1p_{\frac{1}{2}})^{-1}(1p_{\frac{1}{2}})$ state, it is expected that 1p-1h absorption (promoting the single $p_{\frac{1}{2}}$ proton to higher shells) is less probable than a 2p-2h absorption (promoting one of the seven $p_{3/2}$ protons to a higher shell). So the calculation, which included only the Gillet 1p-1h states, is neglecting for this transition a relevant contribution coming from more complex configurations. The correct procedure seems therefore to be that of Kanimura et al. [73] who have coupled dipole and quadrupole vibrations and succeeded in predicting the positions and strengths of resonances both in the γ_0 and the γ_1 channels, with an approach that is qualitatively similar to the assumption of a GDR built on an excited state. The transition to the 7.65 MeV 0^+ state was not observed through direct proton capture, which is consistent with a relatively complex structure for this state, already indicated by the strong transition rate to this state observed in He capture experiments. Completely different results are observed for the γ_3 transition where predicted values overestimate by a factor of ten the experimental data. The speculation is that this 3^- state consists of complex configurations with only 10% admixture of 1p-1h configurations through which it is observed in proton capture.

The unique possibility offered by radiative capture transitions towards the understanding of structures of excited states and their coupling to the GDR, has been exploited by Snover et al. [74] in the range from $E_p = 6$ to $E_p = 23$ MeV. The experiment concerned the 0^+ g.s., the 2^+ 4.43 MeV state, the deformed 0^+ level at 7.66 MeV and the 3^- collective octupole state at 9.63 MeV, which are completely resolved by the use of a large anticoincidence NaI detector. Detailed excitation curves were measured for all four transitions at 90 deg, where absolute values were inferred from normalization to the Allas et al. [69] points, given by

$$\sigma(90)\,[\mu\mathrm{b/sr}] = [2.23 + 0.078(E_\gamma - 12.5)] \qquad [1-42]$$

Angular distributions were taken at $E_p = 12.4$ and $E_p = 14.0$ MeV for the γ_0, γ_1 and γ_3 transitions, showing substantially a negative a_2 coefficient characteristic of dipole radiation and a positive a_1-negative a_3 combination typical of E1-E2 interference. The normalized cross sections for the 0^+ g.s. and the 2^+ transitions are in good agreement

with previous measurements both in absolute value and in energy dependence. Above 14 MeV, the new information is that of a slight dip in the γ_0 yield at $E_p = 14$ MeV and a slight peak at $E_p = 15$ MeV. Otherwise the two curves show a smoothly decreasing cross section from $E_p = 14$ to $E_p = 23$ MeV. There is no evidence for a resonance at $E_x = 28$ MeV (Brassard [71]) nor of a resonance at $E_x = 34$ MeV [67]. The γ_1 excitation peaks at an energy which is displaced by roughly the energy of the first excited 2^+ state, a feature that might be taken as indicating weak coupling between the $0^+ \rightarrow 2^+$ and the $0^+ \rightarrow 1^-$ excitations. Some structure in the two curves appears correlated below $E_x = 28$ MeV which would be interpreted by Kanimura et al. [73], in terms of the dipole-quadrupole coupling. The most dramatic feature of the capture to the 0^+ 7.65 MeV state is its weakness relative to the other measured transitions, in particular to the g.s. GDR. On a qualitative basis this can be reconciled to the fact that the 7.65 MeV state is a deformed state

with a large 4p-4h component and a GDR built upon it will be a combination of 3p-3h, 4p-4h and 5p-5h configurations that do not couple strongly with the $^{11}B + p$ entrance channel. The relative strength of the γ_2 to the γ_0 transition depends on the number of common intrinsic configurations in the two 0^+ (g.s. and 7.65) states. This should in any case be limited to the 1% value obtained by direct comparison of the γ_0 and γ_2 cross sections at the peak of the g.s. GDR (22.5 MeV). A calculation by Tagikawa and Arima [75], based on the description of these 0^+ states as a combination of two intrinsic alpha cluster configurations, gives a value of 1.2% for the γ_2/γ_0 ratio. The strong coupling between GDR's built on the intrinsic configurations of these 0^+ states is contradicted by

the absence of a large number of correlated structures in the γ_0 and γ_2 channels, as is seen for example in ^{16}O, where several of the γ_0 channel structures have also significance in the γ_2 channel [76][77]. The (p, γ_2) cross section peaks are displaced with respect to the (p, γ_0) peaks by an amount roughly similar to the excitation energy of the final state (7.65 MeV), as to be expected if there is weak coupling between the GDR and the 7.65 MeV excitation, but used with caution since the (p, γ_2) strength is weak and may not be representative of the entire γ_2 strength energy behaviour. The γ_3 yield shows narrow asymmetric peaks at $E_x = 27.5$ and $E_x = 27.8$ MeV and this is related to the larger entrance channel angular

momenta possible for E1 capture to the 3^- level, for instance as high as f wave capture followed by decay to 3^-. But the appearence of considerable strength at energies below the weak coupling estimate ($22.5 + 9.6 \approx 32$ MeV) and the large width of the strength distribution indicate the complex nature of this reaction channel.

1-8 GDR's built on p-h excited states in ^{12}C up to $2\hbar\omega$ excitation energy

Extension to high energies ($E_p = 18$ to $E_p = 43$ MeV) has been performed at the Milano cyclotron by a group including the author [78]. The purpose was to complement by the inverse reaction, photonuclear data in the intermediate energy region ($30 \leq E_\gamma \leq 110$ MeV) where data interpretation is for some reason controversial. Above the particle emission threshold in fact, the photon nucleus interaction is known to be collective through the excitation of virtual 1p-1h states and (γ, p) cross sections are well fitted by even a simple single nucleon knock-out scheme up to 300 MeV. But this scheme is unable to explain the remarkable symmetry observed between the (γ, p) and the (γ, n) cross sections over the whole range [79] investigated. Above 140 MeV elementary production processes on single nucleons (impulse approximation) become relevant and boson exchange currents and correlations have been shown to be essential to explain, for example, the two body photodisintegration of deuteron and the total absorption in more complex nuclei (enhancement factor). But relevant information on radiative capture to a large set of ^{12}C excited states was also obtained, thanks to the very good energy resolution of the anticoincidence spectrometer, composed of a central cylindrical 24 cm Ø×32 cm NaI crystal surrounded by a thick shell of NE110 plastic scintillator. Analysis of 7 point angular distributions was possible since the detector was able to be rotated from 35 to 145 deg with respect to the beam direction. Two critical points had to be tackled during the experiment, namely background and pile up. Background rejection is a very important feature in such experiments, since capture cross sections above the GDR are orders of magnitude lower than (p, xn) or $(p, p'\gamma)$ cross sections at the same energy. Moreover the capture photon rate is comparable with the rate in the scintillator volume. Two different systems have therefore been adopted [80]: the relevant neutron background is reduced by time of flight discrimination performed on a 90 cm path by means of the cyclotron beam microsctructure (5 ns every 50 ns), while the residual cosmic ray pulses are almost completely rejected by the anticoincidence with the plastic scintillator shell. The beam current has been limited to about 20 nA in order to

keep the distortion due to the pile-up on the detected spectrum below 5%. In addition pile up of pulses both above or below threshold has been efficiently rejected by the electronics. The high resolving power so achieved (figure 6), allows clear separation of the γ_0 and γ_1 photons throughout the energy range explored and extraction of information for higher transitions to the 9.6(3^-), 12.7(1^+), 13.3(2^-), 15.1(1^+), 16.1(2^+), 18.5(3^-), 19.6(4^-) and 20.6(3^-) states. The photon spectrum in figure 6 is unfolded by the sum of nine response functions, computed by a Monte Carlo code, plus a continuum background. Part of the observed background has probably a physical origin, but instrumental contributions like residual pile-up and bremsstrahlung cannot be excluded. The spectrum is divided into six energy intervals corresponding respectively to the ground state, 4.43 MeV, 9.64 MeV, 12.7 + 13.3 MeV, 15.1 + 16.1 MeV, 18 − 21 MeV excitation energy regions. The i-th interval has been fitted by one or more response functions, properly normalized to the detector efficiency, plus a linear background $B_i(E) = a_i E + b_i$. The parameter b_i is fixed by the requirement of continuity with the background in the adjacent intervals; the free parameters are therefore, for each interval, the slope a_i and the peak areas A_i, the peak width being fixed to the total experimental FWHM resolution, as deduced from a complete set of (p,γ_0) measurements in ^{11}B and ^{12}C [80]. The fit is started from the highest energy interval adjusting b_0 in order to get zero background at the end point of the spectrum; after optimization of the γ_0 peak area the tail of the response function is subtracted from all the higher excitation energy points and the same procedure is repeated to obtain a_i and A_i for the following intervals. The c.m. differential cross sections can be written

$$\frac{d\sigma}{d\Omega} = A_0[1 + \sum_{k=1}^{2L} Q_k a_k P_k(\cos\vartheta_{cm})] \qquad [1-43]$$

Recall (see [1-2]) that L is the maximum multipolarity order and the Q_k finite solid angle correction factors are, in the geometry of this experiment, nearly unity. The experimental data have been fitted to expression [1-43] limiting the sum to $L \leq 2$. A few analyses performed including higher order terms gave results systematically consistent with $a_5 = 0$. If only E1, M1 and E2 multipolarities are considered to be effective, the a_L coefficients are related to the multipole transition amplitudes $|E_L|^2$ and their interference terms $(E_L E_{L'})$ as summarized in table 1. The fit is unambiguous only when a complete angular range is

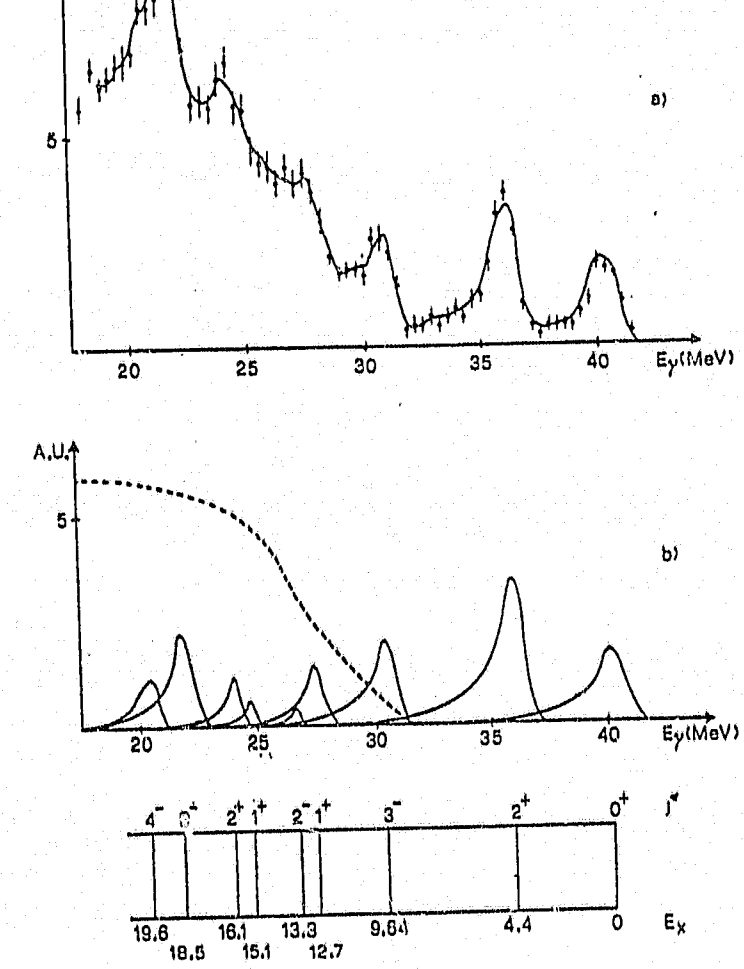

FIGURE 6 A photon spectrum from the reaction $^{11}B(p,\gamma)^{12}C$ at $E_p = 27$ MeV as it is deconvoluted in the sum of a continuous background (dashed line) and of nine peaks corresponding to transitions to a selected set of compound nucleus excited states.

scanned in the measurements. Since our data include angles from 35 deg to 125 deg only, further constraints have been imposed

$$\frac{d\sigma}{d\Omega} \geq 0 \qquad \frac{d\sigma}{d\Omega}(180) \leq \frac{d\sigma}{d\Omega}(150) \leq \frac{d\sigma}{d\Omega}(125) \qquad [1-44]$$

which are consistent with all the available theoretical estimates. As concerns the (p, γ_0) cross section and angular distributions, three different calculations can be compared to our data. The Bologna group [81] computes the electric transition matrix elements using RPA/Skyrme3 wave functions for the ^{12}C ground and scattering state. Tensor correlations, which are known to influence E1 strength above 30 MeV are neglected. Exchange currents are included by the use of the Siegert theorem. The continuous curve in figure 7 is the RPA result: the agreement is fairly good both in magnitude and energy dependence up to about $E_\gamma = 50$ MeV. Above this energy a gradually increasing deviation is observed for the a_1 and a_2 coefficients. The change of slope in a_3 and a_4 coefficients above 35 MeV in our data, probably related to a fast increase of E2 absorption above the GDR, is not reproduced and the calculation shows a more regular behaviour. The discrepancy could be due to the smoother energy distribution of RPA E2 strength in ^{12}C. The Bochum group [82] adopts a semi-direct interaction model, where ground state correlations are introduced in the energy independent shell model wave functions through a Yukava type effective N-N potential. Tensor correlations are partially included by a renormalization of the residual interaction strength to the dipole rule. Exchange currents are explicitely included. A better trend in the higher energy region is obtained as shown by the dotted curve in figure 7. Since the most significant difference in the two models is in the residual interaction used, we might speculate that also tensor correlations begin to influence the dipole cross section above 50 MeV. A third possible approach consists in a simple proton knock out model [83] if calculations are limited to the (γ, p_0) channel.But the evidence is that there is a strong dependence of the computed cross section from the adopted shell or optical model potentials [84][85], with no single particle potential being able to fit simultaneously the integrated cross section and its angular dependence (Figure 8). Besides a direct knock out model is inconsistent with the observed symmetry between (γ, p) and $\gamma, n)$ cross section, which can be accounted for only by including correlations in the nuclear wave functions. Proton capture experiments provide also information on the capture cross sections to various excited states of the compound nucleus. In ^{12}C we have observed up to 8 photon

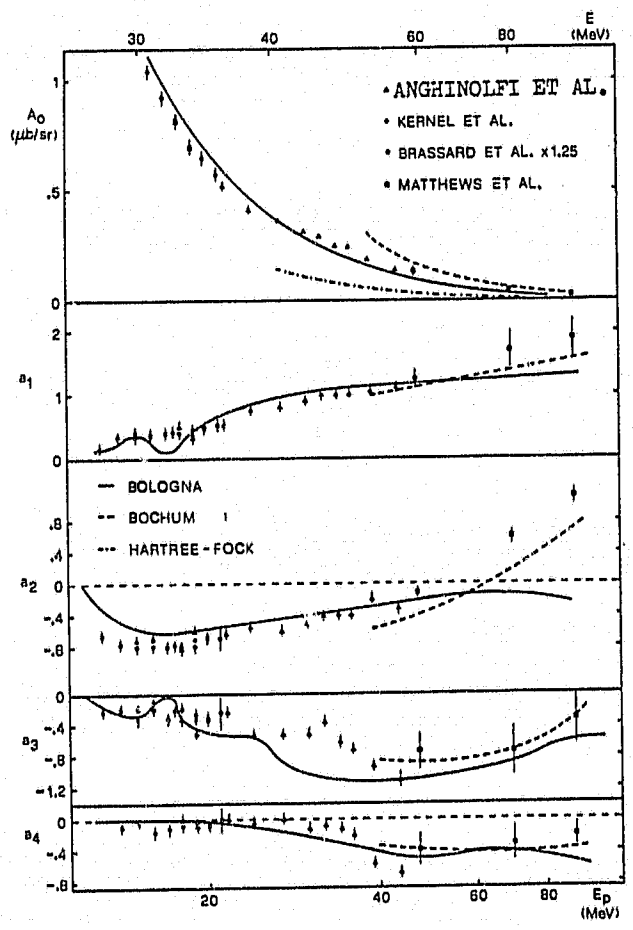

FIGURE 7 Angular distribution coefficients for the $^{11}B(p,\gamma_0)^{12}C$ compared to the theoretical calculations of reference [81] (full curves) and reference [82] (dashed lines).

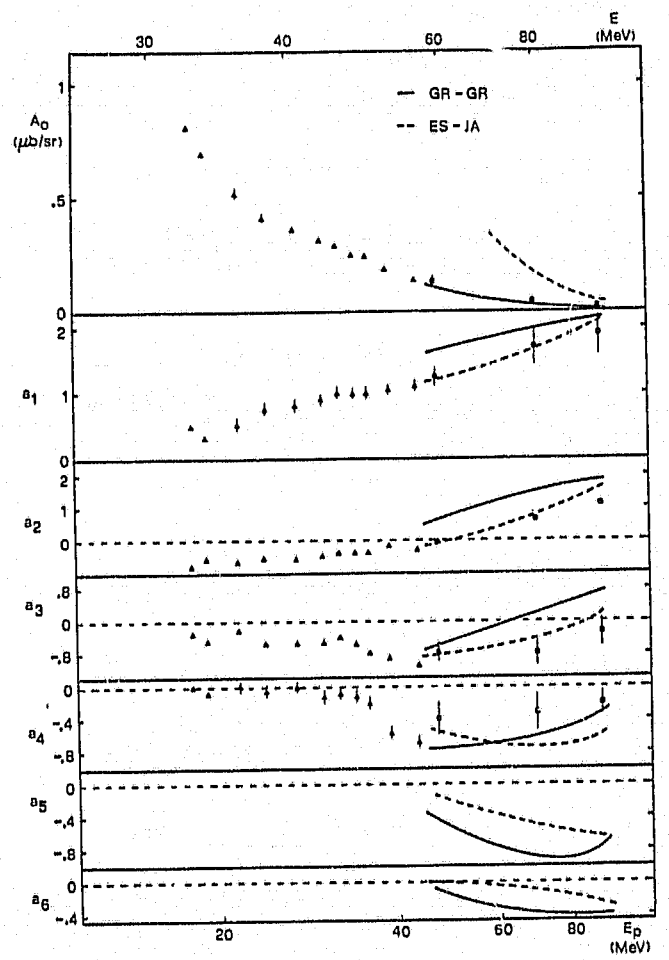

FIGURE 8 Angular distribution coefficients for the $^{11}B(p,\gamma_0)^{12}C$ compared to the predictions of a knock out model using different optical potentials.

peaks corresponding to all states having a large (or sufficiently large) spectroscopic factor for a 1p-1h configuration with the hole in the $1p_{\frac{3}{2}}$ shell. The integrated cross sections are recorded in figure 9 together with all existing data at lower energies. A systematic feature of these cross sections is the existence of giant dipole resonances based on each excited state of ^{12}C. Resonances have been in fact observed at all angles at 22.5, 25.5, 27.4, (28.5), 31.0, 33.2, 37 and 43 MeV. In figure 10-a are reported the integrated cross section.

$$\sigma_{int} = \int_{thresh}^{60\,\mathrm{MeV}} \sigma_{p\gamma_x}(\omega)d\omega \qquad [1-45]$$

from which the average excitation energy in each transition is computed

$$< E >= \int_{thresh}^{60\,\mathrm{MeV}} \omega\sigma_{p,\gamma_x}(\omega)d\Omega/\sigma_{int} \qquad [1-46]$$

In order to perform integration the (p,γ_x) cross sections were extrapolated to the threshold point using both a linear dependence and a Breit-Wigner resonant shape. Even with uncertainties associated with the assumed extrapolation, the resonance energy shifts upwards roughly proportionally to the excitation energy E_x of the coupled level (figure 10-b). The integrated cross section is almost equal; for the γ_0 and the γ_1 transitions; the other channels also show similar cross sections but of lower magnitude (Figure 10-a). These facts, together with the dominant E1 behaviour assigned by the angular distributions (figures 11, 12 and 13), support the very simple and attractive model where we have the new evidence that one can build a collective excitation not only upon the g.s. of a nucleus, but in practice also on a large set of excited states showing a dominant or significant single particle nature. In particular such a GDR can be built even upon states at $E_x \approx 20\,\mathrm{MeV}$ which correspond to the $1\hbar\omega$ excitation in the p-h scheme.

1-9 Second harmonic GDR and single particle states in ^{12}C

The existence of considerable proton capture strength, concentrated not only in the first few excited states, but also in the high lying states of light nuclei, was first remarked by Kovash et al. [86] for capture to ^{12}C, ^{13}N and ^{28}Si at 40, 60 and 80 MeV proton energy at an angle of 60 deg. An anticoincidence NaI-plastic scintillator spectrometer was used which ensured 3.8% resolution at $E_\gamma = 50\,\mathrm{MeV}$ and an efficient neutron rejection by the

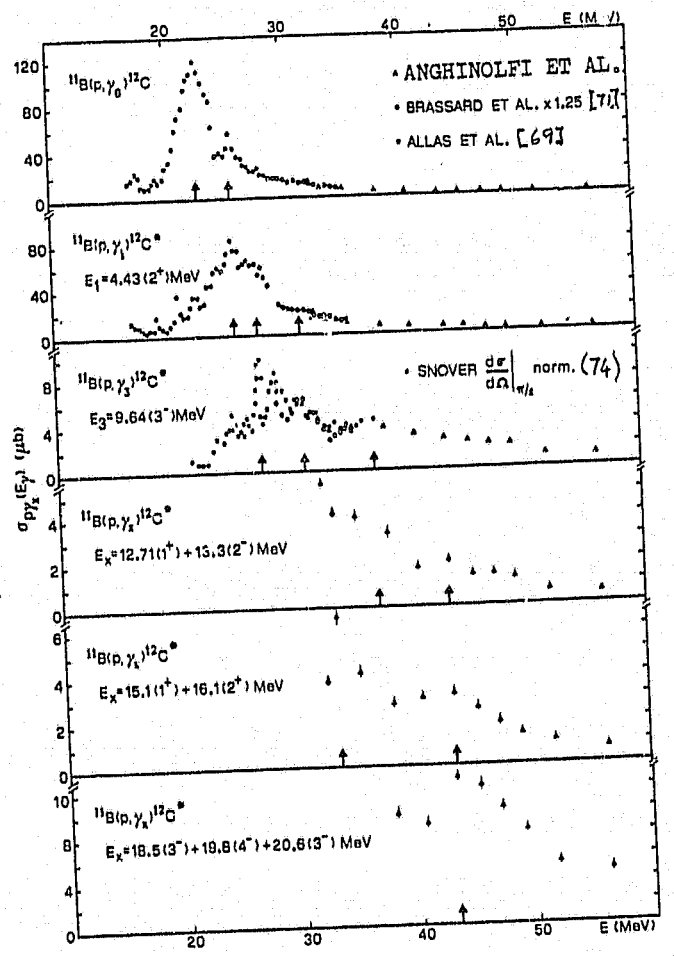

FIGURE 9 Total cross section for radiative capture transitions to the ground and excited states of ^{12}C as a function of excitation energy. All reaction channels show resonances.

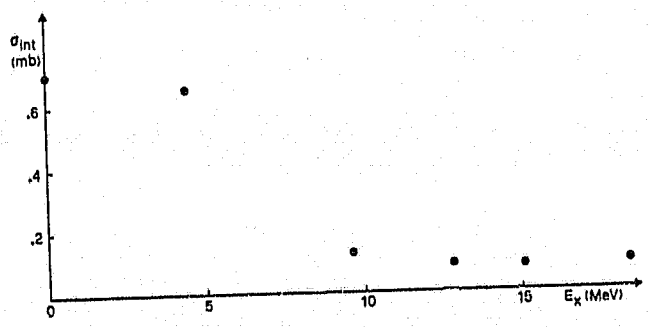

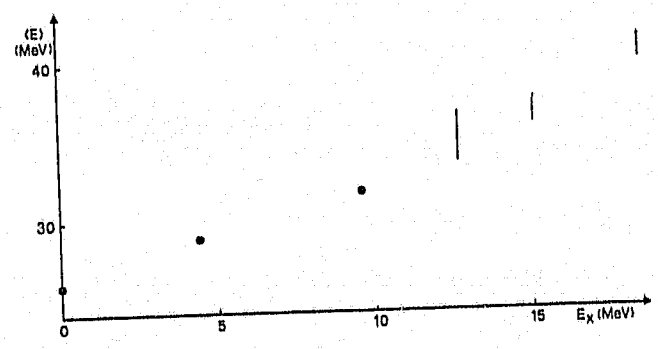

FIGURE 10 a)Total cross section for different final states in ^{12}C populated by proton radiative capture, as a function of excitation energy.
b) Centroid resonance energy as a function of the final state excitation energy. A linear behaviour is shown by the data.

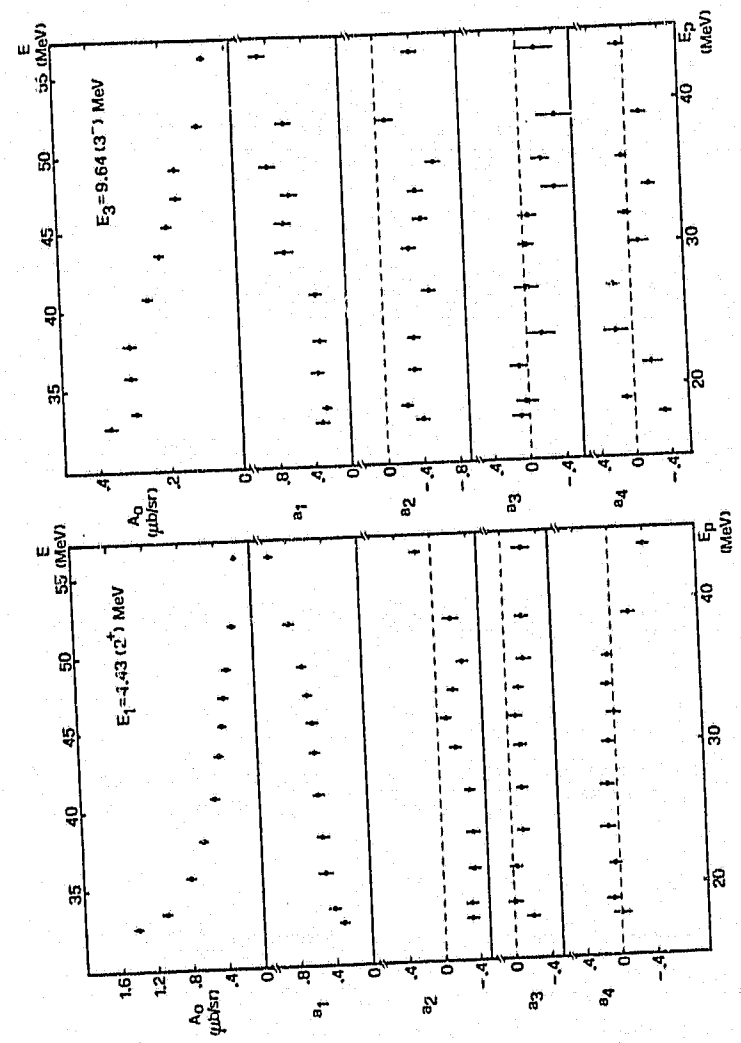

FIGURE 11 Angular distribution coefficients for proton radiative capture to final ^{12}C states at excitation energies of 4.43 MeV and 9.64 MeV.

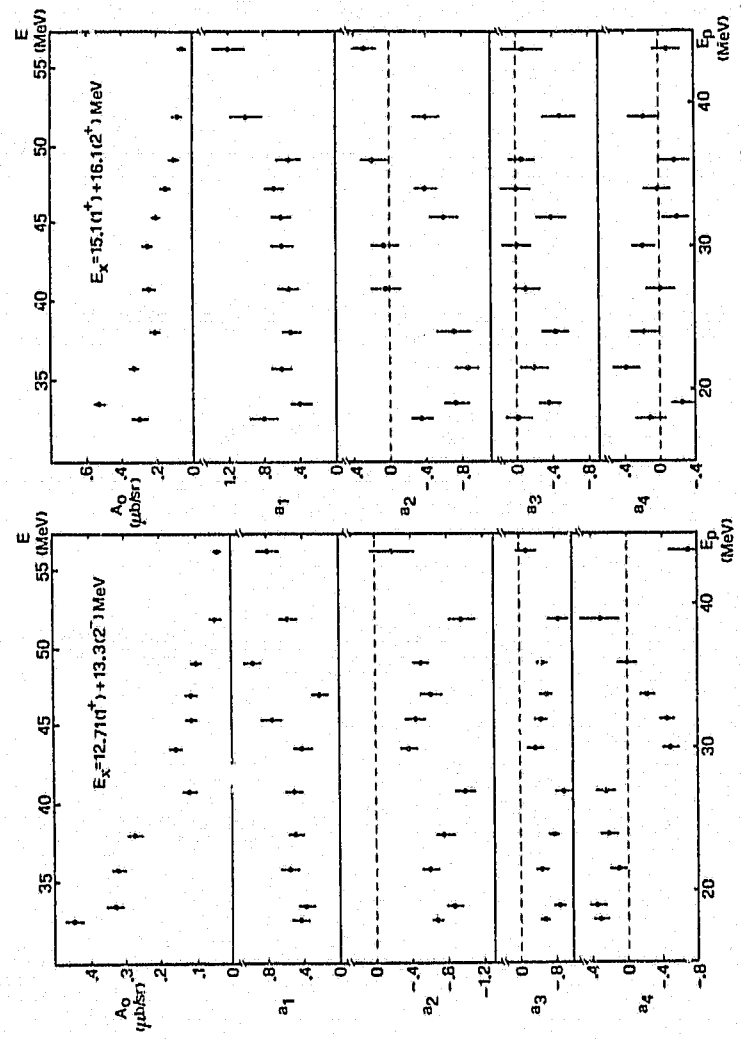

FIGURE 12 Angular distribution coefficients for proton radiative capture to final ^{12}C states at excitation energies of 12.71 + 13.3 MeV and 15.1 + 16.1 MeV.

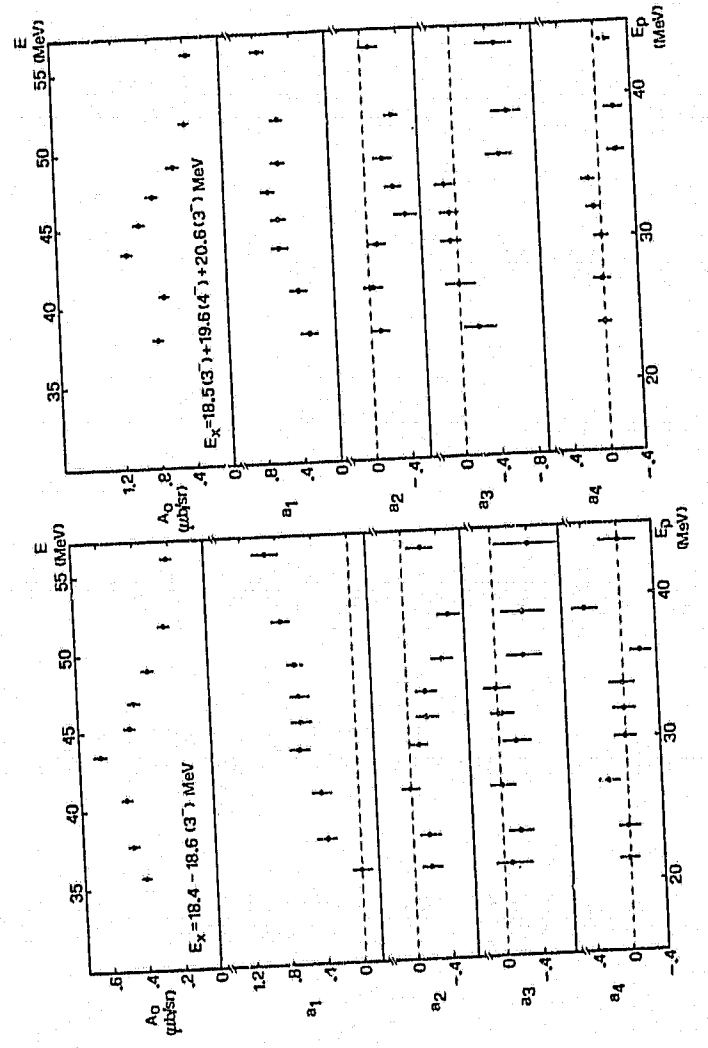

FIGURE 13 Angular distribution coefficients for proton radiative capture to final ^{12}C states at excitation energies of 18.4 + 18.6 MeV and 18.5 + 19.6 + 20.6 MeV.

time of flight technique with a 2.1ns FWHM resolution. All spectra showed transitions to the ground and first excited states. In addition a peak at 19.2 MeV is observed in ^{12}C at $E_p = 40$ and $E_p = 60$ MeV, and persists as a shoulder at $E_p = 80$ MeV. The peak moves with bombarding energy as expected for radiative proton capture to a state or a narrow group of states around 19.2 ± 0.6 MeV, with a differential cross section of $0.96 \pm 0.3\ \mu$b/sr at 40 MeV and $0.12 \pm 0.04\ \mu$b/sr at $E_p = 60$ MeV. Similarly a peak at 13.8 MeV excitation energy is seen in ^{28}Si, carrying a considerable strength and behaving in energy as observed for ^{12}C, indicating capture to a group of states at 13.8 ± 0.6 MeV with a differential cross section of $1.0 \pm 0.3\ \mu$b/sr at $E_p = 40$ MeV. If one thinks of these reactions as a direct process in which the proton radiates enough energy to drop into the appropriate particle orbit then, for target nuclei having a hole in the outermost shell, the transition should be favoured to those states having a large superposition with 1p-1h configurations. These states are therefore expected to have in ^{12}C a $(1p_{\frac{3}{2}})^{-1}1d_{\frac{5}{2}}$ configuration summming to $J^\pi = 4^-$ and in ^{28}Si a $(1d_{\frac{5}{2}})^{-1}f_{\frac{7}{2}}$ summing to $J^\pi = 6^-$. In (e,e') experiments [87] a 19.2 MeV 4^- state has been identified for ^{12}C and a 14.3 MeV 6^- state has been identified for ^{28}Si, in rather good agreement with the observations of Kovash. A shape much broader than in (e,e') experiments is observed in the corresponding (p,γ) peaks, suggesting that more members of the same 1p-1h configuration participate to some extent to the transition. Furthermore it is known the the 6^- state at ≈ 14 MeV in ^{28}Si decays 100% M1 to the 6^-, $T = 0$ state at 11 MeV and there is not evidence for a strong E1 decay of the 19.2 MeV state in ^{12}C to low lying states. Therefore these configurations should all have their electric dipole sum rule concentrated into transitions to or from states of higher energy. For example f wave capture on ^{11}B could produce a $(1p_{\frac{3}{2}})^{-1}1f_{\frac{7}{2}}$ state to decay by M1 to a $(1p_{\frac{3}{2}})^{-1}1d_{\frac{5}{2}}$ state. Similarly a g wave proton capture on ^{27}Al could produce a $(1d_{\frac{5}{2}})^{-1}1g_{\frac{9}{2}}$ resonance to decay E1 to a $(1d_{\frac{5}{2}})^{-1}1f_{\frac{7}{2}}$ state. Such a fact is confirmed experimentally and suggests the presence of second harmonic resonant capture ($2\hbar\omega$) that drops E1 to first harmonic ($1\hbar\omega$) excitations. Further support to the relevance assumed in proton capture by single particle states is supplied by capture to ^{13}N states where the dominant radiative transition is to the third excited $\frac{5}{2}^+$ state that has a substantial $d_{\frac{5}{2}}$ spectroscopic factor. Bumps observed at lower γ energy could not be related to capture reactions, due to the lack of energy points

taken and because there was not a one to one correspondence to reported levels in ^{13}N.

Extensive investigations of proton capture to a group of states around 19.2 MeV has been performed by a Triangle Ohio Indiana [88] collaboration which has produced a combined set of data, taken from just above the g.s. GDR up to $E_p = 60$ MeV, using the Triangle FN Tandem, the Triangle Cyclograaff and the Indiana cyclotron. A 60 deg yield curve taken in steps of 0.5 MeV from 23 to 32 MeV and larger steps above, an unpolarized angular distribution at $E_p = 28.7$ and an analyzing power [1-7] measurement at the same proton energy are discussed in terms of a direct capture mechanism also in comparison to what this approach predicts for capture transition to the ground and first excited states in ^{12}C. Very similar scintillation detectors were used at the two laboratories; they included an anticoincidence shield, additional gain stabilisation circuitry and time of flight $n - \gamma$ separation. Gamma spectra showed peaks having centroid energies corresponding to the ground state and states at 4.43, 9.64, 13.35, 15.11, 16.58, 18.52, 19.65 and 20.68 MeV. The line shape corresponding to these states, plus a background contribution evaluated at about 10% of the total yield, gave good fits to the observed spectra, producing absolute errors in the quoted cross sections of about 20%, these included normalization uncertainties between sets of data taken at the two laboratories. Combined unpolarized data and analyzing powers produced at the same energies, were deconvoluted together with previous results by the usual Legendre polynomial expansion [1-43], including the geometry factors Q_k. A direct capture model calculation was performed. The reaction is viewed as a mechanism in which the incoming nucleon undergoes a radiative transition from its scattering state to a single particle (bound or unbound) state of the residual nucleus. For nucleons captured by a 0 spin target to a definite ℓj final state via an electric transition of multipolarity L the total cross section is given by

$$\sigma_0^L = 2\pi\epsilon_L^2 \hbar c \left(\frac{e^2}{\hbar c}\right) \frac{k_\gamma}{E_a k_a} (2j+1) \frac{L+1}{L(2L+1)} \frac{k_\gamma^{2L}}{[(2L-1)!!]^2} \sum_{\ell_a j_a} |T^L_{\ell j, \ell_a j_a}|^2 \qquad [1-47]$$

Here ϵ_L is the effective charge, given for a target of mass A and charge Z and a projectile of charge z, by

taken and because there was not a one to one correspondence to reported levels in ^{19}N.

Extensive investigations of proton capture to a group of states around 19.2 MeV has been performed by a Triangle Ohio Indiana [88] collaboration which has produced a combined set of data, taken from just above the g.s. GDR up to $E_p = 60$ MeV, using the Triangle FN Tandem, the Triangle Cyclograaff and the Indiana cyclotron. A 60 deg yield curve taken in steps of 0.5 MeV from 23 to 32 MeV and larger steps above, an unpolarized angular distribution at $E_p = 28.7$ and an analyzing power [1-7] measurement at the same proton energy are discussed in terms of a direct capture mechanism also in comparison to what this approach predicts for capture transition to the ground and first excited states in ^{12}C. Very similar scintillation detectors were used at the two laboratories; they included an anticoincidence shield, additional gain stabilisation circuitry and time of flight $n - \gamma$ separation. Gamma spectra showed peaks having centroid energies corresponding to the ground state and states at 4.43, 9.64, 13.35, 15.11, 16.58, 18.52, 19.65 and 20.68 MeV. The line shape corresponding to these states, plus a background contribution evaluated at about 10% of the total yield, gave good fits to the observed spectra, producing absolute errors in the quoted cross sections of about 20%, these included normalization uncertainties between sets of data taken at the two laboratories. Combined unpolarized data and analyzing powers produced at the same energies, were deconvoluted together with previous results by the usual Legendre polynomial expansion [1-43], including the geometry factors Q_k. A direct capture model calculation was performed. The reaction is viewed as a mechanism in which the incoming nucleon undergoes a radiative transition from its scattering state to a single particle (bound or unbound) state of the residual nucleus. For nucleons captured by a 0 spin target to a definite ℓj final state via an electric transition of multipolarity L the total cross section is given by

$$\sigma_0^L = 2\pi\epsilon_L^2 \hbar c \left(\frac{e^2}{\hbar c}\right) \frac{k_\gamma}{E_a k_a} (2j+1) \frac{L+1}{L(2L+1)} \frac{k_\gamma^{2L}}{[(2L-1)!!]^2} \sum_{\ell_a j_a} \left| T^L_{\ell j, \ell_a j_a} \right|^2 \qquad [1-47]$$

Here ϵ_L is the effective charge, given for a target of mass A and charge Z and a projectile of charge z, by

$$\epsilon_L = [A^L z + (-1)^L Z]/(1+A)^L \qquad [1-48]$$

The quantities ℓ_a and j_a are the orbital and total angular momentum for the proton partial wave in the incident state. When it is assumed that the direct capture process depends only on the final state parentage to the target ground state plus a single nucleon, the matrix elements do not depend on the spin of the target nucleus. The case for a target with spin J_a is therefore given by

$$\sigma^L_{J_a} = \frac{2J_f+1}{(2J_a+1)(2j+1)}\sigma^L_0 \qquad [1-49]$$

where J_f is the total angular momentum of the final state and j is the total angular momentum of the particle in the final state. The transition matrix elements $T^L_{Lj,\ell_a j_a}$ are computed using the Lafferty and Cotanch [80] expression of the electromagnetic operators that includes the Siegert theorem since the nuclear current operator is replaced by the charge density operator. All but the first term of the complete expansion, scaled according to E_γ/mc^2 (0.03 for this case), are rejected. In the case where the nucleon is captured into a final state which is a continuum state having an energy E_f and a width Γ, the total cross section is obtained by integrating over the energy of the final state.

$$\sigma^L = \int\int \frac{d^2\sigma(E_f)}{d\Omega dE_f} dE_f d\Omega \qquad [1-50]$$

If a Breit Wigner shape is assumed for the cross section as a function of E_f, integration is equivalent to multiplying the cross section at the centroid energy E_f by a factor $\pi\Gamma/2$. Angular coefficients were also calculated starting from the transition matrix elements $T^L_{Lj,\ell_a j_a}$ using the formalism of Weller. Direct E1 plus E2 calculations were compared to both excitation function and angular distribution coefficients of the γ_0 and γ_1 captures in ^{12}C. It is observed that the direct capture cross section has the wrong energy dependence and underestimates by a factor of about 5 the experimental values around the peak energy, while at higher energies the direct capture model gives a satisfactory agreement. The angular distribution coefficients calculation is in remarkable agreement with the data but this has to be taken with some caution, since it has already been noticed that the

GDR has little effect, for example, on the a_2 coefficient since this depends basically on the gross average potential well and since a_1 and a_3 are very small and consequently affected by large statistical errors right in the region above the GDR, where the effect of a resonant capture is expected to produce a change of the order of 2 for the a_1/a_3 ratio. Two general conclusions, applicable to the γ_{10} transition too, are drawn. First the typical giant resonances observed in proton capture give an enhancement of the order of 5 above the direct capture model predictions. The opening of more channels and the spread-out of the CDR built upon highly excited states should reduce this factor. Secondly it is difficult to observe GDR-related effects on the angular distributions, at least at low energies where a_1 and a_3 in particular are confused with zero. More possibilities of seeing departures from a direct mechanism in an angular distribution, should be offered at higher energies but we cannot ignore possible deviations of the E2 strength from direct capture predictions, with a consequent reduction of every E1 enhancement. Nor we can ignore the possible presence of many intereference terms in a_1 and a_3, that could introduce large variations in them.even for small phase changes. In any case the observation of significant departures from a direct capture mechanism should be very reliably taken as the effect of a resonant phenomenon. Three different calculations were performed for the (p,γ_{19}) reaction channel. In the first the assumption is that the single particle dominant strength is $d_{\frac{5}{2}}$ and that the $d_{\frac{5}{2}}$ single particle state is bound. A convenient Woods Saxon potential ($V = 63.3\,\mathrm{MeV}$, $r_0 = 1.25\,\mathrm{fm}$, $a = 0.65\,\mathrm{fm}$ and $V_{so} = 8.75\,\mathrm{MeV}$) placed the $d_{\frac{5}{2}}$ state just below the proton threshold at 15 MeV. This value is clearly unphysical but the energy in the cross section kinematic factors is taken to be 19.2 MeV. The proton binding energy is $-1.0\,\mathrm{MeV}$. The continuum wave function was generated from the optical model potential that fitted 30 MeV proton elastic scattering data [90]. In the second and third calculation the final state was treated as a continuum state described by an optical potential having the imaginary part alternatively set at 0 and 0.5. A summary of the adopted incident and final state potentials is given in table 11 while a summary of the calculated angular distributions is given in table 12. It is claimed that the bound final state calculation already gives a good description of both the main features of the excitation function, that incidentally peaks around 30 MeV

TABLE 11

Woods Saxon potential parameters

Parameter	Incident potential	Final state pot.
V(MeV)	45.2	55
W(MeV)	3.38	0.0-0.5
V_{so}(MeV)	7.79	6.64
r_0(fm)	1.09	1.23
r_s(fm)	1.3	1.16
r_{so}(fm)	0.98	1.03
a_0(fm)	0.59	0.66
a_{so}(fm)	0.97	0.66
r_c(fm)	1.29	1.10

TABLE 12

Computed angular distribution coefficients

	Bound	Cont. $W = 0$	Cont. $W = .5$	Exper.
a_1	0.44	0.56	0.35	0.37 ± 0.05
a_2	-0.57	-0.52	-0.52	-0.50 ± 0.09
a_3	-0.16	-0.22	-0.20	-0.27 ± 0.07
b_1	0.084	0.092	0.096	0.02 ± 0.016
b_2	-0.044	-0.041	-0.040	-0.027 ± 0.008
b_3	-0.022	-0.026	-0.027	-0.016 ± 0.0006

and 81% of its total is accounted for strength by the E1 contribution alone, and of the angular distributions with the exception of the b_1 coefficient. However the energy dependence of the data is not reproduced above 30 MeV. The investigated energy dependence of the optical potential used to describe the initial state was found insignificant regarding a better agreement between data and calculations. The situation is unexpectedly worse for the more realistic continuum final state calculations, and seems to suggest the presence of additional strength in the data: a giant resonance, enhanced by a factor of three above the

direct capture being one possibility, according to Londergan and Ludeking [92] who give a direct contribution already in marked disagreement with the present one.

The above mentioned work of Londergan and Ludeking [92] deserves attention, in view of the concepts of direct and semidirect processes that it includes and of the further refinements of Blatt et al. [93] that resulted so succesfully in explaining remarkable analogies in proton radiative capture to adjacent nuclei. For nucleon radiative capture reactions the transition amplitude

$$M_{fi}^{(\lambda)} = -\int d\vec{r} < \psi_f | \vec{J}(\vec{r}) \cdot \vec{A}_\lambda(\vec{r}) | \psi_i > \qquad [1-51]$$

is calculated. Here ψ_i is the nuclear wave function which is composed of an incident proton of momentum k_i and the ground state of the target nucleus, ψ_f is the final state wave function. $\vec{A}_\lambda(\vec{r})$ is the electromagnetic potential for the creation of a photon with momentum $\vec{k}_\lambda$, energy $\omega_\gamma = |\vec{k}|$, elicity λ and polarization $\vec{\epsilon}_\gamma(\vec{k})$ and is given by

$$\vec{A}_\lambda(\vec{r}) = \frac{2\pi}{\omega_\gamma} \vec{\epsilon}^*(\vec{k}_\gamma) e^{-i\vec{k}_\gamma \cdot \vec{r}} \qquad [1-52]$$

The current operator is expressed only in terms of one body convection and spin magnetic currents and has the form

$$\vec{J}(\vec{r}) = e \sum_{\alpha=1}^{A} \{ [\frac{1+\tau_3(\alpha)}{2iM_N}] \frac{1}{2} [\delta(\vec{r}_\alpha - \vec{r}) \vec{\nabla}_\alpha - \vec{\nabla}_\alpha \delta(\vec{r}_\alpha - \vec{r})] + \delta(\vec{r}_\alpha - \vec{r}) \frac{\mu_\alpha}{2M_N} \vec{\sigma}(\alpha) \times \vec{\nabla} \} \qquad [1-53]$$

μ_α being the nucleon magnetic moment and $\tau_3(\alpha)$ the isospin component. Siegert theorem has been used to replace the divergence of the one body current by the matrix elements of a one body operator between the initial and final wave functions and the magnetic multipole contribution has been added separately. The transition matrix elements are calculated in a spectator formalism: i.e. the incident nucleon is assumed to radiate a photon in the presence of the strong target field under the following hypotheses: i) the incident and final wave functions can be factored into a single particle wave function times an internal wave function for the residual nucleus ii) the residual nucleus remains in the same internal

state throughout the reaction. In other words the $(A-1)$ particles core remains in its ground state. In particular it is assumed that the g.s. of ^{11}B can be represented by a $(1p_{\frac{3}{2}})^{-1}$ state and that the final states populated are either the ^{12}C g.s. or particle hole states with a $(1p_{\frac{3}{2}})^{-1}$ component. The incoming proton wave function was deduced from a nucleon-nucleus potential of the form

$$\vec{U}(\vec{r}) = V_C(r) - [V_0 f(r) + 4aW_D \frac{d}{dr} f(r)] + \frac{1}{m^2} V_{so} \frac{1}{r} \frac{d}{dr} f(r) \vec{L} \cdot \vec{\sigma} \qquad [1-54]$$

with V_D and W_{so} taken from Halderson and Philpott who fitted proton scattering off ^{12}C. The form factor $f(r)$ is a Woods Saxon well with radius $r_0 = 1.25$ fm and diffuseness $a = 0.55$ fm while the coulomb potential $V_C(r)$ is that due to a charged sphere of radius $1.25A^{1/3}$ fm. The final proton single particle wave functions were computed from the potential of Birkholtz which is basically similar to the one above with $W_D = 0$. The $1d_{\frac{5}{2}}$ wave function, calculated with this potential gives results which are unbound but confining it inside a spherical box of radius 10 fm produces results equivalent to more realistic calculations that employ continuum wave functions in the final state. Computed (p, γ_0) angular distributions show a large E1 dominance at $E_p \approx 7$ MeV and a forward shift at higher energy where higher order electric multipoles and the spin magnetisation current start to play a role. Calculations were made for the (p, γ_{19}) transition, with all the $1d_{\frac{5}{2}}$ strength concentrated at 19.2 MeV, despite the Gillet and Vinh-Mau RPA calculations which showed that strength is rather distributed amongst a set of 2^-, 3^- and 4^- $(T=0, T=1)$ particle-hole states in an energy range from 18.4 to 20.6 MeV. For the (p, γ_{19}) angular distributions the E1 dominance is seen at $E_p = 21$ MeV with a strongly forward peaking as the energy increases. It is obviously necessary to cater for the fragmentation of the $1d_{\frac{5}{2}}$ strength over a much wider energy range or to consider a more realistic distribution of particle-hole strength in the 18.4 – 20.6 MeV range that includes $1d_{\frac{5}{2}}$, $1d_{\frac{3}{2}}$ and $2s_{\frac{1}{2}}$ particle hole states coupled to a $1p_{\frac{3}{2}}$ hole as predicted by Gillet and Vinh-Mau. For the latter case a calculation has been performed, while for the former case a previous work of Tsai and Londergan [94] showed that almost 80% of the $d_{\frac{5}{2}}$ strength is concentrated in the energy range of interest, and therefore the computed results multiplied by 0.8 should give a very reasonable estimate of the cross section values. As a matter of fact the two

calculations do not differ significantly. Comparison of this direct calculation to the (p,γ_0) the $(p,\gamma_{0,6})$ and the (p,γ_{19}) data shows similar results. The experimental peak occurs at a higher energy than predicted, the magnitude of the cross section at the resonance peak is larger than computed, the energy dependence is not reproduced. This was succesfully attributed by Brown for the (p,γ_0) transition, to the coupling of the photon to a coherent set of particle-hole states which were coupled to the initial state via the residual interaction. Assuming that all of the electric dipole strength is contained in a single state at $1\hbar\omega$ excitation energy, the "qualitative" effect of coupling to the giant dipole resonance (the particle hole coherent set) can be taken into account by multiplying the E1 contribution to the direct capture amplitude by an enhancement factor

$$M_{DSD}(E1) \approx M_D(E1)\left[1+\frac{\Delta E}{E_\gamma - E_R + i\frac{\Gamma_R}{2}}\right] \qquad [1-54]$$

where M_{DSD} includes both the direct capture part M_D and the semidirect part. ΔE is the shift in energy between the dipole state and the average unperturbed particle-hole state, E_R and Γ_R are the energy and width of the GDR, and E_γ is the photon energy. For the g.s. GDR a good fit is obtained using $\Delta E = 4.0\,\mathrm{MeV}$, $E_R = 22.5\,\mathrm{MeV}$ and $\Gamma_R = 3.5\,\mathrm{MeV}$. With nearly identical ($E_R = 23\,\mathrm{MeV}$ and $\Delta E = 4.0\,\mathrm{MeV}$) values and a reasonable $\Gamma_R = 12.0\,\mathrm{MeV}$, the agreement is also very good for the γ_{19} transition. The same parameters do not give satisfactory fits to the $\gamma_{0,6}$ excitation function testifying, as already remarked , that the 9.63^- state has not a dominant 1p-1h configuration. From these results and the experimental evidence of Anghinolfi et al. [78], the following behaviour emerges (and we shall see later how it becomes general for light nuclei):

1) In radiative capture reactions we expect to see large (p,γ) transitions to every state which is strongly excited in proton stripping reactions on the same target nucleus; that is to states that have a large superposition with a 1p-1h configuration having a proton in a shell model orbit and the target nucleus as a core.

2) Every such state will have a giant dipole resonance whose energy will in first approximation be identical to the photon energy of the GDR built on the g.s. and whose width will increase as the excitation energy of the state increases.

3) The dominant reaction mechanism is the semidirect one in which the incident proton creates a particle-hole pair via the residual interaction and makes a transition into a single particle state. The particle-hole pair then couples to the photon producing the resonance.

Further support to the single particle character of the proton radiative capture to many of the excited states in light nuclei comes from the analysis of data belonging to neighbouring nuclei and to states which can be described as the target core plus a proton in a single particle orbit. Remarkable similarities have been first observed by Blatt et al. [93] for the reactions $^{11}B(p,\gamma)^{12}C$ and $^{12}C(p,\gamma)^{13}N$ but a similar behaviour has also been observed for nuclear pairs like ^{28}Si and ^{29}P or ^{16}O and ^{17}F. Comparing gamma spectra collected at the same proton energy, $E_p = 28.5\,MeV$, for the $^{11}B(p,\gamma)^{12}C$ and $^{12}C(p,\gamma)^{13}N$, the dominant feature in the ^{12}C spectrum is the capture to a cluster of states around 19 MeV which are of $(1p_{\frac{3}{2}})^{-1}1d_{\frac{5}{2}}$ in character, while the ^{13}N spectrum is dominated by the transition to the $\frac{5}{2}^+$ third excited state. The gamma ray energies corresponding to these transitions are nearly identical. Equally similar in character are the captures to the ground state of ^{13}N, which is $(1p_{\frac{1}{2}})$ in character and to the 2^+ 4.43 MeV first excited state in ^{12}C which is basically a $(1p_{\frac{3}{2}})^{-1}1p_{\frac{1}{2}}$ state. The excitation curves, angular distributions and analyzing powers for these pairs of transitions are, within the experimental errors, significantly similar. A generalized direct plus semidirect model has been proposed which is effective in predicting these remarkable similarities. The basic assumptions of this model are that

i) the initial and final states in the capture process can be represented by states constructed from orthogonal one nucleon configurations and

ii) the electromagnetic transition operator can be represented as a sum of one body operators. The extent to which violation of this second hypothesis is important in spectroscopic applications is not treated though the interaction Hamiltonian does necessarily contain two body operators due to the exchange of charged mesons between nucleons. The transition amplitude is written as

$$M = < J_f M_f T_f T_{f3} | H^\lambda | J_i M_i s m_s T_i T_{i3} t t_3 > = < \psi_f | H^\lambda | \psi_i > \qquad [1-55]$$

where the initial state is characterized by the target nucleus quantum numbers $J_i\, M_i,\, T_i\, T_{i3}$ and the projectile quantum numbers $s\, m_s\, t\, t_3$; the final state for the compound nucleus has the quantum numbers $J_f\, M_f\ T_f\, T_{f3}$ and H^λ is the electromagnetic Hamiltonian that creates a photon with energy $E_\gamma = E_i - E_f$ and elicity λ. The differential cross section and analyzing power are given by

$$\sigma = \frac{1}{2s+1}\frac{1}{2J_i+1}\sum_{m_i,m_s,M_f,\lambda} MM\dagger = \frac{1}{2s+1}\frac{1}{2J_i+1}\mathrm{Tr}(MM\dagger) \qquad [1-56]$$

$$\sigma A_y = \frac{1}{2s+1}\frac{1}{2J_i+1}\sum_{m_i,m_s,M_f,\lambda} M\sigma_y M\dagger = \frac{1}{2s+1}\frac{1}{2J_i+1}\mathrm{Tr}(M\sigma_y M\dagger) \qquad [1-57]$$

With the formalism of projection operators, introducing $P + Q = 1$, where P is the operator that projects from the space of the nuclear Hamiltonian that part which corresponds to a nucleon coupled to the target ground state (Q is its complement), one gets easily

$$M = < P\psi_f|H^\lambda|P\psi_i > + < P\psi_f|H^\lambda|Q\psi_i > + \\ < Q\psi_f|H^\lambda|P\psi_i > + < Q\psi_f|H^\lambda|Q\psi_i > \qquad [1-58]$$

The first term where both the initial and final state look like the target ground state plus a nucleon in a shell model orbit, is the usual direct term. The second and third term include core excitation in the initial or final state and are what normally is retained as a semidirect transition. Due to the hypothesis made on the exclusively one-body operator character of H^λ, only the components of $Q\psi_i$ and $Q\psi_f$ which are a one particle-one hole excitations of the target ground state, can contribute to the semidirect amplitudes. Introducing $q(P)+r = 1$ where $q(P)$ is the projection operator that projects from the space of the nuclear Hamiltonian that part which corresponds to all configurations consisting of a nucleon coupled to a one particle-one hole excitation of the target core (r is the complement) and defining $A(P)$ from the $q(P)\psi_i = A(P)P\psi_i$ one can write

$$< P\psi_f|H^\lambda|Q\psi_i > = < P\psi_f|H^\lambda|q(P)\psi_i > = < P\psi_f|H^\lambda A_i(P)|P\psi_i > \qquad [1-59]$$

$$< Q\psi_f|H^\lambda|P\psi_i >=< q(P)\psi_f|H^\lambda|P\psi_i >=< P\psi_f|A_f(P)^\dagger H^\lambda|P\psi_i > \qquad [1-60]$$

Of course $q(P)$ is not necessarily identified with physically excited states of the target since many of the excited states are known to have a more complex configuration than the one described by $q(P)$. In other words the partition of the Q space in this generalized model is in terms of the particle-hole excitations of the target ground state and not of the physically excited states of the target itself. The transition amplitude is then written as

$$M =< P\psi_f|H^\lambda_{eff}|P\psi_i > + < Q\psi_f|H^\lambda|\psi_i >= M_{dsd} + < Q\psi_f|H^\lambda|\psi_i > \qquad [1-61]$$

where

$$H^\lambda_{eff} = H^\lambda + H^\lambda A_i(P) + A_f(P)\dagger H^\lambda \qquad [1-62]$$

and M_{dsd} is analogous to the direct semidirect amplitude originally introduced by Brown for electric dipole capture in the long wavelength approximation. In this formulation are populated those components of the final state whose parentage derives from the projectile and target in the entrance channel both in the direct amplitude and in the semidirect via one particle one hole excitations of the target nucleus, included in the effective Hamiltonian H^λ_{eff}. Neglecting non-direct mechanisms included in the second term of [1-61], one can compare nucleon radiative captures to closed shell and closed shell plus one nucleon nuclei. $< P\psi_f|$ is proportional to the square root of the spectroscopic factors $(C^2S)^{1/2}$ where C is the Clebsh Gordan coefficient for the coupling of nucleon and target isospins to the compound nucleus isospin. So we can write

$$\begin{aligned} M_{dsd} &= \sum_j (C^2S)^{1/2} < J_iM_ijm|J_fM_f > M_{dsd}(j) \\ &= \sum_j (C^2S)^{1/2} < J_iM_ijm|J_fM_f >< jm|h^\lambda_{dsd}|sm_s > \end{aligned} \qquad [1-63]$$

where j is the final state single particle angular momentum constrained by $|J_i - J_f| \leq j \leq J_i + J_f$. The cross section and analyzing power can be rewritten in terms of M_{dsd} as

$$\sigma = \frac{2J_f+1}{(2s+1)(2J_i+1)} \sum_j \frac{1}{2j+1} (C^2S)^{1/2} \sum_{m_s, m_\lambda} [M_{dsd}(j) M\,\dagger_{dsd}(j)] \qquad [1-64]$$

$$\sigma A_y = \frac{2J_f+1}{(2s+1)(2J_i+1)} \sum_j \frac{1}{2j+1} (C^2S)^{1/2} \sum_{m_s, m_\lambda} [M_{dsd}(j) \sigma_y M\,\dagger_{dsd}(j)] \qquad [1-65]$$

The nuclear structure information can be assumed as entirely contained in the angular momenta and spectroscopic factors since, though M_{dsd} has a structure dependence due to the average nuclear field of the target g.s. and of the coherent 1p-1h excitation of the target g.s., the effect of it can be considered , in adjacent nuclei, smaller than the 20% uncertainty that is carried by the spectroscopic factors. If two transitions are dynamically equivalent, in the sense that will be clarified soon, then M_{dsd} should be equivalent in the two cases. For a core target being a closed shell nucleus $J_i = 0$ then $j_f = J_f = j$ and $T_f = t_f$, therefore

$$\sigma(0, j_f, j_f) = \frac{1}{2s+1} C^2S(0, j_f, j_f, t_f) \mathrm{Tr}[M_{dsd}(j_f) M\,\dagger_{dsd}(j_f)] \qquad [1-66]$$

and

$$A_y(0, j_f, j_f) = \frac{\mathrm{Tr}[M_{dsd}(j_f) \sigma_y M\,\dagger_{dsd}(j_f)]}{\mathrm{Tr}[M_{dsd}(j_f) M\,\dagger_{dsd}(j_f)]} \qquad [1-67]$$

The comparison with a transition to a state in an adjacent closed shell nucleus is meaningful only if the transition is dominated by a state with $j = j_f$, in which case one has

$$\sigma(J_i, j_f, J_f) = \frac{2J_f+1}{(2J_i+1)(2j_f+1)(2s+1)} C^2S(J_i, j_f, J_f, T_f) \mathrm{Tr}[M_{dsd}(j_f) M\,\dagger_{dsd}(j_f)] \qquad [1-68]$$

and

$$A_y(J_i, j_f, J_f) = \frac{\mathrm{Tr}[M_{dsd}(j_f) \sigma_y M\,\dagger_{dsd}(j_f)]}{\mathrm{Tr}[M_{dsd}(j_f) M\,\dagger_{dsd}(j_f)]} \qquad [1-69]$$

If the kinematical conditions in the two reactions are similar, then

$$M_{dsd}(j_f)\big|_{J_i,j_f,J_f} = M_{dsd}(j_f)\big|_{0,j_f,j_f} \qquad [1-70]$$

and one can draw two immediate very important conclusions from the model.

i) The analyzing powers are identical

ii) The cross sections will have the same behaviour and will be related by

$$\frac{\sigma(J_i,j_f,J_f)}{\sigma(0,j_f,j_f)} = \frac{2(J_f+1)}{(2J_i+1)(2j_f+1)} \frac{C^2S(J_i,j_f,J_f,T_f)}{C^2S(0,j_f,j_f,t_f)} \qquad [1-71]$$

The model finds great support from the experimental case, where the conditions under which the model calculations were performed, are in practice fulfilled as it can be seen from Table 13.

TABLE 13

Compared reactions and kinematics

Case	Fin. Nucl.	E_p	$E_p(c.m.)$	E_γ	Orbit ℓ_j	E_x	J_π
a	^{12}C	28.5	26.1	27.7	$d_{5/2}$	19	$1^-,2^-,3^-,4^-$
b	^{13}N	28.5	26.3	21.9	$d_{5/2}$	3.53	$5/2^+$
c	^{12}C	28.5	26.1	37.9	$p_{1/2}$	4.43	2^+
d	^{13}N	28.5	26.3	28.4	$p_{1/2}$	0	$1/2^+$

Comparison of cases a and b must take into account that while the state at 3.5 MeV in ^{13}N is well resolved, contributions to the 19 MeV excitation energy region in ^{12}C may come from few $4^-,3^-,2^-$, or 1^- states, giving to the ratio of the total cross sections the form

$$R = \sum_{J_f=1,4;T} R(J_f,T) = [(\tfrac{3}{48})C^2S(\tfrac{3}{2},\tfrac{5}{2},1^-,T) + (\tfrac{5}{48})C^2S(\tfrac{3}{2},\tfrac{5}{2},2^-,T) + (\tfrac{7}{48})C^2S(\tfrac{3}{2},\tfrac{5}{2},3^-,T) + (\tfrac{9}{48})C^2S(\tfrac{3}{2},\tfrac{5}{2},4^-,T)\frac{1}{C^2S(0,\frac{5}{2},\frac{5}{2}^+,\frac{1}{2})} \qquad [1-72]$$

The observed γ_{10} transition should have contributions from $(4^-,1)$, $(4^-,1)$ and $(3^-,1)$ states. Taking for the spectroscopic factors of all three states a value of 0.9, which is equally

close to those calculated by Donnelly and Walker (0.984)[95] and by Hanna et al. (0.862)[96] for the $(3^-, 1)$, and a value of 0.5 for the $C^2S(0, \frac{5}{2}, \frac{5}{2}+\frac{1}{2})$ we get a value of $R = 0.94$ as experimentally found. Comparison for cases c and d where the spectroscopic factors are $C^2S(\frac{3}{2}, \frac{1}{2}, 2, 0) = 1.41$ as established by Adelberger [97] and $C^2S(0, \frac{1}{2}, \frac{1}{2}, 2, 0) = 0.48$ as measured by Peterson and Hamill [98], gives $R = 0.92$ as experimentally observed.

Evidence has been also established by Blatt et al. [99] of the existence of a $3\hbar\omega$ resonance built upon $2\hbar\omega$ states in ^{13}C. In fact capture strength to final states in the vicinity of 42 MeV has been seen and the yield curve for these transitions from $E_p = 45$ to $E_p = 70$ MeV [$E_x = 56$ to $E_x = 80$ MeV] shows a very broad peak centered at about $E_x = 65$ MeV.

Polarized proton capture to the ground and first excited states of ^{12}C has firstly been reported by Glavish et al. [100] at proton energies of 6, 8, 9.5, 10.4, 12.5 and 14 MeV, where $A(\vartheta)$ were measured as a complement to previous work with unpolarized beams. Since it was proved that

$$\sigma(\vartheta) = A_0[1 + a_1P_1 + a_2P_2] \qquad [1-73]$$

and therefore one has to expect

$$A(\vartheta) = \sum_{k=1} b_k \sin(k\vartheta)[1 + a_1P_1 + a_2P_2]^{-1} \qquad [1-74]$$

the b_k coefficients can be extracted from the data. These are basically consistent with a $\sin(2\vartheta)$ behaviour as shown by the very small b_1 and b_3 values necessary (e.g. $b_1 = 0$, $b_2 = -0.14$ and $b_3 = -0.04$ at $E_p = 8$ MeV) and the average simpler situation is that describing the giant resonance for the (p, γ_0) transition as characterized by an $a_2 = -0.60$ and a $b_2 = -0.18$ with all other coefficients set to zero. Following the same arguments [60] that led to an expression for a_2 one has

$$a_2 = -0.445\mathrm{Re}(\alpha\beta*) + 1.336\mathrm{Re}(\alpha\gamma*) + 0.60\mathrm{Re}(\beta\gamma*) + 0.40|\beta^2| - 0.40|\gamma^2| \qquad [1-75]$$

$$b_2 = -0.474\mathrm{Im}(\alpha\beta*) - 0.947\mathrm{Im}(\alpha\gamma*) - 1.061\mathrm{Im}(\beta\gamma*) \qquad [1-76]$$

$$|\alpha^2| + |\beta^2| + |\gamma^2| = 1 \qquad [1-77]$$

with $\alpha = s_{\frac{1}{2}}\, e^{i\phi_s}$, $\beta = d_{\frac{3}{2}}\, e^{i(\phi_d - \delta)}$ and $\gamma = d_{\frac{5}{2}}\, e^{i\phi_d}$. Five unknowns, namely $s_{\frac{1}{2}}$, $d_{\frac{3}{2}}$, $d_{\frac{5}{2}}$, $\phi_d - \phi_s$ and δ cannot be determined uniquely from a set of three equations and one has to consider paths into the configuration space for such quantities. When these paths are calculated for $\delta = 0, \pm 15$ deg, there are two solutions: one very little sensitive to the selected δ value (solution I) and one quite sensitive to it (solution II). The overall limit values obtained combining the two solutions indicate a minimum $|s_{\frac{1}{2}}|^2$ value between 0.02 and 0.08 (as opposed to a 0.01 value from unpolarized data only), a minimum $|d_{\frac{3}{2}}|^2$ between 0.07 and 0.23 (previously 0.10), and a maximum $|d_{\frac{3}{2}}|^2$ value between 0.14 and 0.49 (previously 0.52). It is worth noting that predicted Coulomb phase shifts ($\delta = 0$, $\phi_d, \phi_s = 18 - 27$ deg) are only possible within solution I. The discussion previously reported [69] is still valid.

1-10 Radiative proton capture on and above the GDR in ^{13}N

The reaction $^{12}\mathrm{C}(p,\gamma)^{13}\mathrm{N}$ has been studied in the range $9 < E_p < 24$ MeV by Berghofer et al.[101]. The radiative captures analysed included firstly the (p,γ_0) transition from $E_p = 14.0$ to $E_p = 24.4$ MeV, compared to data from other experiments below and above the GDR. The analysis concerned as well the (p,γ_1) transition to the 2.37 MeV $\frac{1}{2}^+$ state from $E_p = 19.8$ to $E_p = 24.4$ MeV and finally the (p,γ_{2+3}) to the unresolved doublet at 3.51 ($\frac{3}{2}^-$) and 3.55 ($\frac{5}{2}^+$) MeV, which confirmed previous data taken by the same group with poorer gamma energy resolution and larger energy steps. Inelastic scattering to the 12.71 MeV ($1^+, T = 0$) and the 15.11 MeV ($1^+, T = 1$) levels was also considered in great detail. Gamma rays were detected by a large (25.4 cm, Ø×25.4 cm) NaI crystal surrounded by a thick anticoincidence plastic scintillator placed laterally and in front, for a total FWHM resolution of 3% at 15.11 MeV obtained when count rate was kept low. For all (p,γ_x) transitions 90 deg excitation functions were provided and seven point angular distributions for the (p,γ_0) channel were collected at various energies, in particular in correspondence with specific structures of the excitation function. The strength of the

γ_0 GDR is split into two broad resonances centered at $E_p = 13$ and $E_p = 20.5$ MeV, with perhaps some strength remaining in the energy region around 32 MeV as shown in the earlier data of Fisher et al.[102], but not so evident in more recent [103], high resolution data. On the low energy side of the first main structure at 13 MeV, apart from the sharp ^{13}N excited states populated by p capture, it is important to notice the two strong destructive dips at $E_x = 11.74\,(E_p = 10.62)$ and $E_x = 14.04\,(E_p = 13.12)$ MeV. The latter can be ascribed to destructive interference of the 13.05 MeV broad structure, with the $d_{\frac{3}{2}}$ resonance observed at $E_x = 13.96\,(E_p = 13.04)$ MeV in $^{12}C(p,p)^{12}C$ elastic scattering by LeVine and Parker [104]. This assumption is very reasonable since the g.s. of ^{13}N is $\frac{1}{2}^-$ and is simply connected by E1 transition to this $\frac{3}{2}^+$ structure. Further, since the destructive minima are observed at 90 deg to the beam direction, it is required that the interfering waves must have the same parity. This suggests a search for $\pi = +$ states as candidates for the former structure, which can be reconciled with a similar negative interference with a $d_{\frac{5}{2}}$ state, seen by polarized protons at $E_x = 11.82$ MeV by Wienhard [105] and unpolarized protons at $E_x = 11.49$ MeV by Meyer and Plattner [106]. The interpretation of other secondary structures is much more complex, with the exception perhaps of the broad peak at $E_x = 15.31$ MeV $E_p = 14.5$ MeV $\Gamma = 380$ keV, for which could be postulated a double level: one level at $E_p = 14.8$ MeV ($\Gamma = 300$ keV) and one at $E_p = 15.2$ MeV ($\Gamma = 300$ keV), that could be related to structures observed in other reaction channels. Regarding the nature of the broad maximum at $E_p = 13$ MeV, the angular distributions measured in this experiment from $E_p \approx 10$ to $E_p \approx 24$ MeV, give some clear indications. The a_1 coefficient slowly increases from about 0 at $E_p = 10$ MeV, to 0.35 at $E_p \approx 16.5$ MeV, i.e. in the region of the first broad maximum. In the same region the a_2 coefficient is basically constant at an average value of -0.6. When we compare the experimental findings with the calculated (p,γ) angular distributions of Table 14 we can basically identify the experimental behaviour with that due to a $\frac{3}{2}^+$ resonance for which a_2 should be -0.5, with the a_1 behaviour ascribable to E1-E2 interference due to a possible $\frac{1}{2}^+$ quadrupole resonance probably distributed at 24 MeV $< E_\gamma <$ 32 MeV, as the a_1 increase with energy suggests.

Conclusively the broad background is ascribed to a $1p$ state with $J^\pi = \frac{3}{2}^+$ whilst the two relevant minima come from interference with $\frac{3}{2}^+$ levels of 3p-2h configuration.

TABLE 14

Computed $^{12}C(p,\gamma_0)^{13}N$ *angular distributions*

ℓ_p	j_p	Type	Angular distr.
0	$\frac{1}{2}$	E1	$2P_0$
2	$\frac{3}{2}$	E1	$4(P_0 - 0.5P_2)$
1	$\frac{1}{2}$	M1	$2P_0$
1	$\frac{3}{2}$	M1	$4(P_0 - 0.5P_2)$
1	$\frac{3}{2}$	E2	$4(P_0 + 0.5P_2)$
3	$\frac{5}{2}$	E2	$6(P_0 + 0.57P_2 - 0.57P_4)$

The other energy peak at ≈ 20 MeV has been observed in many other reaction channels [107], namely elastic proton scattering off ^{12}C, inelastic proton scattering to the 4.43 MeV, 12.7 MeV and 15.11 MeV states in ^{12}C, implying that all reaction channels go through the same doorway state. The fit to elastic proton scattering data between 20 and 30 MeV by means of an optical model scattering amplitude, modified to include resonant terms, is dominated by the $d_{\frac{3}{2}}$ wave supporting $J^\pi = \frac{3}{2}^+$ for the 20.4 MeV structure. This result is compatible with the present angular distribution analysis that shows a fairly constant $a_1 = -0.4$ coefficient from 17 to 24 MeV, compatible with an E1 decay from a $\frac{3}{2}^+$ state (Table 14), with an a_2 coefficient increasing further to +0.6 at $E_p = 24$ MeV testifying to the possible interference with an E2 resonance located at high energy, which might also explain the rather isotropic angular distribution of the $^{12}C(p,p'\gamma)^{12}C^*(12.7\,\text{MeV})$ reaction. This overall picture agrees with many body calculations concerning the mass 13 system. ^{13}C and ^{13}N being mirror nuclei are expected to have many corresponding levels and considerably similar should be the reactions $^{12}C(n,\gamma)^{13}C$ and $^{12}C(p,\gamma)^{13}N$.

Marangoni et al. [108] calculate the discrete dipole spectrum in ^{13}C, based on a shell model including the energy continuum. Their main assumptions are: i) the Hartree Fock potential is assumed to be a Woods Saxon well with a spin orbit and a Coulomb term; ii)the ^{13}C is described in the model space of 1p and 2p-1h configurations, leaving one particle in the continuum; iii) the residual interaction is a zero range force with a Soper mixture. The states computed with the higher dipole strengths percentage

are listed in Table 15 and support the previous conclusions. A point to note is that the complete dipole spectrum matches the experimental data on $^{12}C(n,\gamma)$ and reproduces as well the main features of the $^{12}C(p,\gamma)^{13}N$ cross section, with the exception of the $T = \frac{3}{2}$ resonance around 24 MeV that in this case is isospin forbidden.

TABLE 15

Discrete dipole states

E_x(MeV)	D%	J^π	T
12.46	5.99	$\frac{1}{2}^+$	$\frac{1}{2}$
13.82	5.13	$\frac{3}{2}^+$	$\frac{1}{2}$
19.39	13.65	$\frac{3}{2}^+$	$\frac{1}{2}$
24.01	26.65	$\frac{3}{2}^+$	$\frac{3}{2}$
24.13	4.78	$\frac{1}{2}^+$	$\frac{3}{2}$
25.19	8.62	$\frac{1}{2}^+$	$\frac{3}{2}$
34.64	5.47	$\frac{3}{2}^+$	$\frac{1}{2}$

It is worth noting that the calculation places a state at 34.64 MeV carrying an appreciable percentage of the dipole strength, which has found experimental support by Fisher et al. [102] and Ferroni et al. [107], with medium resolution gamma spectrometers. Not so direct a confirmation has come from higher resolution experiments. e.g. the 60 deg yield curve of Blatt et al.[93] and the total cross section of Anghinolfi et al.[103]. The work of Berghofer confirmed and complemented a previous investigation of Fisher on (p,γ) transitions to excited states in ^{13}N. The 90 deg (p,γ_1) yield curve to the 2.37 MeV state shows a resonant structure centered at an excitation energy of 22 MeV which corresponds to an excitation energy above the final level of 19.6 MeV, very close to the 20.5 MeV of the main $\frac{3}{2}^+ T = \frac{1}{2}$ structure in the γ_0 yield. The yield curve for the (p,γ_{2+3}) transition shows a somewhat more structured resonance, centered at about $E_x = 25$ MeV ($E_x = 21.5$ MeV above the final level), with secondary maxima at $E_x \approx 28$ MeV and $E_x \approx 32.5$ MeV. Again, although there is not exact correspondence of γ_{2+3} and γ_0 transition structures, there is a simple suggestion in favour of GDR built upon excited states even for ^{13}N.

Radiative capture transitions, in the range 18 MeV $< E_p <$ 44 MeV, have been ob-

served by a group including the author [103], to a quite large set of states in ^{13}N. Precisely collected spectra (Figure 14-a) show transitions to the $\frac{1}{2}^-$ g.s., the unresolved doublet at 3.51($\frac{3}{2}^-$) and 3.55($\frac{5}{2}^+$) MeV, the unresolved $\frac{3}{2}^+$ doublet at 6.9 and 7.9 MeV, a similar doublet at 10.36 and 11.7 MeV and finally a pair of states at 13.5 and 15 MeV. All these transitions show remarkable resonances, whose centroid position shifts upwards with increasing excitation energy of the final state, as seen in Figure 15. Once again, even within the approximations induced by extrapolation of the resonant yield curves with a Breit Wigner shape in the low energy region, where data were missing, the centroid energy computed by equation [1-46] gives results compatible with the assumption of a giant resonance built upon a large set of excited states, once again having a configuration largely superimposed on the initial scattering state configuration. The analysis of (p,γ_0) angular distributions, in terms of the Legendre polynomials [1-48] gives the results of figure 16. Although our data are in larger energy steps, there is substantial agreement with the data of Berghofer et al.[101] in the region of superposition, even considering the large fluctuations of our a_3 and a_4 coefficients from $E_p = 18$ to $E_p = 24$ MeV. Therefore the constantly negative a_2 value supports the E1 character of the broad excitation function, centered at $E_x = 21$ MeV, and the assignment of a $J^\pi = \frac{3}{2}^+$ to the main dipole state involved (Tables 14 and 15). The a_1 coefficient seems to flatten at an average value of +0.38 from $E_x = 24$ to $E_x = 40$ MeV and could complement the idea already expressed by Berghofer of it being due to interference between the main E1 mode and an E2 strength already present at 14 MeV but mostly concentrated in our energy range. Though there is not, at about 34 MeV, a structure as evident as that reported by Fisher it might be significative that minima are present in the a_3 and a_4 coefficients in exact correspondence with the Fisher resonance. An interesting feature of the ^{13}N data is the excitation at the maximum proton energy of 44 MeV, of a large peak corresponding to excitation energies of 20 – 22 MeV, i.e. to the energy of the g.s. GDR in ^{13}N (figure 14-a). Since this was the upper energy limit of this experiment it was not possible to measure the transition strength as a function of the proton energy. Only this kind of measurement, performed at energies above 44 MeV, will be able to establish if the 22 MeV peak originates from a γ decay of higher, second harmonic resonances built upon the g.s. GDR in ^{13}N. The angular distribution shows

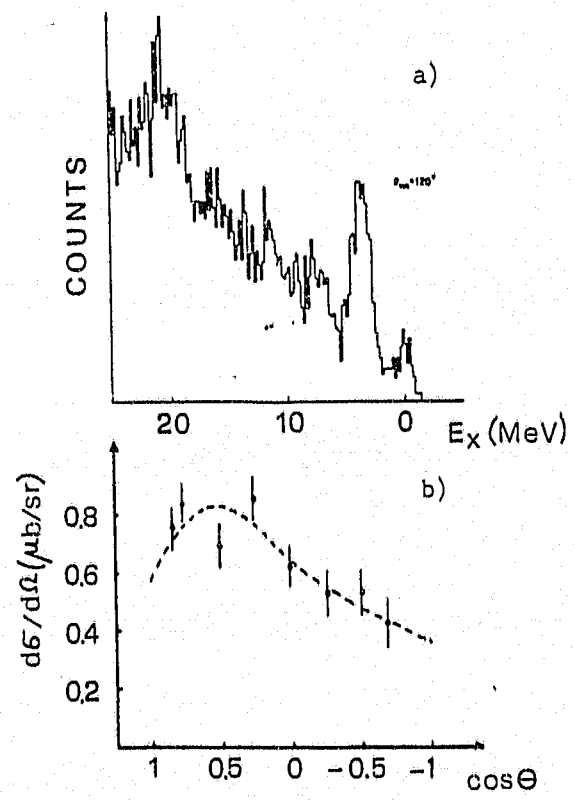

FIGURE 14 a) A photon spectrum from the $^{12}C(p,\gamma)^{13}N$ reaction at $E_p = 44$ MeV showing transitions to different ^{13}N final states including those at excitation energies around 20 MeV.
b) The angular distribution for the reaction $^{12}C(p,\gamma_x)^{13}N^*(E_x = 20\,\text{MeV})$.

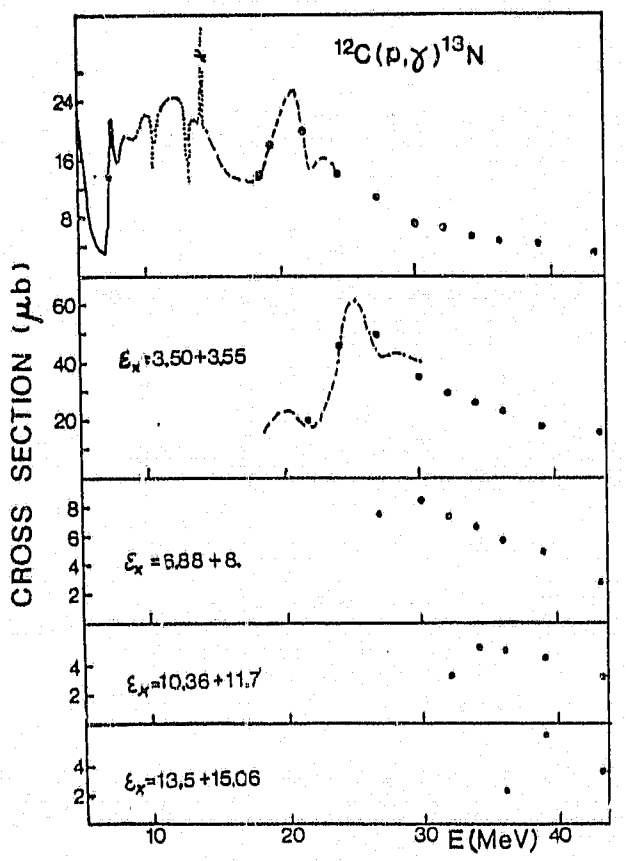

FIGURE 15 Absolute total cross section for proton radiative capture to the ground and excited states ^{13}N as a function of excitation energy. Every channel shows the presence of resonances.

FIGURE 15 Absolute total cross section for proton radiative capture to the ground and excited states in ^{13}N as a function of excitation energy. Every channel shows the presence of resonances.

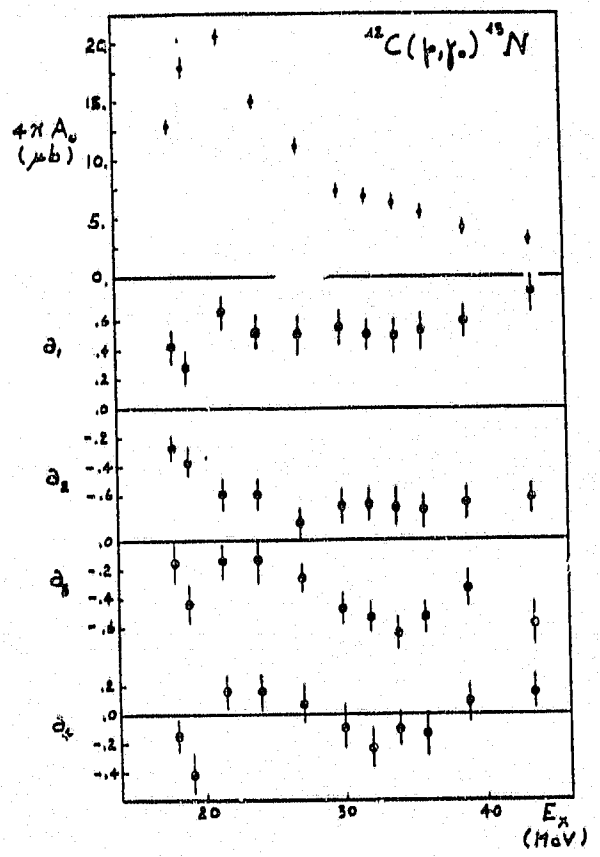

FIGURE 16 Angular distribution coefficients for the reaction $^{12}C(p, \gamma_0)^{13}N$.

(figure 14-b) a 60 deg peaked shape, typical of (E1,E2) interference, and very similar to the angular distribution of the lower energy resonances.

1-11 Radiative proton capture in the GDR region of ^{16}O

The rather complex structure of the g.s. GDR in ^{16}O has first been presented in radiative capture reactions by Cohen et al.[109] in measurements performed in the region $21 \leq E_x \leq 26$ MeV. The Princeton synchrocyclotron provided proton beams up to 19.5 MeV and a 3 in Ø×3 in NaI detector placed at 90 deg to the beam direction allowed convenient spectroscopy. E_p values below 14.5 MeV were obtained by interposition of polyethylene absorbers for a total beam spread of 200 keV. Pure (98.7%) ^{15}N gas was used as a target. The 90 deg differential cross section shows two peaks centered at 21.8 and 24.7 MeV with the latter possibly being a double structured resonance, not completely resolved because of the large statistical errors. Detailed balance is applied to the data for a converted differential cross section $\sigma(\gamma, p)$ of 14 mb/4πsr for the 21.8 MeV peak and an integrated cross section of 41. MeVmb/4πsr in the 21 – 26.8 MeV interval. Absolute values and energy dependence agree well with direct photoproton emission data obtained by bremsstrahlung beams [110]. The splitting of the GDR is reconciled to a conventional shell model calculation of odd parity ^{16}O states of the $1p^{-1}1d$ and $1p^{-1}2s$ type which gives excitation energy and wave functions for the five $1^-, T = 1$ states of these configuration, with the two highest found at 22.6 and 25.2 MeV.

The excitation energy region in ^{16}O from 15.9 to 25.6 MeV was covered in great detail by Tanner et al. [111] who produced the 90 deg yield curve for γ transitions to the g.s. of ^{16}O from a transmission ^{15}N target with thin nickel foil entrance and exit windows. The lowest structure observed is a sharp resonance at $E_p = 4.43$ MeV ($E_x = 16.24$ MeV) almost identical in shape (width = 24 keV) to the resonance at 4.437 MeV observed in the $^{15}N(n,p)^{15}O$ channel. The (p,γ) angular distribution at the top of the resonance is fitted by $W(\vartheta) = 1 + 10\sin^2\vartheta + 0.7\cos\vartheta$, consistent with that expected from a $J^\pi = 1^+$ state formed by protons in channel spin 0. The latter would be purely of the $\sin^2\vartheta$ form and the small $\cos\vartheta$ term experimentally found can confidently be attributed to the presence of $J^\pi = 1^-$ background. Two sharp resonances are found at $E_p = 5.40$ ($E_x = 17.16$) MeV and

$E_p = 5.55\,(E_x = 17.29)$ MeV. The (p,γ) angular distributions measured at four energies near the resonances have an average dependence of $W(\vartheta) = 1 - 0.44P_2$ with small $\cos\vartheta$ terms, not too different from the $W(\vartheta) = 1 - 0.70P_2$ observed in the photoproton emission [112] from these two levels, and large changes in the 0/90 deg ratio are observed around this energy region. The radiation widths limit the selection to $J^\pi = 1, 2^\pm$. The selection compatible both with the angular distributions and the observed drastic changes in the 0/90 deg ratio is that of two 1^- states; the lower is formed by nearly pure s wave protons and the higher is formed by nearly pure d wave protons with an angular momentum phase difference of about 20 deg. There is also evidence that a broad state at $E_p \approx 3$ MeV could underlie the two sharp resonances with an integrated cross section almost comparable to the sum of those belonging to the $E_x = 17.6$ MeV and the $E_x = 17.29$ MeV states. The two resonances observed at 19.05 and 19.56 MeV excitation energy are clearly seen in the $^{16}O(\gamma,n)$ reaction [113] as well, though more structure is observed in this region by neutron experiments. The 90/0 deg ratio measured between $E_p = 8.5$ and $E_p = 9.75$ MeV is everywhere larger than 1 and rules out the assignment of $J^\pi = 2^+$ to these states for which the expected 90/0 deg value is 0.5 independent of the relative admixture of p and f proton waves. The most likely assignment is then $J = 1$. For E_p above 10.01 MeV (E_γ above 21.5 MeV) there is a remarkable convergence amongst $^{16}O(e,e'p)^{16}O$, $^{16}O(\gamma,p)^{15}N$ and $^{16}O(\gamma,n)^{15}O$ and the (p,γ) data of this experiment and of Cohen's one [109] in revealing a large resonant structure at $E_\gamma = 22.3$ MeV connected to a poorly established bump at 21.8 MeV and a a secondary maximum at $E_\gamma = 23.0$ MeV plus an additional doublet at $E_\gamma = 24.4$ and $E_\gamma = 25.1$ MeV. The cross section integrated from 21.2 to 22.8 MeV is 96 MeVμb in (p,γ) or 7.7 MeVmb in (γ,p) assuming, for the (γ,p) points a $W(\vartheta) = 1 + 2.5\sin^2\vartheta$ distribution as observed in $(e,e'p)$ experiments. The gamma ray absorption data [114] integrated with (p,γ) structures observed in this experiment compare favourably with both a shell model calculation that used a square well potential (case (a) of table 16) and one which used harmonic oscillator wave functions (case (b) in table 16) perturbed by a particle-hole force. The comparison is made in Table 16 and one can see that only half of the expected classical sum rule (240 MeVmb) is found in the two peaks at ≈ 22 and ≈ 25 MeV the rest being distributed in the long tail at higher energies or, in smaller

percentage, in the sharp states at lower energy. There is also substantial agreement with earlier work of Elliot [115] and Brown [116].

TABLE 16

Computed ^{16}O *states and exc. fun. structures in* $^{15}N(p,\gamma)^{16}O$

$E_{\gamma_{exp}}$ (MeV)	Γ_{exp} (MeV)	$\int \sigma_{abs}$ (MeV mb)	$\%\sigma_{abs}$	E_γ (a) (MeV)	% sum rule	E_γ (b) (MeV)	% sum rule
17.0	1.0	10.0					
17.13	0.044	0.8	7.7	18.1	1.0	17.5	1.0
17.29	0.090	4.0					
19.05	0.35						
19.56	0.40			19.6	3	19.3	1.0
21.0	0.80	95	50	22.2	73	22.5	58
22.2	0.85						
23.0	0.60						
24.3	1.0						
25.2	0.5	63	33	25.2	20	25.6	39

A detailed study of angular distributions has been subsequently performed by the same group [117] to better establish the character of all structures in the excitation function of proton radiative capture in ^{16}O. Dipole radiation to the g.s. of ^{16}O is expected to give the major contribution to the capture strength and can only come from a dipole state having $J^\pi = 1^-$, and such a state can be excited either by capture of an s wave proton or a d wave proton by ^{15}N. But the angular distributions of the type $W(\vartheta) = A_0 + A_2P_2$ should be able to distinguish between the two cases, being s capture characterized by $A_2/A_0 = 0$ and d wave capture by A_2/A_0 ranging from -1.0 to +0.5. Possible other multipoles, like M1 or E2, should appear appreciably in the odd coefficients. M1 is due to p wave capture in channel spin 1 and produces a term A_1P_1; E2 is due to p or f wave capture and produces terms like A_1P_1 and A_3P_3. All angular distributions were compatible with the expansion [1-2] limited to $k = 3$ since all A_4 values were of the same magnitude of their respective statistical errors. Relative A_0 values were obtained from the 90 deg excitation function

and ratios of A_1/A_0, A_2/A_0 and A_3/A_0 were measured in fine energy steps from $E_x \approx 13$ to $E_x \approx 25$ MeV, where the excitation function seems to contain about ten resonances. General nuclear reaction formalism gives the angular distribution of γ rays radiated from a capture state interpreted in terms of overlapping resonances

$$\frac{d\sigma(E,\vartheta)}{d\Omega} = \frac{k}{E}\sum_{t,t'} W_{t,t'}(\vartheta) S_t(E) S_{t'}^*(E) \qquad [1-78]$$

where k is a constant, t and t' are the reaction channels quantum numbers, S_t the matrix elements and $W_{t,t'}$ the angular term. The sum extends over all t and t' compatible with the conservation laws. Considering that S_t will become negligible for multipolarities higher than 2, one can consider only E1, M1 and E2 radiations to the ground state of ^{16}O and compute the angular terms $W_{tt(t')}$ as listed in Tables 17 and 18.

TABLE 17

Intensity terms W_{tt}

Channnel S	ℓ_p	J^π	Type	W_{tt}
0	1	1^+	M1	$3(P_0 - P_2)$
1	0	1^-	E1	$3P_0$
1	0	2^+	E2	$5(P_0 + 0.5P_2)$
1	1	1^+	M1	$3(P_0 + 0.5P_2$
1	2	1^-	E1	$3(P_0 + 0.5P_2$
1	3	2^+	E2	$5(P_0 + 4/7P_2 - 4/7P_4)$

From these predictions it is easy to see that the absence of A_4 terms means that 2^+ states formed by f wave capture do not contribute to the observed intensity, but the A_1 and A_3 coefficients are most probably related to E1 E2 interference although E1 M1 interference cannot be ruled out.

It also means that large negative values and significant A_1 variations with energy require d wave $J^\pi = 1^-$ states and their interference with s wave $J^\pi = 1^-$ states. It is the region above 18 MeV which is assumed to be due predominantly to E1 radiation and the angular distributions show some marked general trend.

TABLE 18

Interference terms $W_{tt'}$

ℓ_p	Type	ℓ'_p	type	$W_{tt'}$
0	E1	2	E1	$(3\sqrt{2})P_2$
1	E2	3	E2	$(-5\sqrt{3/7}\sqrt{2})(P_2 - 8P_4)$
0	E1	1	E2	$(-3\sqrt{5}/\sqrt{2})P_1$
0	E1	3	E2	$-\sqrt{15}P_3$
2	E1	1	E2	$(3/2\sqrt{5})(P_1 - 6P_3)$
2	E1	3	E2	$(\sqrt{3}/\sqrt{10})(9P_1 - 4P_3)$
0	E1	1	M1	$(3\sqrt{3}/\sqrt{2})P_1$
1	E2	1	M1	$(3\sqrt{15}/2)P_2$
2	E1	1	M1	$(-3\sqrt{3}/2)P_1$
3	E2	1	M1	$2\sqrt{3}P_2$

i) In the range from $\approx$ 20 MeV to $\approx$ 25 MeV the ratios A_1/A_0 and A_3/A_0 show little variation compared to the peaks seen in the A_0 coefficient energy behaviour, with A_3/A_0 approximately constant at -0.09 and A_1/A_0 smoothly increasing from +0.08 to +0.26

ii) The ratio A_2/A_0 always remains compatible with the value of -0.5 expected from E1 radiation following d wave capture, the small variations being accounted for by an eventual s wave capture contribution of less than 5%.

iii) The A_1/A_0 and A_3/A_0 ratios have comparable absolute values and this would indicate that the contribution seen is coming more from E1 E2 than from E1 M1 interference for which A_3/A_0 is expected to be 0.

iv) From Table 18 interference of primary d wave E2 radiation with secondary p wave or f wave E2 radiation gives A_3/A_1 ratios of -6.0 and -0.44 respectively, the latter being closer to the experimental values, which average at -0.8 from 20 to 25 MeV. Again the difference between the pure f wave value of -0.44 and the observed average -0.8 value can be easily reconciled by small admixtures of s wave capture to the E1 contribution or small p wave capture to the E2 contribution.

It is concluded that $^{15}N(p,\gamma)^{16}O$ in the region of the GDR is dominated by two entrance channels: d wave capture followed by E1 radiation and f wave capture followed

by E2 radiation, the latter being about 1% of the E1 mode. This is not incompatible with the seven peaks observed in the A_0 trend but we should note that the relative constancy or smooth behaviour of the angular distribution coefficients fails to reproduce the A_0 fluctuations in the region of interest. A plausible explanation is that of a broad resonance centered at ≈ 23 MeV with a width of ≈ 4 MeV interfering positively or negatively with a set of ten smaller resonances not to be identified with the structures in A_0, and whose total integrated cross section could be less than 6% of the corresponding broadly distributed E1 strength. The average values obtained from 20 MeV to 25 MeV are $A_0 = 45\,\mu$b, $A_1 = 5.8\,\mu$b, $A_2 = -25\,\mu$b and $A_3 = -4.6\,\mu$b and the odd coefficients can be accounted for by an E2 resonance positioned around 30 MeV with a width of 5 to 10 MeV and a peak cross section of about $1\,\mu$b. One has finally to remark on the presence in this region of a peak at 19.08 MeV, characterized by a rapid variation of A_1/A_0 and A_3/A_0, (suggesting interference between states of opposite parity), and a sudden positive variation of A_2/A_0, that from Table 17 can be accounted for by a 2^+ state already identified in inelastic electron scattering at 19.20 MeV. The experimental results in the region of the E1 main contribution, can be compared both with a shell model calculation with harmonic oscillator wave functions perturbed by a particle-hole interaction whose strength was adjusted to place the main dipole strength at 22 – 25 MeV [72], or to a coupled channel calculation where the particle nucleus interaction mechanism is the usual two body complex optical potential and a particle-hole force [118]. The former predicts five states at 13, 17, 19, 22 and 25 MeV, with most of the dipole strength concentrated in the last two, but fails to reproduce by a factor of two the integrated experimental cross section while accounting rather well for the observed A_2/A_0 ratio. The latter is much more realistic and quite succesful. In fact the magnitude of the integrated cross section is in fair agreement with the experimental values, the widths of the calculated peaks are conveniently large and the behaviour of the 90 deg cross section from 12 to 26 MeV is fairly well reproduced. The angular distribution coefficients are generally well reproduced with the exception of the 19 MeV region which is characterized by a sharp 2^+ resonance.

Proton capture reactions followed by radiation to the first and second excited state in ^{16}O were studied by Barnett and Tanner [119] with an improved resolution γ spec-

trometer of 24 Øcm by 32 cm that allowed clear identification of the reaction channels $^{15}N(p,\gamma_{1+2})^{16}O^*$ and $^{15}N(p,\gamma_0)^{16}O$. The excitation function of the g.s. transition is in all respect similar to that already observed by the same group [111] with only an energy shift of 50 – 150 keV between the two cases. The yield curve for the γ_{1+2} transition shows four prominent states at 18.05, 19.00, 19.91 and 20.40 MeV excitation energy with two weaker levels at 19.25 MeV, 22.7 MeV and a shoulder at 23.35 MeV. The lower pair at 18.05 and 19.00 MeV correspond to the two analog states at the expected energies in ^{16}N, a T=1 nucleus. From the strength of γ ray decay a T=1 assignment can also be made for the upper pair of levels at 19.91 and 20.4 MeV and the weaker state at 19.25 MeV could be identified with the level strongly observed in the (p,n) reaction [120]. Despite the improved detector it was still not possible to separate γ_1 and γ_2 transitions to the 6.05 MeV 0^+ and the 6.13 MeV 3^- levels in ^{16}O, never the less the completely different excitation curves for the γ_0 and the γ_{1+2} reactions suggest that very little γ_1 strength is seen in γ_{1+2}. In fact the 6.05 MeV 0^+ level wave function is supposed to have 2p-2h and 4p-4h major components together with about 10% of the 0p-0h g.s. wave function. These do not match the 1p-1h configuration of the entrance channel. Even considering transitions to only the 10% 0p-0h component of the final excited state, this leads to a γ_0/γ_1 braching ratio of 4% that is much higher than the 1% upper limit fixed by the experimental γ_0 and γ_{1+2} yield curves. The fact is that dipole transitions to the 2p-2h component must be relevant and destructively interfering with the 0p-0h component thus destroying any similarity betweeen the two curves. The γ_{1+2} is therefore largely due to deexcitation to the 6.13 MeV 3^- state. This should be due to $2^\pm$, $3^\pm$, $4^\pm$ compound states with the spin 4 state only possible for g and h wave protons, and consequently largely depressed by the angular momentum barrier. Angular momenta of the compound states responsible for the (p,γ_{1+2}) radiation should therefore be $J = 2$ and $J = 3$. In the absence of angular distribution measurements, but comparing the strengths of the three highest (p,γ_{1+2}) with the strength of established E1 γ_0 transitions, it is assumed that the 19.91, 20.40 and 22.7 – 23.4 MeV resonances are E1 in character, with the 20.40 and 22.7 MeV too strong to be E2. The lower γ_{1+2} resonances are an order of magnitude weaker than the higher ones, and no assignment can be made on the grounds of strength. To be noted is that the

pair at 19.91 and 20.40 MeV can also be identified with the 2^+ states obtained coupling the 1^- states of ^{16}O at 12.43 MeV, $T = 0$ and 13.10 MeV, $T = 1$ to the 6.13 MeV 3^- state. The 2^+ possibility is assumed because it can be obtained by p wave capture while 3^+ and 4^+ require the less probable f wave formation. This picture finds support from the experimental evidence of an energy separation between the compund states of 0.49 MeV which comparable to the energy separation of 0.67 MeV of the two coupling states, and also from the fact that the T=0 and T=1 states are known to be mixed by the coulomb force with an intensity component (of one in the other) of $\alpha^2 = 0.15$.This is very well reproduced by the experiment which gives

$$\Gamma_{19.9}/\Gamma_{20.4} = 0.17 = \alpha^2/(1-\alpha^2) \qquad \alpha^2 \approx 0.15 \qquad [1-79]$$

Further insight into this aspect has been achieved by Barnett and Lowe [121] by direct $\gamma_2 - \gamma$ coincidence studies for the $E_x = 19.9$ MeV resonance and the $E_r = 20.4$ MeV one. The $\gamma - \gamma$ yield was not influenced by the 0_2^+ state decay since this takes place entirely by pair emission. The singles spectra were recorded in a 7.6 cm Øx 7.6 cm NaI detector and coincidence 6.13 MeV γ's were detected at the opposite side of the target in a similar 10 cm Øx 13 cm NaI crystal whose energy window was set between 4.8 and 7.0 MeV. The computed efficiency for this crystal at 6.13 MeV for that particular geometry is $\epsilon_A = 0.046 \pm 0.02$. If N is the number of decays per unit of beam charge, $\Delta\Omega_A$ and $\Delta\Omega_B$ are the solid angles subtended by the two detectors ϵ_B the efficiency to high energy γ's of the main detector, then

$$\frac{N_{coinc}}{N_{sing}} = \frac{N\Delta\Omega_A\Delta\Omega_B\epsilon_A\epsilon_B(\gamma_2/\gamma_{1+2})}{N\Delta\Omega_B\epsilon_B} = N\Delta\Omega_A\epsilon_A\left(\frac{\gamma_2}{\gamma_{1+2}}\right) \qquad [1-80]$$

where γ_2/γ_{1+2} is the relative branching ratio for the two γ transitions. Data are perfectly compatible with 100% γ_2 branching and substantiate the model of weak coupling between the 6.13, the 12.43 and the 13.11 MeV states.

The region of the main GDR peak ($E_p = 10.00 - 11.24$ MeV) and the region above 24 MeV excitation energy, were explored at three laboratory angles (32, 45 and 90 deg) by Black et al. [122] in 10 to 20 keV steps, in order to detect any fine structure in the main

GDR peak and to investigate the contribution of the integrated dipole strength to the long tail following the GDR excitation. The 90 deg yield curve is basically in agreement with the corresponding Tanner et al. [111] curve. More definite structures are revealed at the forward angles at $E_x = 21.89$, 22.05, 22.17 and 22.22 MeV all with widths in the interval 50 – 100 keV. These structures correspond with similar ones detected in the (γ, p_0) channel although with an energy shift of 100 keV. In general the (γ, p_0) channel shows more structure out of the GDR peak that is not revealed in the (p, γ_0) channel. The observed sharp structures may well be those ascribed by Gillet to interference between simple 1p-1h and more complex multiparticle multihole (2p-2h 4p-4h) excitations. The higher energy region gives results in agreement with those of Tanner [111] although it is again necessary to shift the two energy scales by about 200 keV, to obtain perfect matching in the region of superposition. Two pronounced shoulders are found at $E_x = 25.5$ MeV and $E_x = 26.4$ MeV in agreement with what is observed in $^{16}O(\gamma, n)^{15}O$. The most remarkable result of this investigation is that the high region makes a substantial contribution to the total dipole strength as seen from the integrated yield value which is 5.4 MeVmb from 25.2 to 29 MeV with an assumed $W(\vartheta) = 1 + 2.5 \sin^2 \vartheta$, and from the fact that the cross section in the same region averages 50% of the cross section between 18.2 and 25.2 MeV i.e. in the peak of the GDR.

The understanding of the configuration of the GDR in ^{16}O and its energy dependence can be improved with polarized proton capture where amplitudes and relative phases associated with the reaction channels which form the GDR can be analyzed. Hanna et al. [123] have analyzed the $^{15}N(\vec{p}, \gamma_0)^{16}O$ reaction at fourteen energies between $E_p = 7.4$ to $E_p = 15.0$ MeV, measuring the analyzing power $A(\vartheta)$ [1-7] at 45, 90 and 135 deg and two additional angles for the strongest peak at $E_p = 10.8$ MeV. Many of the energies were selected to coincide with peaks and valleys of the excitation function. The usual expression [1-8] [1-9] for $W_u(\vartheta)$ and $A(\vartheta)$ have been used to extract the a_k and b_k coefficients with the traditional limit of $k \leq 2L$ if the multipolarity involved is L, $k < L + L'$ if two multipolarities L and L' are interfering, and k even or odd according to whether the two radiations have the same or opposite parity. The experiment shows that throughout the GDR region ($E_x > 20$ MeV) the $A(\vartheta)$'s are largely compatible with the $\sin 2\vartheta$ dependence

expected for a pure E1 radiation with b_1 and b_3 much smaller than b_2 and therefore neglected in the analysis which also included a_1 and a_2 coefficients from unpolarized data. Considering only E1 radiation from 1^- states as the main component of the GDR in ^{16}O then the coefficients a_2 and b_2 alone can be connected to the transition matrix elements and their phases. Referring ℓ, s, and $j = \ell + s$ to the incoming proton, only incident waves with $(\ell = 0, j = \frac{1}{2})$ or $(\ell = 2, j = \frac{3}{2})$ can combine with the $J^\pi = \frac{1}{2}^-$ g.s. of ^{15}N to form a compound $J^\pi = 1^-$ state in ^{16}O. The corresponding amplitudes can be written as $s_{\frac{1}{2}} e^{i\Phi_s}$ and $d_{\frac{3}{2}} e^{i\Phi_d}$ with the angular coefficients given by

$$\begin{aligned} a_2 &= -0.5 d_{\frac{3}{2}}^2 + 1.414 s_{\frac{1}{2}} d_{\frac{3}{2}} \cos(\Phi_d - \Phi_s) \\ b_2 &= -1.5 s_{\frac{1}{2}} d_{\frac{3}{2}} \sin(\Phi_d - \Phi_s) \qquad [1-81] \\ s^2 + d^2 &= 1.0 \qquad \text{normalization} \end{aligned}$$

for a total of three equations and three unknowns. The fact that the equations are quadratic allows two mathematical solutions to be compatible with the data. One shows a dominant $d_{\frac{3}{2}}$ capture with $|d_{\frac{3}{2}}|^2$ averaging 90% and the other being mainly attributable to $s_{\frac{1}{2}}$ capture with $|s_{\frac{1}{2}}|^2$ averaging 80%. Both agree in predicting an almost constant $d_{\frac{3}{2}}$ or $s_{\frac{1}{2}}$ behaviour all over the energy rangeof interest attributing the large fluctuations observed in the A_0 term uniquely to the large oscillations of the realtive phase $\Phi_d - \Phi_s$ between the two interfering waves. Bound state calculations and neutron polarization data favour the $d_{\frac{3}{2}}$ dominance. Still in the range $E_p = 8\,\text{MeV}$ to $E_p = 16\,\text{MeV}$, convincing evidence of E2 strength can be achieved by precision angular distribution measurements, where a_3 and a_4 are sensitive to the presence of quadrupole strength (Table 1). But quantitative information is not possible by unpolarized data only. The a_k and b_k coefficients have been extracted from precision, seven points, angular distributions and analyzing powers by Hanna et al.[124] and reported in Table 19.

In the $j-j$ coupling scheme, to the extent that multipoles higher than E2 and also M1 can be excluded, four complex amplitudes contribute to the E1 and E2 radiations: $s_{\frac{1}{2}} e^{i\Phi_s}$, $d_{\frac{3}{2}} e^{i\Phi_d}$, $p_{\frac{1}{2}} e^{i\Phi_p}$ and $f_{\frac{5}{2}} e^{i\Phi_f}$, which coupled to the $J^\pi = \frac{1}{2}^-$ g.s. of ^{15}N give $0^+\,1^-$, $1^-\,2^-$, $1^+\,2^+$, $2^+\,3^+$compound nucleus states which can decay by E1(1^-) or E2(2^+) radiation to the 0^+ g.s. of ^{16}O. The $a_2\,a_3\,a_4$, $b_2\,b_3\,b_4$ coefficients and the overall normalisation are

TABLE 19

Unpolarized and polarized angular distribution coefficients

E_p(MeV)	a_1	b_1	a_2	b_2	a_3	b_3	a_4	b_4
8.69	-0.05	0.066	-0.528	0.223	-0.205	-0.045	-0.022	-0.03
9.50	0.078	0.064	-0.248	0.326	0.129	0.000	-0.053	-0.010
10.10	0.051	0.046	-0.537	0.267	-0.161	-0.010	-0.017	-0.002
10.40	0.019	0.022	-0.566	0.301	-0.073	0.015	-0.040	0.003
11.50	0.203	-0.006	-0.403	0.297	-0.111	0.043	-0.072	-0.002
12.60	0.158	0.061	-0.640	0.248	-0.156	0.011	-0.022	0.015
13.00	0.208	0.064	-0.607	0.281	-0.178	0.037	-0.073	-0.004
14.50	0.301	0.017	-0.603	0.246	-0.142	0.032	-0.002	0.027
15.70	0.324	0.017	-0.543	0.244	-0.127	0.062	-0.075	0.030

sufficient to determine the seven unknown quantities, i.e. the four amplitudes $s_{\frac{1}{2}}$, $d_{\frac{3}{2}}$, $p_{\frac{1}{2}}$, $f_{\frac{5}{2}}$ and the relative phases. The system of quadratic equations produces two different solutions, one corresponding to a predominant $d_{\frac{3}{2}}$ E1 part, the other to a predominant $s_{\frac{1}{2}}$ E1 part. Both agree in giving an E2 strength centered at ≈ 24 MeV for a maximum value around 6 μb and a total width of not less than 8 MeV, and in reproducing independently the a_1 and b_1 coefficients, without the need of including any M1 component in the calculation. The observed E2 strength lies slightly above the GDR peak and is thus presumed to be isovector in character contrary to the isoscalar E2 component, reported in (p,p') experiments [125] at an energy a few MeV below the GDR peak. The isovector sum rule

$$\int \sigma(E2)dE/E^2 = 4\,10^{-4}\frac{NZ}{A^{\frac{1}{3}}}(\frac{\text{mb}}{\text{MeV}}) \qquad [1-82]$$

is exhausted to 30% by the (p,γ) data and to about 60% if a similar E2 strength is expected for the neutron channel.

Specific attention to the γ_{1+2} channel has been paid by Chew et al. [126] in the range $E_p = 6 - 19.6$ MeV ($E_x = 18 - 30$ MeV). The ^{15}N$(p,\gamma_0)^{16}$O 90 deg yield agrees with Black's data [122] and shows no significant structure above the well known GDR, but a

slowly decreasing tail. The excitation function for the $^{15}N(p,\gamma_{1+2})^{16}O^*$ shows three new peaks at E_p = 13.45, 15.25, 16.20 MeV in addition to the already known structures at E_p = 6.32, 7.33, 8.30 and 8.53 MeV. The coincidence method already described has been applied to the 6.32 and 7.33 MeV resonances

and again the measured coinc./singles ratio for the $\gamma - \gamma_{6.13}$ pair is in good agreement with a 100% γ_2 branching ratio, indicating that these two states decay through the $J^\pi = 3^-$ second excited state of ^{16}O. For the 13.45, 15.25 and 16.20 MeV resonances, the coinc./singles ratio in a corresponding pair of photon spectra is affected by much larger errors than in the case of lower peaks. Nevertheless the yield in coincidence mode is almost equivalent in magnitude and width to the singles yield multiplied by the factor $\Delta\Omega_A\epsilon_A$ and this is taken as a clear indication of selective decay to the 6.13 MeV 3^- state. In the aim of selecting transitions to the 6.05 MeV 0^+ first excited state in ^{16}O, the reaction $^{13}C(^3He,\gamma_{1+2})^{16}O^*$ was studied in parallel to proton capture to the same doublet of ^{16}O excited states. The interest for this lies in the fact that, as already mentioned, the 6.05 MeV 0^+ state is believed to have a small (10%) superposition with the 0^+ g.s. wave function, being otherwise dominated by 4p-4h and 2p-2h configurations to which a 3p-3h compound state as it is presumably formed by ^3He capture in ^{13}C, can decay. The single γ_{1+2} yield is explored from $E_{^3He}$ = 4. to $E_{^3He}$ = 12 MeV spanning the excitation region from ≈ 24 MeV to ≈ 32 MeV, with evidence confirmed of a resonance [127] at $E_{^3He}$ = 4.5 MeV (E_x = 26.45 MeV). The coincidence $\gamma - \gamma_{6.13}$ technique is once more applied but very little evidence remains of the yield curve peak in coincidence mode, when this is compared to the singles yield multiplied by $\Delta\Omega_A\epsilon_A$, implying that the decay is essentially to the $J^\pi = 0^+$ first excited state at 6.05 MeV. The possibility of such a decrease in coincidence yield being due to an unfortunate angular correlation pattern in the selected geometry of two detectors diametrically opposed at ϑ_{lab} = 90 deg has been at this stage evaluated for $J^\pi = 2^+, 3^+$ and 4^+ for the resonance and any $\ell_{^3He}$ from 0 to 4. Angular correlation calculations give results that are still compatible with a 2^+ assignment for the resonance. Therefore only specific angular correlation measurements can rule out the 2^+ hypothesis in favour of the 0^+ assignment. The strength of the 26.45 MeV state is such that it most probably is $J^\pi = 1^-, T = 1$ forming part of the

deformed GDR in ^{16}O, of which we see, by the explored transition the 3p-3h component, the rest being probably located above $E_x = 32.6\,MeV$. As concerns the proton entrance channel, all compound states seem to decay to the 3^-, $T = 0$ second excited state and since E1 or M1 decays have to be preferred to eventual E2, the probabilities are restricted to $J^\pi = 2^\pm$, $3^\pm$, $4^\pm$ assignment to such compound states. To make firmer spin assignments requires measurements of angular distributions and Chew's group performed them [128] at 34 energies, both on and off resonance, in the range $E_p = 6 - 22\,MeV$ ($E_x = 18 - 33\,MeV$) spanning angles from 0 to 150 deg for $6 \leq E_p \leq 10\,MeV$ and angles from 20 to 146 deg for $10 \leq E_p \leq 21\,MeV$. Due to the very large variations of the angular distribution shape around the $E_p = 8.86\,MeV$ ($E_x = 20.43\,MeV$) resonance, a set of angular correlations was measured with the main 25.4 cm Ø× 30.5 cm detector positioned at ($\vartheta = 90, \varphi = 0$) and in coincidence with either of three 12.7 cm Ø×15.2 cm at (0,90), (90,180) and (90,90) each with an energy window at $4.5 - 8\,MeV$. The 90 deg $^{15}N(p,\gamma_0)^{16}O$ excitation function is in very good agreement with previous results so is the (p,γ_{1+2})one, except for the resonance at $E_p = 7.60\,MeV$[119]which is not found during this experiment. Seven major resonances were located at $E_p = 6.29$, 7.31, 8.29, 8.86, 13.49, 15.25 and 16.25 MeV. Absolute cross sections were measured considering the γ yield, the detector efficiency, absorption in the target and beam pipe and dead time. The $(\frac{d\sigma}{d\Omega})_{90}(p,\gamma_0) = 27.7 \pm 8.3\,\mu b\,sr$ at $E_p = 10.8\,MeV$,is in agreement within the experimental errors with Black's data [122] ($19.5 \pm 3.5\,\mu bsr$) but definitely larger than the Earle and Tanner [117] value ($14.0 \pm 4.0\,\mu bsr$). The (p,γ_0) angular distributions show a_1 values oscillating around the zero line up to about $E_p = 11\,MeV$, then rising continuously to reach a value of $\approx +0.5$ at $E_p = 20.5\,MeV$ ($E_x \approx 31\,MeV$). The a_2 coefficient remains negative in the energy range of this experiment showing pronounced fluctuations at the lower energies and stabilizing around -0.5 above $E_p = 12\,MeV$. The a_3 and a_4 coefficients are very small and compatible with 0 except maybe for the slightly negative a_3 values at $E_p > 17\,MeV$, thus confirming the predominant E1 character of proton capture to the ground state. The (p,γ_{1+2}) angular distributions show an a_1 coefficient steadily increasing from

≈ 0 at $E_p < 10\,MeV$ to an average of $+0.4$ at $E_p \approx 21\,MeV$, with some high positive values at the lowest explored energy ($\approx 6\,MeV$). The a_2 coefficient shows pronounced fluc-

tuations, being positive at the $E_p = 6.29$ MeV resonance, negative at the $E_p = 7.31$ MeV one, positive at the $E_p = 8.29$ MeV peak, largely fluctuating across the $E_p = 8.86$ MeV resonance, setting to positive values from $E_p = 10.5$ MeV to $E_p = 12$ MeV and then assuming a smooth trend with negative values all the way from $E_p = 12$ MeV to $E_p = 21$ MeV. The a_3 and a_4 values are hardly distinguishable from zero, with the largest statistical errors, thus bringing us to consider that the E1 and M1 transition modes are the leading ones in the decay to first and second excited states. All seven resonances have been shown to mainly decay to the 6.13 MeV, $T = 0$ state, with only the $E_p = 8.86$ MeV one needing to be reconsidered, following the new evidence of abnormal angular distributions. Assuming E1 or M1 transitions to the 6.13 MeV, 3^- state, implies that compound nuclear levels with $J^\pi = 2^\pm$, $3^\pm$, $4^\pm$ are involved. For spin 3, depending on channel spin and orbital momentum mixing, a_2 varies in the range $+0.37 - +0.50$; for spin 2 a_2 varies from -0.30 to -0.35 and for spin 4 a_2 is in the range $-0.07 \div -0.14$. Based on the a_2 values no distinction is possible between spin 2 and 4 and the assignment for the lowest resonances is as from Table 20, the strength of the transitions being compatible with both a $T = 0, 1$ value.

TABLE 20

J^π and T assignments based on a_2 values and strengths

E_p(MeV)	E_x(MeV)	a_2	J^π	T
6.29	18.02	> 0	3	0,1
7.31	18.89	< 0	2,4	0,1
8.29	19.90	> 0	3	0,1
8.86	20.43	fluct.		1
13.49	24.77	< 0	2^+, 4^+	1
15.25	26.42	< 0	2^+, 4^+	1
16.25	27.36	< 0	2^+, 4^+	1

The strength of the highest four states looks typical of isospin allowed E1 or M1 transitions to a T=0 state. So it is natural to assign T=1 to these resonances and a 2^+ or 4^+ J^π value to the three highest in accordance with negative a_2 values for these peaks. Since the 6.13 MeV state wave function has basically the $(1p_{\frac{1}{2}})^{-1}1d_{\frac{5}{2}}$ and the

$(1p_{\frac{3}{2}})^{-1}1d_{\frac{5}{2}}$ components, states formed by protons captured in the $f_{\frac{7}{2}}$ shell will have a basic component $(1p_{\frac{3}{2}})^{-1}1f_{\frac{7}{2}}$ and should have large E1 widths to the 6.13 MeV state as suggested from the strength of these transitions. The $f_{\frac{7}{2}}$ capture can form $J^\pi = 3^+, 4^+$ hence a possible but not conclusive suggestion is that the 13.49, 15.25 and 16.25 MeV resonances can be identified with 4^+ states. The a_2 coefficient varies from +0.1 just below the 8.86 MeV resonance to -0.7 just above, and this cannot be accounted for by any means by a pure spin state decaying to a 3^- state. One possibility, suggested by the a_2 value just above the resonance, which is typical of an E1 transition to a 0^+ state, is that this resonance is in fact composed of two close levels, responsible for the large variation observed in the angular distributions. Previous $\gamma - \gamma_{6.13}$ coincidence results excluded such a possibility and the actual angular correlations which give $W = 0.5\,(\vartheta = 90, \varphi = 180)$ or $W = 0.75\,(90,90)$ or $W = 1.75\,(0,0)$, strongly suggest that only γ_2 radiation is observed. The more likely explanation is that a single state interferes with an energy independent coherent background. As a matter of fact either a $j = 2$ resonant spin interfering with an energy independent $J =$ background of amplitude $0.275\Phi_{J=2}$, or vice-versa (as concerns spins), give rather good fits of the a_2 coefficients for $E_p = 8.5$ to $E_p = 9.2$ MeV. A strong M2 state is observed in inelastic electron scattering at $E_x = 20.4$ MeV [129]. This state has $J^\pi = 2^-\ T = 1$ and could decay via M1 to the 6.13 MeV state, and since the wave function of this state has a large superposition with that of an M1 excitation performed upon the 6.13 MeV state, the identification of the two 20.4 MeV states as the same level is very plausible. The main feature of the observed GDR based on the g.s. ($E_x \approx 18 - 29$ MeV) and on the 6.13 MeV second excited state ($E_x \approx 23 - 32$ MeV) of ^{16}O can be summarized as follows. The γ_0 excitation function is characterized by a general rise in yield, with several resonances of $\Gamma \approx 1$ MeV superimposed on this and an almost constant a_2 coefficient across the GDR region. The picture that emerges is that of a broad vibrational state having a wave function with large overlap to a proton coupled to the ^{15}N core and therefore a expected width of several MeV in the proton capture channel. This cannot be identi with any of the too sharp structures in the excitation function but can be responsible for the almost constant a_2 values and, through the admixture of a small part of its amplitude in the wave functions of the individual sharper levels, evidently characterized by more

complex configurations, of the structured excitation function. The γ_{1+2} excitation function is similarly characterized by a general rise in yield above $E_x = 23\,\text{MeV}$ with a_2 having a broad negative minimum in the region $E_x = 23 - 32\,\text{MeV}$, insensitive to whether the angular distribution is performed in coincidence with one of the three secondary maxima in the excitation function or in between them. This is again consistent with the presence of a broad vibrational state responsible for the capture in this region. Evidence for $J = 2$ or $J = 4$ compound states is provided by the data. Assuming that the 6.13 MeV state wave function is essentially that of a $(1p_{\frac{1}{2}})^{-1}1d_{\frac{5}{2}}$ configuration, possible GDR configurations are those where the particle is further promoted to a $2\hbar\omega$ shell such as $(1p_{\frac{1}{2}})^{-1}2p$, $(1p_{\frac{1}{2}})^{-1}1f$ or those in which an extra particle is promoted out of the $1p$ shell such as $(1p_{\frac{1}{2}})^{-2}1d^2$, $(1p_{\frac{1}{2}})^{-2}1d2s$, $(1p_{\frac{1}{2}})^{-1}(1p_{\frac{3}{2}})^{-1}1d^2$, $(1p_{\frac{1}{2}})^{-1}(1p_{\frac{3}{2}})^{-1}2s1d$, the 1p-1h configurations being able alone to account for the capture radiative widths.

The GDR region in ^{16}O has been reconsidered by O'Connel and Hanna [130] who performed a series of very detailed measurements on the $^{15}\text{N}(p,\gamma_0)^{16}\text{O}$ reaction including 90 deg excitation functions from $E_p = 8.45\,\text{MeV}$ to $E_p = 18\,\text{MeV}$, in steps of 20, 40 or 100 keV, and also eight angles angular distributions from $\vartheta = 22$ to $\vartheta = 135$ deg in steps of 100 125 250 keV from $E_p = 8.6\,\text{MeV}$ to $E_p = 18\,\text{MeV}$. Angular distributions were expanded in Legendre polynomials [1-2] alternatively for $k = 0 - 4$ or $k = 0 - 3$ with the results on a_4 coefficients constantly equal to zero and not taken into account. Structures in the 90 deg yields are in good agreement both with previous (p,γ_0) measurements [117] produced in the same energy region and with corresponding (γ,p_0) [131] and (γ,n_0) [132] measurements. They show up at $E_x = 20.9$, 22.15, 22.9, 24.25 MeV, and, but smaller, at $E_x = 24.85\,\text{MeV}$. Above $E_x = 25.4\,\text{MeV}$ the yield curve falls smoothly. The absolute cross section value at $E_x = 22.15\,\text{MeV}$ is of 12.9 mb. The angular distributions show an a_1 coefficient fluctuating around zero from $E_p = 8.61\,\text{MeV}$ to $E_p = 10.5\,\text{MeV}$. Then a_1 is positive and appreciably increases with energy with perhaps some little structure. The a_2 coefficient is generally negative but shows definite maxima at $E_x = 21\,\text{MeV}$ and in the range $E_x = 22.5 - 24\,\text{MeV}$, being otherwise nearly constant at -0.55. The a_3 coefficient is obviously affected by larger statistical errors but shows compatibility with zero up to $E_p = 12\,\text{MeV}$, then becoming slightly negative and decreasing with energy. The

most striking result, rather new w respect to other, lower statistics, larger energy step experiments, is the correlation of the a_2 structures with the structures in the excitation function. The latter have also correspondence with narrow resonances observed in other reactions, *specifically* there is a resonance at $E_x \approx 21$ MeV observed in $^{12}C(\alpha,\gamma)^{16}O$, a resonance at $E_x \approx 22.7$ MeV observed in $^{14}N(d,\gamma_0)^{16}O$ and a pair of resonances at $E_x \approx 25$ MeV and $E_x \approx 25.3$ MeV observed in $^{13}C(^3He,\gamma)^{16}O$. The picture that emerges is that a_2 and A_0 are dominated by 1p-1h E1 strength from a broadly distributed state wh in interferes with narrow np-nh configurations of the same spin and parity as the 4p-4h at $E_x \approx 21$ MeV, the 2p-2h at $E_x \approx 22.7$ MeV and the 3p-3h at $E_x > 25$ MeV. A fit assuming five resonances at 20.95, 22.15, 22.89, 24.07 and 25.12 MeV with Γ values of respectively 0.32, 0.73, 0.32, 0.59 and 3.15 MeV, can perfectly account for the observed excitation function. The two broad resonances at 22.15 and 25.12 MeV give the dominant E1 contribution and interfere with the remaining one which carries only a small fraction of the E1 strength. Resorting to polarized proton data in the same energy region we have the convincing evidence of the entrance channel being dominated by a $d_{\frac{3}{2}}$ configuration (80%) [123], with the rest left to the $s_{\frac{1}{2}}$ configuration. The continuum state is therefore mainly a $(1p_{\frac{1}{2}})^{-1}1d_{\frac{3}{2}}$ with some admixture of $(1p_{\frac{1}{2}})^{-1}2s_{\frac{1}{2}}$. Shell model calculations including a particle-hole correlation assuming a zero range force with a Soper mixture, by Brown et al. [113], give the dipole states in ^{16}O reported in table 21 with the last two carrying the most part of the E1 strength.

TABLE 21

Dipole states configuration in ^{16}O

E_x(MeV)	$p_{\frac{1}{2}}^{-1}s_{\frac{1}{2}}$	$p_{\frac{1}{2}}^{-1}d_{\frac{3}{2}}$	$p_{\frac{3}{2}}^{-1}s_{\frac{1}{2}}$	$p_{\frac{3}{2}}^{-1}d_{\frac{5}{2}}$	$p_{\frac{3}{2}}^{-1}d_{\frac{3}{2}}$	strength
13.3	1.0	-0.02	-0.06	-0.02	0.02	1%
17.6	0.01	0.90	-0.09	-0.38	-0.21	1%
20.0	0.06	-0.02	0.96	-0.24	-0.08	1%
22.2	0.04	0.35	0.20	0.90	-0.20	68%
25.0	-0.01	0.27	0.10	0.09	0.95	28%

The mismatch between the continuum channel configuration and the dipole states

configuration is remarkable but the doorway state model [133] has been succesfully applied [134] to the $^{15}N(p,\gamma_0)^{16}O$ problem and accounts for the rather important contribution of p and n channels to the total E1 strength. The γ_1, γ_2, γ_3 and γ_4 transitions were not resolved in this experiment but the comprehensive γ_{1-4} excitation function shows structures in qualitative agreement with those already observed in the γ_{1+2} channel only. The doorway state model is specifically applied to proton capture by Glavish and Mavis [135] and is reviewed and compared to the direct-semidirect model by Hanna [136]. In the doorway state approach the direct term enters naturally as the first step in the radiative capture process. With specific attention to $p + {}^{15}N$ [136] the $d_{\frac{3}{2}}$ or $s_{\frac{1}{2}}$ proton makes a radiative transition from a continuum state to fill the $p_{\frac{1}{2}}$ shell hole of the ^{15}N core. Alternatively the direct capture may excite a p-h state such as for example a $(p_{\frac{3}{2}})^{-1}d_{\frac{5}{2}}$ or a $(p_{\frac{1}{2}})^{-1}d_{\frac{3}{2}}$, that we have seen dominate the E1 transitions calculated in ^{16}O by Brown [116]. This accounts for the mismatch of continuum and dipole configurations in $^{15}N(p,\gamma_0)^{16}O$ since it is the two dipole states that make a radiative transition to the g.s. of ^{16}O, acting as the primary doorway states. But more complex configurations can be involved since the primary doorway may well excite secondary 2p-2h or many particles-many holes doorway states which at any step may revert to states of the GDR and radiatively deexcite. As a matter of fact the direct-semidirect model and the doorway state model are equivalent approaches to the same problem, the former dealing with hydrodynamical properties of the GDR and the latter with its microscopic nature.

1-12 GDR's built on excited ^{16}O states

Extension of (p,γ) measurements above the GDR region in ^{16}O has been firstly performed by a group including the author at the Milano cyclotron [137] where unpolarized protons from $E_p = 18$ to $E_p = 40$ MeV were available. Seven point angular distributions were measured at ten proton energies: 18.1, 19.7, 20.7, 21.7, 23.8, 25.8, 27.8, 31.8, 35.8 and 39.8 MeV respectively. They were subsequently fitted by a four term Legendre polynomial expansion [1-43] to obtain $a_1 \ldots a_4$ coefficients and total cross section for the γ_0 channel and a series of transitions all to 1p 1h final states in ^{16}O, for which the corresponding γ peaks could confidently be extracted from the collected photon spectra (Figure 17).

configuration is remarkable but the doorway state model [133] has been succesfully applied [134] to the $^{15}N(p,\gamma_0)^{16}O$ problem and accounts for the rather important contribution of p and n channels to the total E1 strength. The γ_1, γ_2, γ_3 and γ_4 transitions were not resolved in this experiment but the comprehensive γ_{1-4} excitation function shows structures in qualitative agreement with those already observed in the γ_{1+2} channel only. The doorway state model is specifically applied to proton capture by Glavish and Mavis [135] and is reviewed and compared to the direct-semidirect model by Hanna [136]. In the doorway state approach the direct term enters naturally as the first step in the radiative capture process. With specific attention to $p + ^{15}N$ [136] the $d_{\frac{3}{2}}$ or $s_{\frac{1}{2}}$ proton makes a radiative transition from a continuum state to fill the $p_{\frac{1}{2}}$ shell hole of the ^{15}N core. Alternatively the direct capture may excite a p-h state such as for example a $(p_{\frac{1}{2}})^{-1}d_{\frac{5}{2}}$ or a $(p_{\frac{1}{2}})^{-1}d_{\frac{3}{2}}$, that we have seen dominate the E1 transitions calculated in ^{16}O by Brown [116]. This accounts for the mismatch of continuum and dipole configurations in $^{15}N(p,\gamma_0)^{16}O$ since it is the two dipole states that make a radiative transition to the g.s. of ^{16}O, acting as the primary doorway states. But more complex configurations can be involved since the primary doorway may well excite secondary 2p-2h or many particles-many holes doorway states which at any step may revert to states of the GDR and radiatively deexcite. As a matter of fact the direct-semidirect model and the doorway state model are equivalent approaches to the same problem, the former dealing with hydrodynamical properties of the GDR and the latter with its microscopic nature.

1-12 GDR's built on excited ^{16}O states

Extension of (p,γ) measurements above the GDR region in ^{16}O has been firstly performed by a group including the author at the Milano cyclotron [137] where unpolarized protons from $E_p = 18$ to $E_p = 40$ MeV were available. Seven point angular distributions were measured at ten proton energies: 18.1, 19.7, 20.7, 21.7, 23.8, 25.8, 27.8, 31.8, 35.8 and 39.8 MeV respectively. They were subsequently fitted by a four term Legendre polynomial expansion [1-43] to obtain $a_1 \ldots a_4$ coefficients and total cross section for the γ_0 channel and a series of transitions all to 1p-1h final states in ^{16}O, for which the corresponding γ peaks could confidently be extracted from the collected photon spectra (Figure 17).

These included states at 6.13-6.9, 8.9-9.6, 11.6 and 12.6 + 13.1 MeV all having a dominant $(1p_{\frac{1}{2}})^{-1}$ configuration. The spectrum stripping procedure into nine peaks and a continuous background is indicated by the dashed curves in Figure 17, and requires the knowledge of the intrinsic response function $F(\omega, E_\gamma)$ and efficiency $\epsilon(E_\gamma) = \int F(\omega, E_\gamma)d\omega$, which can be provided by a reliable Monte Carlo calculation [138], to extract single peak areas and infer absolute values to the cross section. The actual line shape $S(\omega, E_\gamma)$ is obtained by Gaussian convolution of the intrinsic response function:

$$S(\omega, E_\gamma) = \int F(\omega', E_\gamma) G\left(\frac{\omega - \omega'}{\sigma_s}\right) d\omega' \qquad [1-83]$$

with the statistical variance σ_s determined from a set of well resolved $^{11}B(p,\gamma_0)^{12}C$ and $^{12}C(p,\gamma_0)^{13}N$ gamma lines [79]. Examples of the angular distributions obtained for the ground and some excited states are given in figures 18 and 19. The ground state transition is summarized in figure 20. The angular distributions (Figure 18) show a forward peaking more pronounced at high energies due to (E1,E2) interference, as revealed by the a_1 and a_2 coefficients, and by the non-zero a_3 and a_4 coefficients sensitive respectively to (E1,E2) interference and to quadrupole strength. High energy (γ, p_0) data [139] require the inclusion of a_5 which depends on (E2,E3) interference and a_6 which depends on $|E3|^2$, showing the presence of a non-negligible electric octupole component. No significant fit improvement is observed in the present data when such addition is attempted. Two theoretical models have been compared to the γ_0 data. One consists of a self consistent RPA calculation [81] where the single particle energies, the bound and scattering state wave functions and the particle-hole interaction are obtained from phenomenological forces. Skyrme-3 type nucleon-nucleon interaction is adopted, which accounts for the long range correlations and neglects tensor terms. Meson exchange currents are accounted for by the use of the Siegert theorem. Dipole and quadrupole matrix elements only are computed and the predictions are for an E1 strength peaked at 21 MeV and then slowly decreasing towards higher energies. The E2 strength peaks at $E_x \approx 21$ MeV but remains considerably high up to 60 MeV where it begins to be bigger than E1. As seen from the comparison with the experimental $a_0 \ldots a_4$ values relative to γ_0 radiation, the capture quadrupole strength is responsible mainly through (E1,E2) of the observed angular coefficients behaviour, the

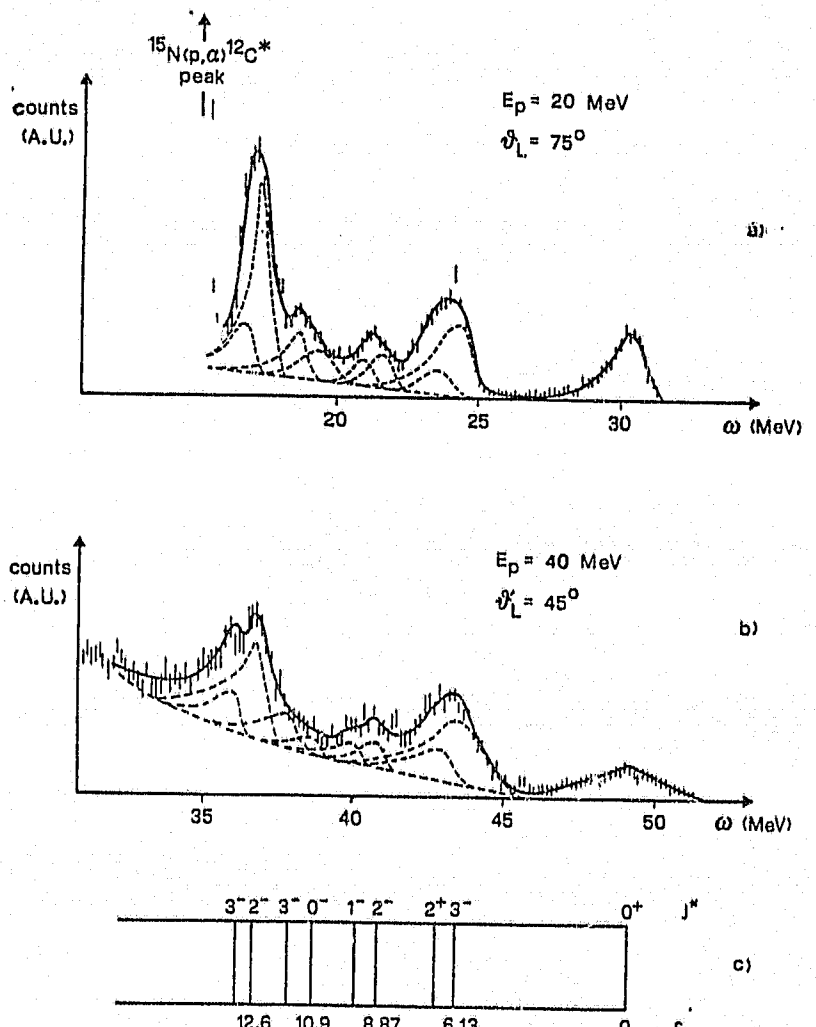

FIGURE 17 Photon spectra from the reaction $^{15}N(p,\gamma)^{16}O$ at $E_p = 20\,MeV$ and $E_p = 40\,MeV$. Shown is the unpeeling of the spectra into a continuous background and a series of peaks corresponding to transitions to a selected set of ^{16}O states.

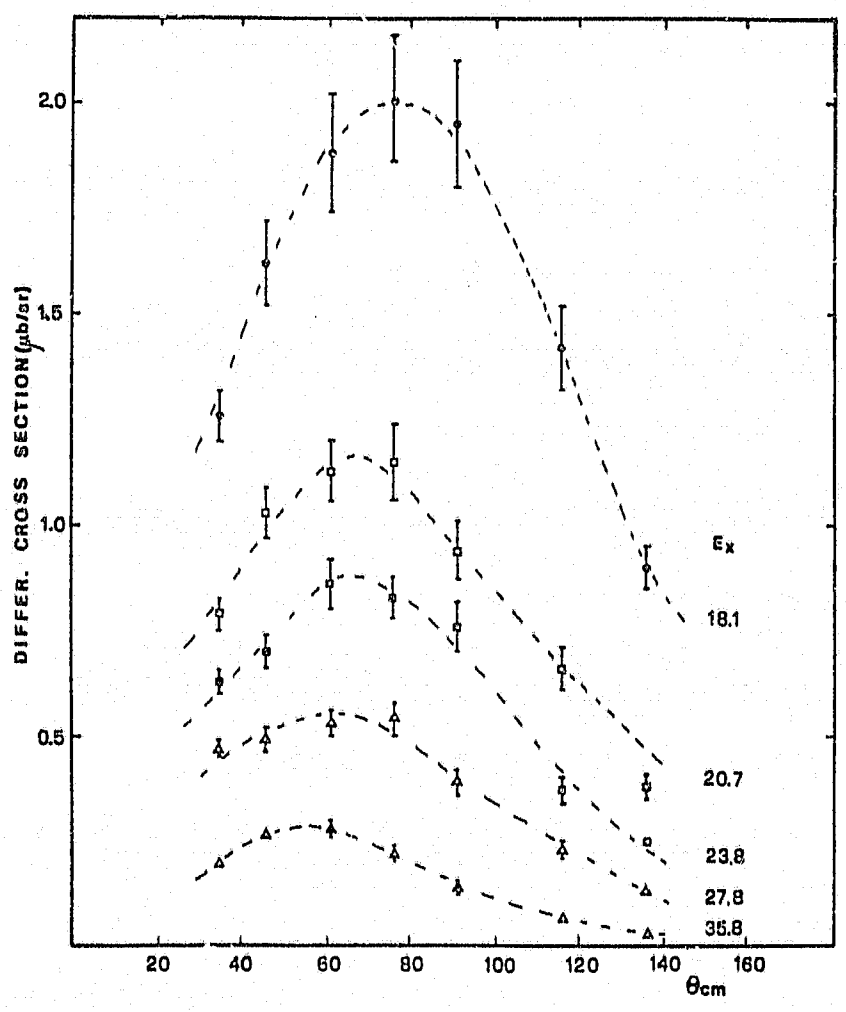

FIGURE 18 Angular distributions for the $^{15}N(p,\gamma_0)^{16}O$ at a few proton energies.

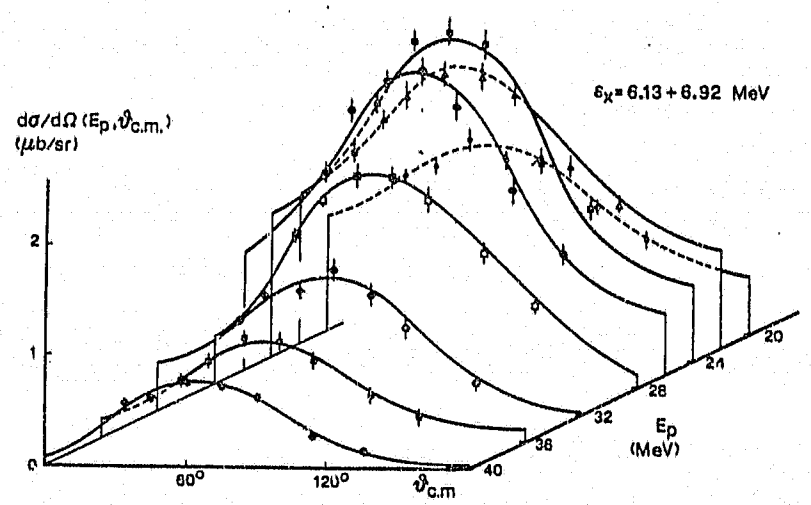

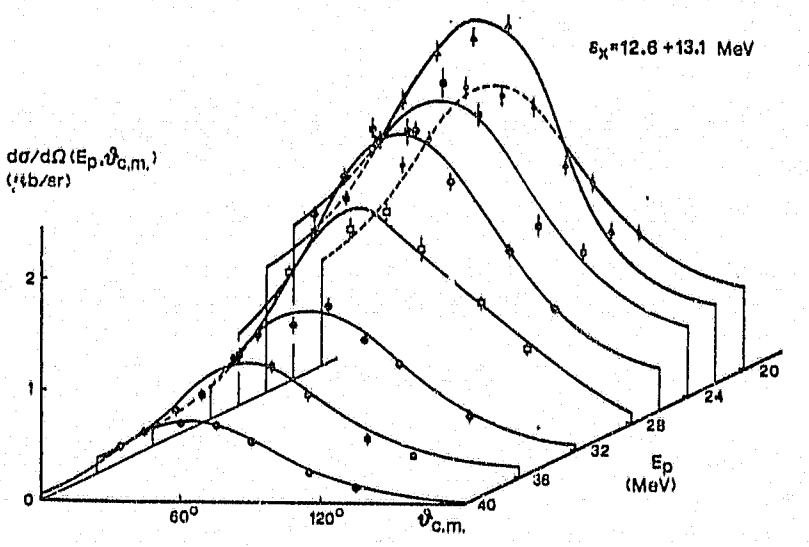

FIGURE 19 Angular ditributions for the reactions $^{15}N(p,\gamma_x)^{16}O^*$ ($E_x = 6.13+6.92$ MeV) and $^{15}N(p,\gamma_x)^{16}O^*$ ($E_x = 12.6 + 13.1$ MeV) at a few proton energies. The curves are Legendre polynomial fits to the data.

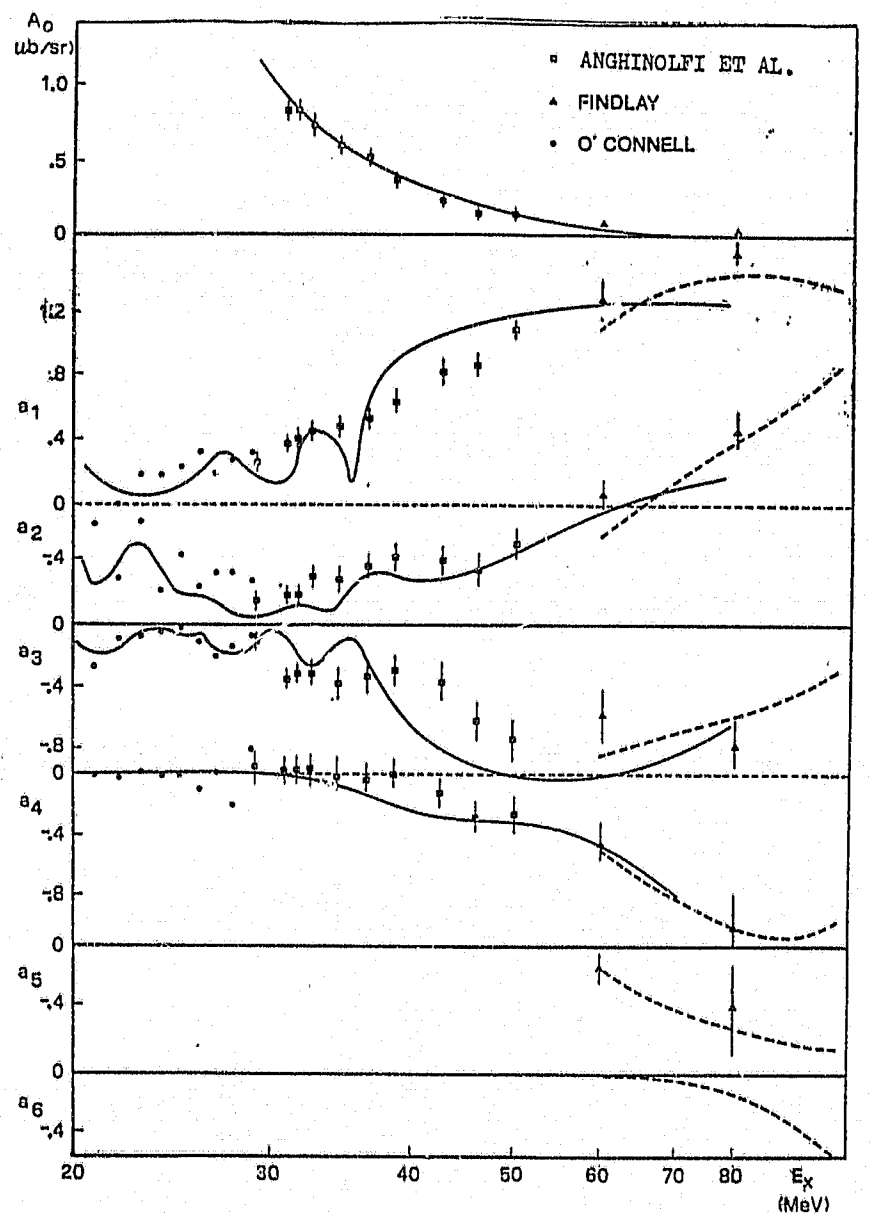

FIGURE 20 Angular distribution coefficients for the reaction $^{15}N(p,\gamma_0)^{16}O$ compared with the theoretical calculations of ref. [81] (full lines) and ref. [82] (dashed curves).

overall agreement being fairly good at least above the GDR specially if we consider the downward shifting of the RPA E2 strength with respect to the experimental points. The second model [82] consists of a a direct plus semidirect interaction, using phenomenological single particle wave functions, where ground state correlations have been included through a Yukawa effective nucleon-nucleon potential. Exchange currents are explicitly included by the use of effective two-body operators, and tensor correlations are partly included by a renormalisation of the residual interaction strength to the dipole sum rule. Above 50 MeV the agreement with the data is better than for the RPA calculation, certainly because tensor correlations begin to influence the dipole cross section at such energies. The total (γ, p_0) cross section is plotted in Figure 21, the integrated value up to 100 MeV is $57.8 \pm 5.$ mbMeV with the cross section above 30 MeV contributing with 8.0 μbMeV. The proton channel thus exhausts 24% of the classical sum rule and 18% of the integrated value as evaluated from total absorption measurements extended up to 100 MeV [140]. Expansion [1-43] has also been applied to (p, γ_x) data, which show smoother angular distributions increasing the difficulty of establishing the correct a_k values. The constraints [1-44] have been imposed with the consequence of an extra 5% uncertainty (40% for a_4) to be added to the statistical errors. The results for the unresolved $6.13 - 6.92$ MeV and the $12.6 - 13.1$ MeV groups of states, reported in Figure 22, can be taken as well representative of the general situation for (p, γ_x) transitions. There is evidence of a dominant E1 absorption, responsible for the large a_2 values, with non negligible (E1,E2) interference contribution to the a_1 and a_3 terms, due to appreciable E2 strength which should be concentrated around $30 - 40$ MeV as observed by the $^{12}C(\alpha, \gamma_x)^{16}O$ reaction [141]. From the energy behaviour of the (p, γ_x) angular distributions and from the integrated cross section reported in Figure 23 for the ground and the excited states transitions, emerges once more the systematic existence of resonances in each channel. If one notices that the final states involved are largely dominated by 1p-1h configurations with a hole in the $1p_{\frac{1}{2}}$ shell, as it is for the continuum initial state, one is naturally led to the description of p radiative capture as a single particle process, extremely selective for the nature of the final excited state (which mostly matches the entrance channel configuration) and dominated by E1 resonance present in each excited state, and clearly identified in their nature by the almost general behaviour

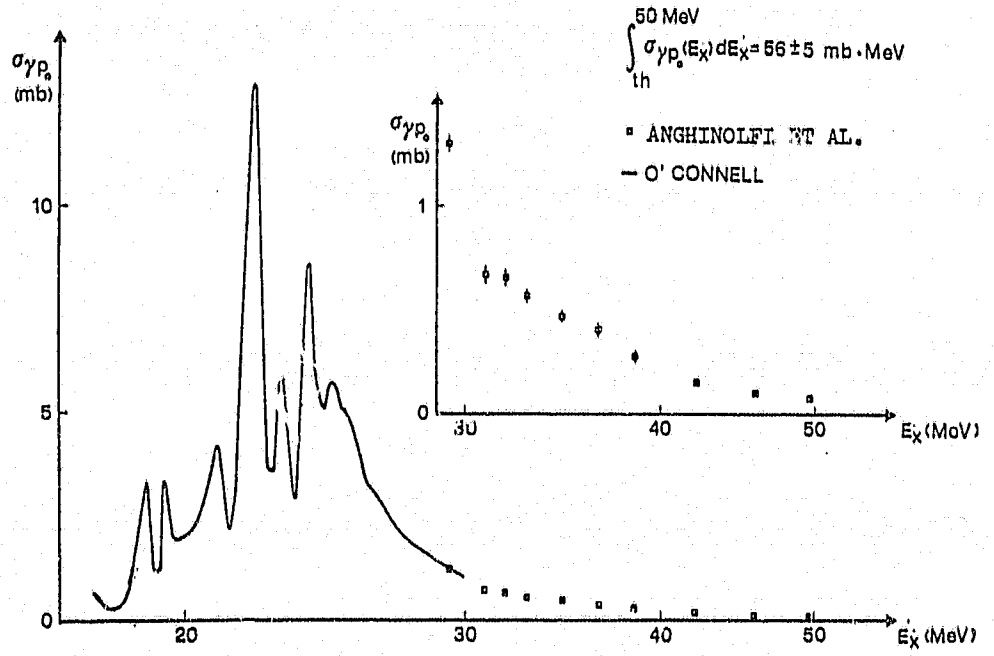

FIGURE 21 Ground state photodisintegration cross section (γp_0) as a function of the incident photon energy.